LINEAR PHASE PERFECT RECONSTRUCTION FILTER BANKS: THEORY, STRUCTURE, DESIGN, AND APPLICATION IN IMAGE COMPRESSION

By

Trac Duy Tran

A dissertation submitted in partial fulfillment of the

requirements for the degree of

Doctor of Philosophy

(Electrical Engineering)

at the

UNIVERSITY OF WISCONSIN – MADISON

1999

Abstract

This dissertation studies the theory, structure, design, and implementation of discrete-time FIR linear phase perfect reconstruction filter banks with arbitrary M channels and arbitrary-length filters. The class of filter banks in consideration has high practical values, and the results reported are the most general solutions in the current literature. The approach consistently taken throughout the dissertation is to parameterize these systems by lattice structures based on the factorizations of the analysis and synthesis polyphase transfer matrices. The lattice robustly enforces the two most desirable properties, namely linear phase and perfect reconstruction, so that they are inherently retained regardless of the quantization of lattice coefficients to any desired level. The various lattices are proven to completely span the set of all possible solutions and to employ the least number of delay elements in the filter bank's implementation.

The novel multi-band linear phase perfect reconstruction filter banks can also be viewed as the generalized lapped orthogonal/biorthogonal transforms with fast, efficient, robust, and modular implementations. The lapped transform elegantly solves the blocking artifact problem in traditional block-transform-based image coders. Extensive image coding examples demonstrate that the new lapped transforms, when appropriately designed and utilized, offer significant improvements in both objective and subjective coding performances over all transforms reported in previous works.

Acknowledgements

First, I wish to express my appreciation and gratitude to my advisor, Professor Truong Q. Nguyen, whose patience, support, guidance, and encouragement have made the completion of this dissertation possible. He has introduced me to the dynamic, tantalizing field of research on filter banks and wavelets, and has taught me most of what I know on the subject. I am also grateful to Dr. Ricardo L. de Queiroz for numerous intellectual discussions on lapped transforms and filter banks and for allowing me to work on the GLBT on the side during my brief three-month tenure at Xerox Corporation. Next, I would like to thank Professor Masaaki Ikehara of Keio University, Japan, with whom I had several rewarding collaborations. Professor Ikehara has greatly influenced the design approach of variable-length lapped transforms in Chapter 6. I am also thankful to Professor Yu-Hen Hu for his enthusiasm, his generous help, and the fruitful collaboration on image and video compression. Special tokens of appreciation go to Professor Akbar Sayeed for serving as a thesis reader, to Professor Damon L. Tull and Professor Mei-Chang Shen for their geniality in serving on my thesis committee. Long-distance collaborations with Soontorn Oraintara of Boston University on multi-dimensional filter banks and Mika Helsingius of Tampere University of Technology, Finland, on generalized zerotree coding are gratefully acknowledged.

I also feel obliged to acknowledge the University of Wisconsin, General Electric, and NSF for providing me most of the necessary financial support over the years.

The special note of gratitude goes to my parents whose unconditional love and tremendous sacrifice have brought me up the person I am today. The early-season harvest of this dissertation is dedicated to them with my utmost respect. I am also thankful to my aunt and uncle who have always treated me like their own son. Another special thank-you note is directed to my brother Tri D. Tran for his constant support. The final and deepest appreciation is reserved for my fianceé Lan K. Nguyen whose love, patience, understanding, and caring throughout my Ph.D. program are unfathomable.

Contents

List of Figures

List of Tables

Chapter 1

Introduction

1.1 Filter Banks and Multirate Systems

There has been a tremendous growth in the field of filter banks (FBs) and multirate systems in the last fifteen years [11], [95], [98], [77]. These systems provide new and effective tools to represent signals for processing, understanding, and compression purposes. For instance, one of the newest addition to the filter bank field is the dyadic wavelet transform which can be interpreted as an iteration on the lowpass output of a two-channel filter bank with certain degrees of regularity (vanishing moments) [13], [43], [44]. As another example, the current image compression standard JPEG [58] is based on the 8×8 Discrete Cosine Transform (DCT) which is nothing more than a well-designed 8-channel linear phase orthogonal filter bank with 8-tap filters [67]. Some classical linear system tools also fit elegantly in the filter bank framework as well: the Discrete Fourier Transform (DFT) can be viewed as a multi-channel uniform filter bank whose filters are modulations of a single complex sinusoid. It is quite accurate to say that filter banks find applications in virtually every signal processing and closely related field: speech, audio, image, and video compression; signal filtering; communication; time-frequency representation and

analysis; statistical signal processing; optical signal processing; computer graphics, etc. Obviously, of extreme importance is the ability to design a FB that can fully exploit the properties and nature of a particular signal or application.

1.2 Application in Image Compression

One particular application that filter banks have found tremendous successes in is the compression of images. Image compression, or image coding, is the technology of image data reduction to save storage space and transmission bandwidth. With the recent explosion of the internet, the search for better image compression techniques is becoming ever more pressing. It is evidently desirable to represent images by the minimum number of binary digits given a fixed level of distortion, or for a given bit budget, to retain as much visual information as possible.

Two dominant techniques in existing image compression standards and implementations are block transform coding and subband coding [32], [58], [66], [104]. Both methods actually exhibit many similarities: operating in the frequency domain, utilizing the same basic building blocks such as bit allocation, quantization, and entropy coding to achieve compression. In the coder, both techniques rely heavily on filter banks to generate the frequency coefficients that can be quantized and entropy coded. In the decoder, filter banks are again employed to combine and reconstruct the signal. Therefore, designing good filter banks plays an integral role in the advancement of image coding technology. A good filter bank has to be able to fully exploit two main principles that make image

compression successful:

- **Reduction of redundancy**. There exists statistical dependency between neighboring pixels in meaningful images. The analysis filters must possess high energy compaction property. In other words, they have to be able to decorrelate the image as much as possible, representing the image by the fewest number of coefficients.

- **Reduction of irrelevancy**. The Human Visual System (HVS) cannot perceive certain deviations of the reconstructed image from the original image. The synthesis filters must be designed to minimize the perceivable difference between the compressed and the original representation. Image properties such as smoothness that human eyes prefer should be retain whereas annoying artifacts such as blocking and ringing should be adequately suppressed.

1.3 Concentration and Approach

M-channel uniform LPPRFBs can be implemented as lapped transforms which can reduce blocking artifacts in traditional block-transform-based image coders [45], [46], [47], [62] at low bit rates. The lapped transform borrows pixels from the adjacent blocks to produce the transform coefficients of the current block. Hence, it takes into account inter-block correlation, provides better energy compaction, and reduces blocking discontinuities drastically. The block-based nature of multi-band lapped transforms also offers numerous other advantages: capable of processing large signals under limited memory constraint, increasing computational parallelism, facilitating region-of-interest coding/decoding, and

providing a finer tiling of the time-frequency plane.

A filter bank that finds application in image coding may also need to have linear phase, finite filter length, real (sometimes rational or even interger) filter coefficients, and perfect reconstruction. In this dissertation, the theory, design, and implementation of M-channel discrete-time FIR linear phase perfect reconstruction filter banks with application in image coding are studied in details. Besides the aforementioned often-desired properties, all of the novel filter banks presented in this work are obtained from the attractive approach of system's parameterization by lattice structures based on the factorization of the analysis and synthesis polyphase matrices. The lattice structurally enforces the linear phase and perfect reconstruction properties on the filter banks, i.e., in the lattice representation both of these properties are retained regardless of coefficient quantization. Not only does the lattice structure offer a powerful FB design tool, it also provides a fast, efficient, and robust structure suitable for hardware implementation. Note that although image compression is the main application in mind, filter banks presented here can benefit numerous other applications as well. The dissertation provides a unique blend of experience in filter bank theory, filter bank structure, filter design, and image compression.

1.4 Outline

The outline is as follows. In **chapter 2**, we offer a review of important background materials, major concepts, as well as previous related works in the theory, design, implementation of multirate systems, filter banks, and their application in image coding. **Chapter 3** lays the foundation for the whole thesis by investigating general filter bank theories concerning the equivalent conditions for the linear phase property and the permissible conditions of existence for linear phase perfect reconstruction systems. These fundamental results are extremely helpful in restricting the search space of possible solutions and they also play key roles in the development of general lattice structures throughout the dissertation.

Chapter 4 next introduces a lattice structure based on the singular value decomposition that propagates the linear phase and the perfect reconstruction property. The lattice is proven to use a minimal number of delay elements and to completely span a large class of linear phase perfect reconstruction filter banks (LPPRFBs): arbitrary channel M, all analysis and synthesis filters have the same FIR length $L = KM$ sharing the same center of symmetry. Under the lapped transform's prizm, these LPPRFBs represent the complete family of generalized lapped biorthogonal transforms (GLBTs) with arbitrary number of channels M and arbitrary large overlapping samples KM. The biorthogonal property allows the novel filter bank to have significantly different analysis and synthesis basis functions which can then be tailored appropriately to fit a particular application.

A generalization step is taken in **chapter 5** where the length of the filters L is not

constrained to be an integer multiple of the number of channels M anymore. This is the true lapped transform whose number of overlapping samples can be chosen arbitrarily. Solutions for both cases of orthogonal and biorthogonal systems are presented.

Chapter 6 discusses the theory, structure, and design of filter banks with variable-length filters, or generalized lapped transforms with variable-length basis functions. The variable-length property leads to extremely fast, low-complexity transforms which are also to reduce ringing artifacts at high compression ratios while being as effective in eliminating blocking artifacts as the traditional lapped transforms in Chapter 4–5. Design procedures and design examples are presented throughout Chapter 4–6.

The successful application of the newly found filter banks in progressive and perceptually progressive image coding is illustrated in **chapter 7**. Our lapped-transform-based embedded coder consistently outperforms the wavelet-based SPIHT coder [71] by a large margin. The improvement in PSNR can be up to an astounding 2.6 dB. Finally, **chapter 8** draws up the final conclusions and presents several future research directions.

Chapter 2

Review

2.1 Introduction

This chapter introduces the notations, symbols, and terminologies as well as reviews some basic definitions and important concepts that are used extensively throughout the dissertation. Discussions of previous works on filter banks and their application in image coding are also provided as motivational background materials.

2.2 Notations

Let $\mathcal{C}, \mathcal{R}, \mathcal{Z}, \mathcal{Z}^+$ denote the sets of complex, real, integer, and positive integer numbers. The symbols $h_i[n]$, $H_i(z)$, and $H_i(e^{j\omega})$ stand for the i-th filter's impulse response (storing the filter's coefficients), its associated z-transform, and its Fourier transform. If a discrete-time filter has finite length, it is called FIR (finite impulse response); otherwise, it is labeled IIR (infinite impulse response). A filter $h_i[n]$ is said to be *causal* if $h_i[n] = 0$, $\forall\ n < 0$, $n \in \mathcal{Z}$, and *anticausal* if $h_i[n] = 0$, $\forall\ n > 0$, $n \in \mathcal{Z}$. When refering to the transfer function or the z-domain representation, the term causal is equivalent to "polynomial in z^{-1}" and the term anticausal is equivalent to "polynomial in z". For various practical

purposes, only FIR and real-coefficient systems are under consideration.

Bold-faced lower case characters are used to denote vectors while bold-faced upper case characters are used to denote matrices. $\mathbf{A}^\dagger$, $\mathbf{A}^T$, $\mathbf{A}^{-1}$, $tr(\mathbf{A})$, $|\mathbf{A}|$, $\rho(\mathbf{A})$, $\mathbf{a}_{i\cdot}$, $\mathbf{a}_{\cdot j}$ denote respectively the conjugate transpose, the transpose, the inverse, the trace, the determinant, the rank, the i-th row, and the j-th column of the matrix $\mathbf{A}$. If a matrix $\mathbf{A}$ has elements as polynomials in z, it is denoted as $\mathbf{A}(z)$. Moreover, if $\mathbf{A}(z)$ has an inverse and its determinant is a pure delay, i.e., $|\mathbf{A}| = z^{-m}$, $m \in \mathcal{Z}$, then $\mathbf{A}(z)$ is called FIR invertible or having FIR inverse.

Several special matrices with reserved symbols are: the polyphase matrix of the analysis bank $\mathbf{E}(z)$, the polyphase matrix of the synthesis bank $\mathbf{R}(z)$, the identity matrix $\mathbf{I}$, the reversal matrix $\mathbf{J}$ ($\mathbf{I}$ flipped left-right or up-down), the null matrix $\mathbf{0}$, the nonvacuous matrix $\mathbf{X}$, and the diagonal matrix with entries being either $+1$ or -1 $\mathbf{D}$. When the size of a matrix or vector is not clear from context, subscripts will be included. For example, $\mathbf{J}_M$ denotes the square reversal matrix of size M, and $\mathbf{0}_{M\times N}$ denotes the $M \times N$ null matrix. M and L are usually reserved for the number of channels and the filter length. Finally, $\mathcal{S}\{\mathbf{a}_1, \mathbf{a}_2, \ldots, \mathbf{a}_n\}$ is used to denote the vector space spanned by the n vectors $\mathbf{a}_1, \mathbf{a}_2, \ldots, \mathbf{a}_n$.

For abbreviations, we use LP, PR, PU, VL, LT, and FB to denote *linear phase*, *perfect reconstruction*, *paraunitary*, *variable length*, *lapped transform*, and *filter bank*, respectively. *Symmetric* and *antisymmetric* are sometimes abbreviated as S and A. The terms – LPPUFB and GenLOT, LPPRFB and GLBT, LPPUFB with filters of different lengths and VLLOT, LPPRFB with filters of different lengths and VLGLBT – are used

interchangeably in the thesis. The term lapped transform usually emphasizes the possible block-based implementation of the filter bank.

2.3 Filter Bank Fundamentals

2.3.1 What is a Filter Bank?

A filter bank is simply a bank of lowpass, bandpass, and highpass filters, each of which covers a band in the frequency spectrum. Other possible components of a filter bank include downsamplers, upsamplers, and delay elements. In this dissertation, we consider the discrete-time M-channel maximally-decimated uniform filter bank as depicted in Figure 1. At the *analysis stage*, the input signal $x[n]$ is passed through a bank of M analysis filters $H_i(z)$, each of which preserves a frequency band of uniform bandwidth $\frac{\pi}{M}$. These M filtered signals are then decimated by M to preserve the system's overall sampling rate (thus this system is commonly labeled as *maximally decimated* or *critically sampled* filter bank). The resulting *subband* signals can be encoded, processed, transmitted, and/or decoded independently or jointly. All of these activities are grouped together in the *processing* block, which is typically not considered as a component of the filter bank. At the *synthesis stage*, the subbands are combined by a set of upsamplers and M synthesis filters $F_i(z)$ to form the reconstructed signal $\hat{x}[n]$. If the filters are ideal, no aliasing occurs and perfect reconstruction is obtained trivially. However, this is not the case in practice, so judicious choices of $H_i(z)$ and $F_i(z)$ need to be made. The most

general perfect reconstruction property can be defined as follows.

Definition 2.1 *A filter bank is said to have perfect reconstruction if its output* $\hat{x}[n]$ *is a pure time-delayed version of its input* $x[n]$*, i.e.,* $\hat{x}[n] = x[n-\ell]$*,* $\ell \in \mathcal{Z}$*.*

This is also the most intuitive definition of perfect reconstruction. Later we shall provide more specific definitions in term of the filter bank's polyphase matrices. Perfect reconstruction is, of course, a very attractive property since it provides a lossless signal representation and it simplifies the error analysis significantly.

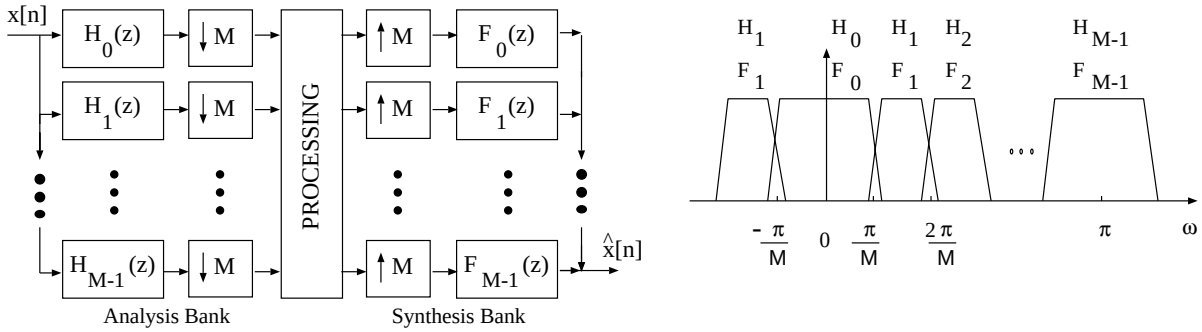

Figure 1: A typical M-channel maximally-decimated uniform filter bank.

2.3.2 Linear Phase Filter Banks

In numerous applications, especially image processing, it is crucial that all analysis and synthesis filters have linear phase. Such system is called a linear phase filter bank (LPFB). Besides the elimination of the phase distortion which is often disastrous in many image processing applications [40], LP filters preserve the locality of the edges, the key to success of hierarchy image coding algorithms [110], [66], [73], [71]. For the same reason, LP filters are also important in frame-to-frame correlation schemes used in video processing and

for event localization in geophysical signal processing. Furthermore, LP filters allow us to employ simple symmetric extension methods to effectively handle the boundaries of finite-length signals [8], [36], [61]. Symmetric extension eliminates the annoying energy leakage due to discontinuities at the borders when circular convolution and periodic extension are used to implement non-LP filter banks. Finally, from an implementation perspective, the symmetry of the filters helps reducing the number of multipliers needed by a factor of 2.

The most general condition for an L-tap FIR linear phase filter is that its impulse response $h[n]$ must satisfies the equation: $h[n] = c\,h[L-n]$ for some $c \in \mathcal{C}$ with $|c| = 1$ [95]. Since we only deal with real-coefficient filters, this condition simplifies to either $h[n] = h[L-1-n]$ (symmetric filter) or $h[n] = -h[L-1-n]$ (antisymmetric filter). Depending on whether $h[n]$ is odd-length or even-length, symmetric or antisymmetric, we have four types of real-coefficient LP filters as summarized in Table 1. Notice that some of these filters cannot cover certain frequency. A filter bank with all Type 4 filters certainly cannot have perfect reconstruction: signal component at DC ($\omega = 0$) is discarded in the analysis bank and cannot be recovered.

2.3.3 Polyphase Representation

Consider a filter h_i of an M-channel filter bank in z-domain $H_i(z) = \sum_{n=-\infty}^{\infty} h_i[n]\, z^{-n}$. Even-indexed and odd-indexed coefficients can be separated as

$$H_i(z) \;=\; \sum_{n=-\infty}^{\infty} h_i[2n]\, z^{-2n} + \sum_{n=-\infty}^{\infty} h_i[2n+1]\, z^{-2n-1}$$

Type	*Length*	*Symmetry*	*Zero Locations*	*Special Characteristics*
1	odd	S	–	good lowpass, bandpass, highpass
2	even	S	at π	good lowpass, bandpass
3	odd	A	at 0 and π	good bandpass, middle coefficient is 0
4	even	A	at 0	good bandpass, highpass

Table 1: Four types of real-coefficient LP filters.

Define

$$E_{i0}(z) \triangleq \sum_{n=-\infty}^{\infty} h_i[2n]\, z^{-n} \quad \text{and} \quad E_{i1}(z) \triangleq \sum_{n=-\infty}^{\infty} h_i[2n+1]\, z^{-n}$$

as two *polyphase components* of $H_i(z)$. We can then represent $H_i(z)$ as

$$H_i(z) = E_{i0}(z^2) + z^{-1}E_{i1}(z^2).$$

More generally speaking, $H_i(z)$ can be characterized equivalently by its M polyphase components for any given positive integer M:

$$H_i(z) = \sum_{\ell=0}^{M-1} z^{-\ell}\, E_{i\ell}(z^M) \qquad \text{(Type I polyphase)}, \tag{2.1}$$

where

$$E_{i\ell}(z) = \sum_{n=-\infty}^{\infty} h_i[nM+\ell]\, z^{-n}. \tag{2.2}$$

Another polyphase representation of $H_i(z)$ is given by

$$H_i(z) = \sum_{\ell=0}^{M-1} z^{-(M-1-\ell)}\, R_{\ell i}(z^M) \qquad \text{(Type II polyphase)}, \tag{2.3}$$

with $R_{\ell i}(z) = E_{i(M-1-\ell)}(z)$.

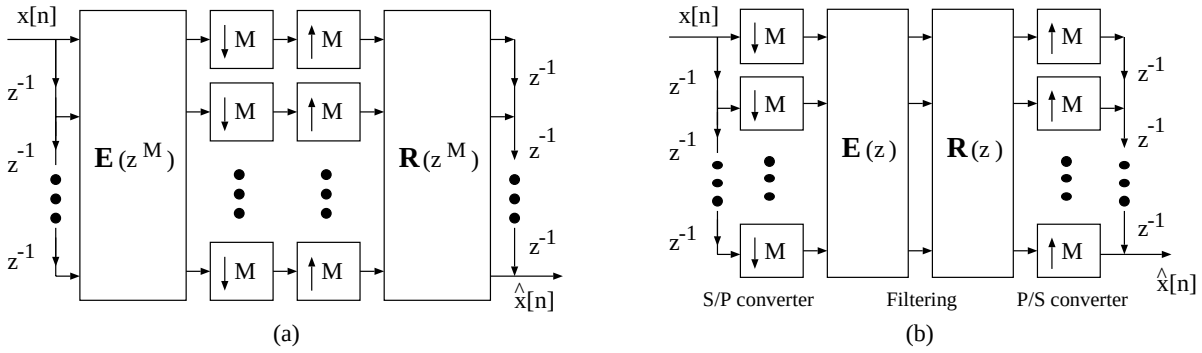

Figure 2: Equivalent polyphase representations of an M-channel filter bank.

Armed with the polyphase representations, let us reconsider the M-channel critically sampled filter bank depicted in Figure 1. Again, the coding and quantization errors in the processing step are ignored. Define the $M \times M$ matrix $\mathbf{E}(z) \triangleq [\ E_{i\ell}(z)\ ]$ as the polyphase matrix of the analysis bank. The Type I polyphase in Eq.(2.1) yields

$$\begin{bmatrix} H_0(z) \\ H_1(z) \\ \vdots \\ H_{M-1}(z) \end{bmatrix} = \mathbf{E}(z^M) \begin{bmatrix} 1 \\ z^{-1} \\ \vdots \\ z^{-(M-1)} \end{bmatrix}. \tag{2.4}$$

Similarly, the synthesis bank can be represented by the Type II polyphase matrix $\mathbf{R}(z) \triangleq [\ R_{\ell i}(z)\ ]$ as follows

$$\begin{bmatrix} F_0(z) & F_1(z) & \dots & F_{M-1}(z) \end{bmatrix} = \begin{bmatrix} z^{-(M-1)} & z^{-(M-2)} & \dots & 1 \end{bmatrix} \mathbf{R}(z^M). \tag{2.5}$$

Eq.(2.4) and Eq.(2.5) produce the equivalent filter bank in Figure 2(a). The noble identities illustrated in Figure 3 can then be applied to obtain another representation shown in Figure 2(b) where the delay chain and the downsamplers at the analysis stage work as

a serial-to-parallel converter. At the synthesis bank, the upsamplers and the delay chain can be thought of as a parallel-to-serial converter.

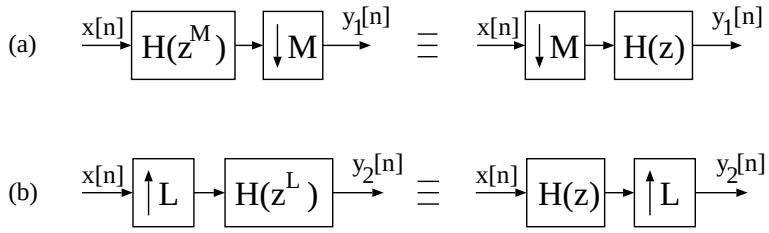

Figure 3: Noble identities.

The latter polyphase representation in Figure 2(b) proves to be very useful, both theoretically and practically, in filter bank design and application. Not only does it allow the processing of signals at lower rates, but it also simplifies filter bank theory dramatically. As demonstrated throughout the dissertation, polyphase matrices are cornerstones in the lattice structure design method. In light of the polyphase representation, we can now define some FB terminologies in a more mathematically precise manner. First, it is a simple exercise to show that when $\mathbf{R}(z)\mathbf{E}(z) = \mathbf{I}$, the output $\hat{x}[n]$ is a delayed version of the input $x[n]$. Hence, perfect reconstruction is guaranteed if the polyphase matrix $\mathbf{E}(z)$ is invertible.

Definition 2.2 *A filter bank is said to have perfect reconstruction if its polyphase matrices* $\mathbf{R}(z)$ *and* $\mathbf{E}(z)$ *satisfy the following equation*

$$\mathbf{R}(z)\,\mathbf{E}(z) \;=\; z^{-\ell}\,\mathbf{I}, \qquad \ell \in \mathcal{Z}. \tag{2.6}$$

The reader should note that Definition 2.2 is not as general as Definition 2.1; more general condition can be found in [95]. However, Definition 2.2 still covers a huge class of

PR filter banks. In fact, for a FB to have practical values, many more restrictions need to be imposed. For instance, to obtain stable synthesis filters, $\mathbf{E}(z)$ must be invertible with strictly minimum-phase determinant, i.e., its determinant has all zeros inside the unit circle (except zero at $z = \infty$ as in z^{-1}). With this requirement, stability is established, but the synthesis filters will most likely turn out to be IIR. To obtain FIR synthesis filters, we need the following constraints on the determinants of both polyphase matrices.

Theorem 2.3 *Every perfect reconstruction filter bank as defined in Definition 2.2 with FIR analysis and synthesis filters must have*

$$|\mathbf{R}(z)| \;=\; z^{-m} \quad \textit{and} \quad |\mathbf{E}(z)| \;=\; z^{-n} \qquad m, n \in \mathcal{Z}. \tag{2.7}$$

In other words, the determinants of both analysis and synthesis polyphase matrix of an FIR PRFB have to be monomials. The proof of Theorem 2.3 can be found in [95]. It relies on a straightforward implication from Definition 2.2: $|\mathbf{R}(z)|\,|\mathbf{E}(z)| \;=\; z^{-M\ell}$.

Paraunitary (sometimes loosely called orthogonal) filter banks are often desired in practice. The orthogonality of the filters is a very natural choice. After all, filters with ideal brick-wall responses are orthogonal. The definition of paraunitary FB below is used throughout the dissertation.

Definition 2.4 *A filter bank is said to be paraunitary if its polyphase matrices satisfy the following relation*

$$\mathbf{R}(z) \;=\; z^{-K}\mathbf{E}^{\dagger}(z^{-1}), \tag{2.8}$$

where K is the order of $\mathbf{E}(z)$. For real-coefficient paraunitary filter banks,

$$\mathbf{R}(z) \;=\; z^{-K}\mathbf{E}^{T}(z^{-1}). \tag{2.9}$$

Equivalently, the impulse responses of a real-coefficient paraunitary filter bank have to satisfy the following time-domain constraint [95]:

$$\sum_{n=-\infty}^{\infty} h_j[n]\, h_k^T[n-\ell M] \;=\; \delta[\ell]\,\delta[j-k], \qquad \ell \in \mathcal{Z}. \tag{2.10}$$

As Eq.(2.10) suggests, paraunitary filter banks impose very strict constraints on the filters' coefficients. Besides the obvious orthogonality of the impulse responses of the filters, their shift-by-M versions (the overlapping tails) must be orthogonal to each other also. Furthermore, the synthesis filters are simply time-reversed versions of the analysis filters: $f_i[n] = h_i[L-1-n]$. These are penalties that one has to pay to obtain simple yet high-performance systems. PU filter banks avoid the costly procedure of matrix inversion in the optimization process (synthesis banks can be trivially obtained), and their orthogonal filters usually lead to high energy compaction. In the case where $\mathbf{E}(z)$ may not be paraunitary but Eq.(2.6) holds, we say the FB is *biorthogonal*.

Definition 2.5 *A filter bank is said to be biorthogonal if its polyphase matrices satisfy the following relation*

$$\mathbf{R}(z) \;=\; z^{-K}\mathbf{E}^{-1}(z^{-1}), \tag{2.11}$$

where K is chosen appropriately so that the resulting synthesis filters are causal.

Remarks. The definition of biorthogonality in Eq.(2.11) is equivalent to the definition of perfect reconstruction in Eq.(2.6) with two additional constraints: (i) the synthesis filters are causal; (ii) the synthesis filters are FIR. In the case when all analysis and synthesis filters have the same length L, K is simply the order of $\mathbf{E}(z)$. Definition

2.5 does cover orthogonal systems as well (when $\mathbf{E}^{-1}$ is chosen to be $\mathbf{E}^T$). In practice, high-performance biorthogonal systems are usually close to satisfying Eq.(2.9) and Eq.(2.10). In this dissertation, biorthogonality and perfect reconstruction are often used interchangeably.

2.3.4 Lattice Structure

One of the more important theoretical developments in filter bank design is the concept of the *lattice structure*, where the filter bank is factorized into a cascade of elementary building blocks. These blocks are parameterized by a set of lattice coefficients that completely characterize a given filter bank. The space of possible lattice parameters can be used as a design space over which certain secondary FB properties are optimized for. These lattice factorizations lead to fast and efficient algorithms for the subband computations, since they reduce the filter description to a minimal set of delay elements. The modular form of a lattice factorization lends itself nicely to VLSI implementations, and PR property is retained in spite of lattice coefficient quantization.

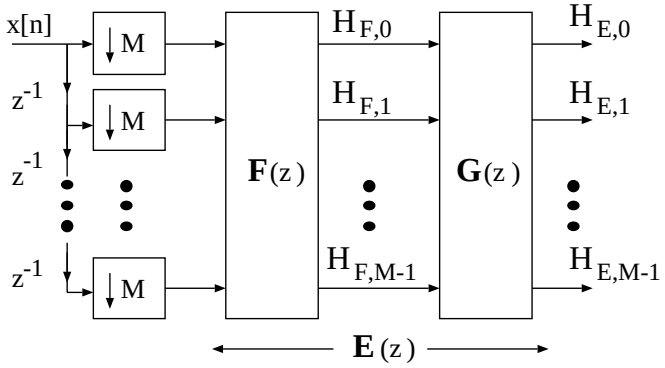

Figure 4: A stage of the lattice structure.

The essential concept of the lattice structure can be best illustrated in Figure 4. Suppose we are given a set of filters $\{H_{F,i}(z)\}$ with the associated polyphase matrix $\mathbf{F}(z)$ satisfying a certain set of desired properties. We would like to design a low-ordered structure $\mathbf{G}(z)$ to translate $\{H_{F,i}(z)\}$ into another set of filters $\{H_{E,i}(z)\}$ of higher order, represented by the new polyphase matrix $\mathbf{E}(z) = \mathbf{G}(z)\mathbf{F}(z)$, in such a way that $\{H_{E,i}(z)\}$ still possesses the same set of desired properties as $\{H_{F,i}(z)\}$. A high-complexity filter bank can be designed by cascading a multiple of simple lattice building blocks together as shown in Figure 5, i.e., $\mathbf{E}(z) = \mathbf{G}_K(z)\,\mathbf{G}_{K-1}(z) \cdots \mathbf{G}_1(z)\;\mathbf{G}_0(z)$. It is easy to see from Eq.(2.6) and Eq.(2.9) that the resulting FB has PR or is PU if each of the building blocks $\mathbf{G}_i(z)$ is invertible or paraunitary, respectively.

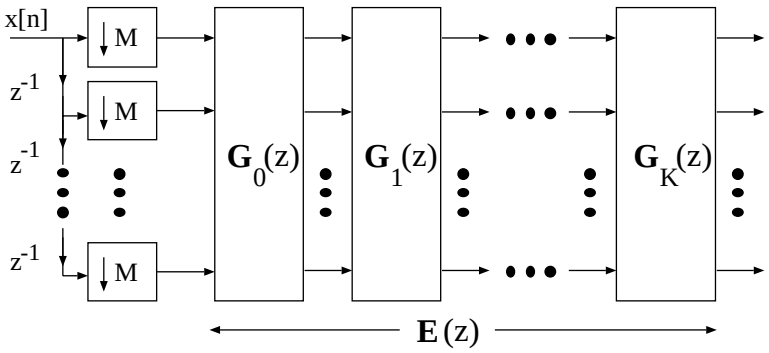

Figure 5: High-order filter bank as a cascade of lattice structure stages.

The free parameters, or the degrees of freedom, in each $\mathbf{G}_i(z)$ structure are often called the *lattice coefficients*. Thanks to the property propagation (which is mathematically imposed), the FB still retains its attractive properties when its lattice coefficients are varied arbitrarily. This leads to the robustness of the system under coefficient quantization. To see this more clearly, consider the parameterization of an $N \times N$ orthogonal

matrix (here $\mathbf{G}_i(z)$ is simply $\mathbf{U}_i$, propagating orthogonality). It is well-known that any orthogonal matrix $\mathbf{U}_i$ can always be factored into a series of $\frac{N(N-1)}{2}$ Givens (planar) rotations [19], [25], [95] as illustrated in Figure 6 (drawn for $N = 4$), where each rotation has the following form

$$\mathbf{U}_{\theta_i} = \begin{bmatrix} \cos\theta_i & \sin\theta_i \\ -\sin\theta_i & \cos\theta_i \end{bmatrix}. \tag{2.12}$$

The free parameters, or the lattice coefficients, in this case are the rotation angles. Any realization of the set of rotation angles gives rise to an orthogonal matrix. On the other hand, any orthogonal matrix can be completely characterized by $\frac{N(N-1)}{2}$ rotation angles. Under this parameterization, $\mathbf{U}_i$ is guaranteed to be orthogonal in spite of any quantization of the parameters since the quantized rotation

$$\hat{\mathbf{U}}_{\theta_i} = \begin{bmatrix} \cos Q[\theta_i] & \sin Q[\theta_i] \\ -\sin Q[\theta_i] & \cos Q[\theta_i] \end{bmatrix}$$

is still orthogonal (here $Q[.]$ stands for a generic quantization operator).

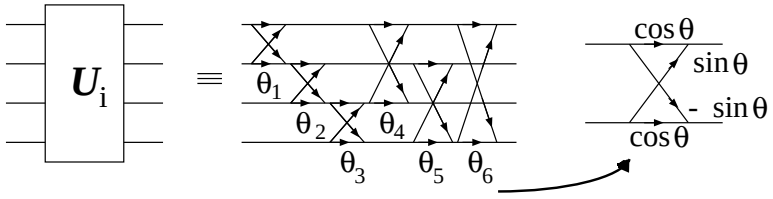

Figure 6: Parameterization of an orthogonal matrix.

Besides robustness, there are two important theoretical concepts associated with the lattice structure factorization: *completeness* and *minimality* [95]. The first is concerned with the generality of the solution, whereas the latter deals with the practicality of the solution.

- Completeness: the lattice should cover all possible solutions, i.e., any FB possessing all of the desired properties can always be realized by a certain set of lattice coefficients.
- Minimality: the FB implementation based on the lattice employs the least number of delay elements.

Every novel filter banks presented in this dissertation are obtained from a certain type of lattice structure. The aforementioned key concepts of completeness and minimality will be discussed and proven throughout.

2.4 Two-Channel Filter Banks

The simplest maximally-decimated filter bank shown in Figure 7 was introduced in the early 1980's. It has only two channels. These 2-channel PRFBs have been studied and characterized thoroughly with many different design methods based on spectral factorization [50], [74], [35], lattice structure [96], [53], [101], [97], time-domain optimization [51], quadratic-constrained least-squares (QCLS) optimization [55], Lagrange multiplier approaches [26], ect.

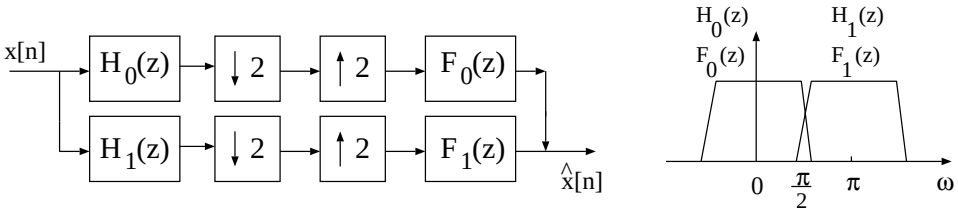

Figure 7: A typical two-channel filter bank.

The most popular and also the most successful design method in 2-channel PRFB design is *spectral factorization*. This elegant, conceptually simple design procedure can be explained in a few lines. By examining the transfer function of the filter bank, one can derive the relationship between the output $\hat{X}(z)$ and the input $X(z)$:

$$\begin{aligned}\hat{X}(z) \;=\; & \tfrac{1}{2}\,[\,F_0(z)\,H_0(z) + F_1(z)\,H_1(z)\,]\,X(z) \\ & + \tfrac{1}{2}\,[\,F_0(z)\,H_0(-z) + F_1(z)\,H_1(-z)\,]\,X(-z). \qquad (2.13)\end{aligned}$$

Perfect reconstruction with ℓ delays can be obtained with non-ideal filters if $\hat{X}(z) = z^{-\ell}X(z)$, leading to the following intuitive conditions:

$$F_0(z)\,H_0(-z) + F_1(z)\,H_1(-z) \;=\; 0 \quad \text{Aliasing Cancellation} \qquad (2.14)$$

$$F_0(z)\,H_0(z) + F_1(z)\,H_1(z) \;=\; 2z^{-\ell} \quad \text{Distortion Elimination.} \qquad (2.15)$$

The choices of $F_0(z) = H_1(-z)$ and $F_1(z) = -H_0(-z)$ cancel aliasing totally and reduce Eq.(2.15) to the design of a lowpass halfband filter $P_0(z) \stackrel{\triangle}{=} F_0(z)H_0(z)$ because the distortion elimination then simplifies to

$$P_0(z) - P_0(-z) \;=\; 2z^{-\ell}. \qquad (2.16)$$

Thus, the design of a 2-channel PR filter bank can be accomplished in two steps:

1. Design a lowpass filter $P_0(z)$ satisfying Eq.(2.16).
2. Factor $P_0(z)$ to obtain $H_0(z)$ and $F_0(z)$ (thus justified the name — spectral factorization). $H_1(z)$ and $F_1(z)$ are then chosen to cancel aliasing as described above.

LP filters can be obtained if the lowpass halfband filter $P_0(z)$ is chosen to have LP and spectral factorization is carried out appropriately [77].

2.5 Wavelets and Their Relation to Filter Banks

The wavelet transform is an octave-band representation of signals. The discrete dyadic wavelet transform can be obtained by iterating a 2-channel PR filter bank on its lowpass output as shown in Figure 8. For a true wavelet, one iterates on the lowpass output only, whereas for a wavelet-packet decomposition, one may iterate on any output. It is easy to see that as long as the original 2-channel system serving as the basic building block has perfect reconstruction, $x[n]$ can be recovered losslessly after a finite delay.

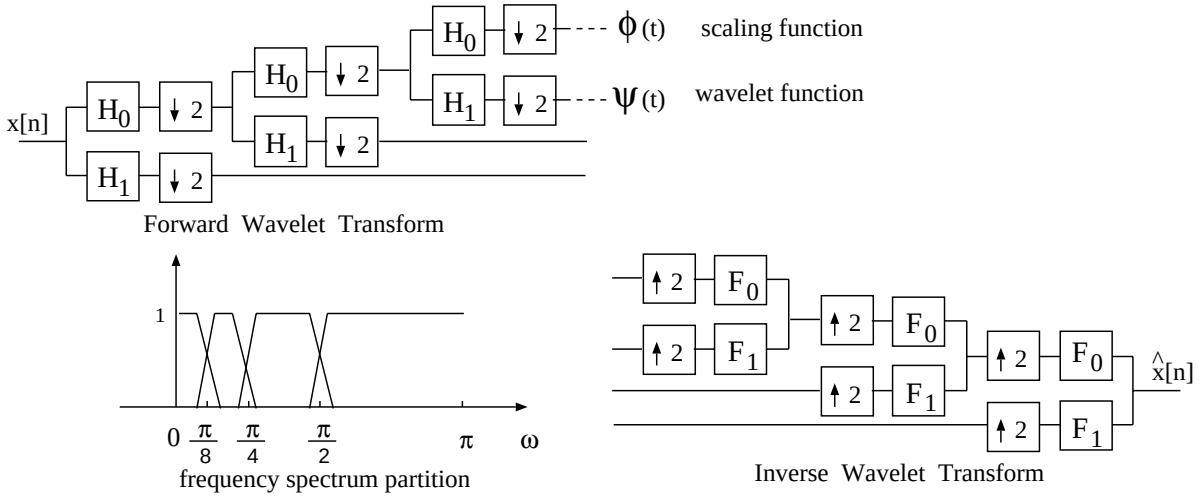

Figure 8: The discrete dyadic wavelet transform as iteration of a 2-channel filter bank.

The wavelet transform can also be thought of as a multiresolution decomposition of a signal into its coarse and detail components. In the case of images, the wavelet representation is well-matched to psychovisual models, and compression systems based on the wavelet transform thus far yield superior objective (mean-square error MSE, peak signal-to-noise ratio PSNR) and subjective (perceptual quality of the reconstructed images) performance comparing to other methods at medium and high compression ratios

[3], [73], [71], [72], [110], [112].

The "wavelet idea" of iterating a filter bank on its lowpass output has introduced many new considerations into the field of filter design. When applying the wavelet transform to lossy image coding, one is concerned with the smoothness of the iterated lowpass filter because any quantization noise will appear in the decompressed image as mainly linear combinations of the wavelet transform bases called *scaling function* $\phi(t)$ and *wavelet function* $\psi(t)$ (see Figure 8). If these basis functions are not smooth, then perceptually unacceptable artifacts will result. In fact, only around five iterations of the filtering-and-downsampling operation are needed to obtain the impulse responses resembling the infinite limits. A filter that is not designed with wavelet iteration in mind has its scaling and wavelet function quickly diverge upon a few iterations [77], [98]. Daubechies has shown that imposing N *vanishing wavelet moments*

$$\int t^k \psi(t) dt = 0, \quad 0 \leq k \leq N-1, \tag{2.17}$$

is a means of ensuring smoothness [13]. This condition is equivalent to imposing an N-th order zero ($N \leq L-1$) at $\omega = \pi$ on the lowpass filter:

$$\sum_n (-1)^n \, n^k \, h_0[n] \;=\; 0, \qquad k \in \mathcal{Z}, \qquad 0 \leq k \leq N-1. \tag{2.18}$$

In frequency domain, the wavelet transform simply mimics an M-band nonuniform partitioning of the frequency spectrum as depicted in Figure 8. This may lead to low energy compaction, especially when applying to signals with significant-energy narrow-bandwidth components at medium to high-frequency band. In this dissertation, we shall

demonstrate that M-channel uniform filter banks, when designed and utilized appropriately, prove to be much better alternatives – they consistently offers significantly higher energy compaction over state-of-the-art wavelets.

2.6 M-Channel Filter Banks

M-channel linear phase perfect reconstruction filter bank is our focus of study. There are numerous advantages and its potential is tremendous. Some existing M-channel LPPRFBs with fast algorithms already found success in image coding: the *discrete cosine transform* (DCT), the *lapped orthogonal transform* (LOT), and its generalized version GenLOT. M-channel filter banks can provide finer frequency spectrum partitioning without severe penalties in delay or filter performance. The considerable increase in the degrees of freedom allows M-channel filter banks to have much more flexibility in adapting to a particular class of signals or a particular application. For examples, M-channel filter banks can satisfy both linear phase and paraunitary simultaneously (the DCT and the LOT are two vivid examples) while 2-channel systems cannot (except the trivial Haar wavelet, $h_0[n] = \frac{1}{\sqrt{2}}[1 \;\; 1]$, $h_1[n] = \frac{1}{\sqrt{2}}[1 \;\; -1]$, as shown in [95], [98]). Finally, M-channel LPPRFBs can give rise to M-band linear phase orthogonal/biorthogonal wavelets as discussed in a later section.

2.6.1 Generalization Difficulties

Most works on linear phase FIR perfect reconstruction filter banks deal with two-channel systems and all solutions have been found. In the general M-channel case, there are still many open problems. The challenges are clearly visible once we investigate the general transfer function of a FB with arbitrarily large number of channels M. Define $W \stackrel{\Delta}{=} e^{-j2\pi/M}$, the reconstructed signal $\hat{X}(z)$ can be shown [95] to be

$$\hat{X}(z) = \frac{1}{M} \sum_{\ell=0}^{M-1} X(zW^{\ell}) \sum_{i=0}^{M-1} H_i(zW^{\ell}) F_i(z). \tag{2.19}$$

To make an analogy with the 2-channel case, Eq.(2.19) can be rewritten in terms of the distortion function $T(z)$ and the aliasing functions $A_\ell(z)$

$$\begin{aligned} \hat{X}(z) &= \frac{1}{M} X(z) \sum_{i=0}^{M-1} H_i(z) F_i(z) + \frac{1}{M} \sum_{\ell=1}^{M-1} X(zW^{\ell}) \sum_{i=0}^{M-1} H_i(zW^{\ell}) F_i(z) \\ &= T(z)X(z) + \sum_{\ell=1}^{M-1} A_\ell(z) X(zW^{\ell}), \end{aligned} \tag{2.20}$$

where

$$T(z) \stackrel{\Delta}{=} \frac{1}{M} \sum_{i=0}^{M-1} H_i(z) F_i(z), \tag{2.21}$$

and

$$A_\ell(z) \stackrel{\Delta}{=} \frac{1}{M} \sum_{i=0}^{M-1} H_i(zW^{\ell}) F_i(z), \qquad 1 \le \ell \le M-1. \tag{2.22}$$

Spectral factorization is not simple anymore. At this point in time, it is unclear to FB designers what the general choices of $H_i(z)$ and $F_i(z)$ are such that all aliasing terms $A_\ell(z)$ are annihilated and the distortion function $T(z)$ becomes a pure delay $z^{-\ell}$. Limiting the discussion to LPPRFB design, one has to rely upon other approaches such as lattice

structure parameterization [75], [62], time-domain optimization [51], [55], [70], and cosine modulation [41]. The most attractive amongst these is the lattice structure approach based on the factorization of the polyphase matrices $\mathbf{E}(z)$ and $\mathbf{R}(z)$. As aforementioned, the lattice structure offers fast implementation with a minimal number of delay elements, retains both LP and PR properties regardless of lattice coefficient quantization, and if it is general enough, covers a complete class of FB with certain desired properties. The DCT, the LOT, and the GenLOT are all fast-computable transforms based on the same lattice structure.

2.6.2 The Discrete Cosine Transform

From a statistical signal processing standpoint, the DCT is a robust approximation to the optimal discrete-time *Karhunen-Loève transform* (KLT) of a first-order Gauss-Markov process with a positive correlation coefficient ρ when $\rho \to 1$ [67]. The KLT is optimal in the energy compaction sense, i.e, among unitary transforms, the KLT packs signal energy into the fewest number of coefficients. However, the KLT is signal-dependent, therefore, computationally complex and expensive. DCT has proven to be a much better alternative in practice: it is signal independent, it has linear phase, real coefficients, and fast algorithms. The DCT coefficients $\mathbf{X}$ and the input image pixels $\mathbf{x}$ are related by the following equations:

$$X[m] = \alpha_m \sum_{n=0}^{M-1} x[n] \cos\left[\frac{\pi m}{2M}(2n+1)\right], \quad 0 \le m \le M-1, \tag{2.23}$$

with

$$\alpha_m = \begin{cases} \sqrt{1/M}, & m = 0 \\ \sqrt{2/M}, & 1 \leq m \leq M-1. \end{cases}$$

From a filter bank standpoint, DCT is the most basic M-channel LPPUFB. Its polyphase matrix has order 0 (independent of z) and can be written in the following form:

$$\mathbf{E}_0 = \frac{1}{\sqrt{2}} \begin{bmatrix} \mathbf{U}_0 & \mathbf{U}_0\mathbf{J} \\ \mathbf{V}_0\mathbf{J} & -\mathbf{V}_0 \end{bmatrix} = \frac{1}{\sqrt{2}} \begin{bmatrix} \mathbf{U}_0 & \mathbf{0} \\ \mathbf{0} & \mathbf{V}_0 \end{bmatrix} \begin{bmatrix} \mathbf{I} & \mathbf{J} \\ \mathbf{J} & -\mathbf{I} \end{bmatrix}. \tag{2.24}$$

It is clear that $\mathbf{E}_0$ is orthogonal if and only if $\mathbf{U}_0$ and $\mathbf{V}_0$ are orthogonal. For $\mathbf{E}_0$ to represent the DCT, we need two special orthogonal matrices. However, any choice of orthogonal $\mathbf{U}_0$ and $\mathbf{V}_0$ does result in an M-channel M-tap LPPUFB. The frequency and impulse response of the DCT filters are depicted in Figure 9. Note that all of the DCT's basis functions have linear phase; half of them are symmetric (ones associated with $\mathbf{U}_0$), the other half antisymmetric (ones associated with $\mathbf{V}_0$). We shall later prove that this is the necessary condition for all even-channel even-length LPPR systems. Besides being a real-coefficient transform with fast implementation, the DCT places heavy emphasis on the lowpass frequency spectrum. Therefore, for real-world image and video signals, it provides superior energy compaction over other classical transforms such as the FFT.

2.6.3 The Lapped Orthogonal Transform

Despite being the transform of choice in several international standards, the DCT still has its share of shortcomings. First of all, the DCT's basis functions are not overlapped: each pixel block is transformed independently. This often creates a loss of compression due

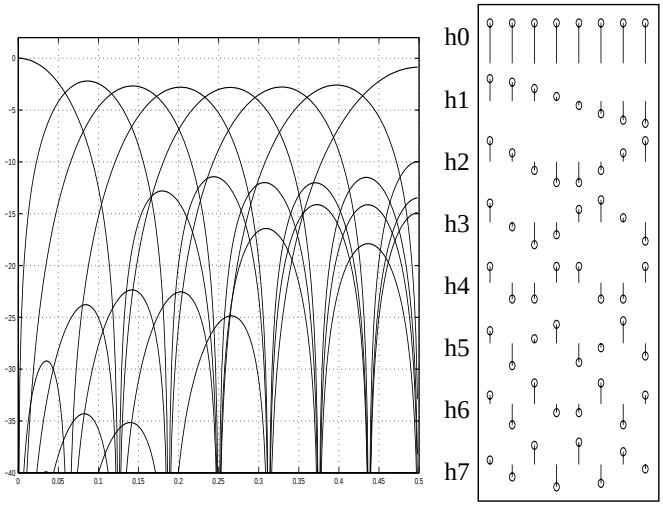

Figure 9: The DCT's frequency and impulse response.

to existing correlation across the blocks. More importantly, annoying blocking artifacts due to the discontinuities between block boundaries occurs at high compression ratios. These problems motivate the development of an overlapped blocking scheme, resulting in the lapped orthogonal transform (LOT) popularized by Malvar [45], [46], [47].

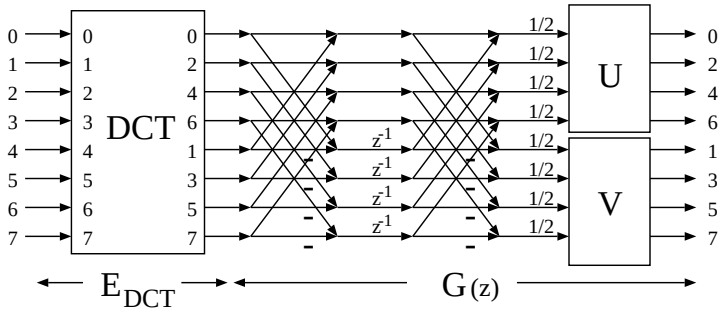

Figure 10: The lapped orthogonal transform.

From a FB perspective, the lapped orthogonal transform is simply an even-channel paraunitary filter bank with linear phase filters of length $L = 2M$. The LOT's polyphase

transfer matrix is

$$\begin{aligned}\mathbf{E}_{LOT}(z) &= \frac{1}{2}\begin{bmatrix}\mathbf{U} & \mathbf{0}\\ \mathbf{0} & \mathbf{V}\end{bmatrix}\begin{bmatrix}\mathbf{I} & \mathbf{I}\\ \mathbf{I} & -\mathbf{I}\end{bmatrix}\begin{bmatrix}\mathbf{I} & \mathbf{0}\\ \mathbf{0} & z^{-1}\mathbf{I}\end{bmatrix}\begin{bmatrix}\mathbf{I} & \mathbf{I}\\ \mathbf{I} & -\mathbf{I}\end{bmatrix}\mathbf{E}_{DCT} \qquad (2.25)\\ &\triangleq \mathbf{G}(z)\,\mathbf{E}_{DCT},\end{aligned}$$

where $\mathbf{E}_{DCT}$ denotes the DCT's polyphase matrix, and $\mathbf{U}$ and $\mathbf{V}$ are orthogonal matrices of size $\frac{M}{2}$. Hence, $\mathbf{U}$ and $\mathbf{V}$ can be parameterized by a set of rotation angles as in Eq.(2.12). As an overlapping block transform, rather than processing one block independently from the next, the LOT borrows pixels from a neighboring block to produce the outputs of the current block. Thanks to overlapping input windows, the LOT can elegantly solve the DCT's blocking problem: it partly smooths out the block boundaries. The frequency and impulse responses of the LOT optimized for image coding is shown in Figure 11. The reader can immediately notice significant improvements in the frequency responses of the LOT's filters comparing to the DCT's.

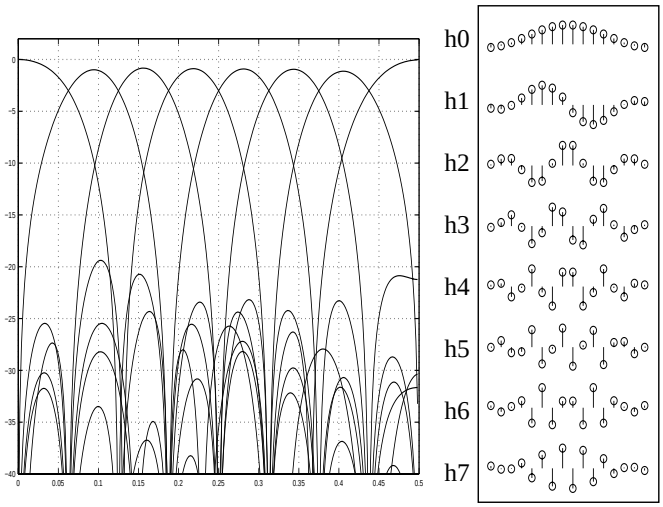

Figure 11: The LOT's frequency and impulse response.

2.6.4 The Generalized Lapped Orthogonal Transform

To further reduce blocking effect, longer data overlaps might be needed. Besides, there is no concrete evidence on why one has to restrict the block size to $2M$. This leads to the development of the generalized lapped orthogonal transform (GenLOT) [62]. From Eq.(2.25), one can quickly observe that the building block $\mathbf{G}(z)$ increases the filter length by M and all of its factors are orthogonal. A closer examination reveals that $\mathbf{G}(z)$ propagates the linear phase property of the filters as well. In other words, $\mathbf{G}(z)$ is a stage of the lattice structure approach introduced in Section 2.3.4 where the propagating properties are chosen to be linear phase and paraunitary. A cascade of many $\mathbf{G}_i(z)$ blocks, each has exactly the same form as in Eq.(2.25), yields a highly complex LPPU system that the original authors named GenLOT. The resulting polyphase matrix is given by

$$\mathbf{E}_{GenLOT}(z) \;=\; \mathbf{G}_{K-1}(z)\,\mathbf{G}_{K-2}(z)\,\cdots\,\mathbf{G}_1(z)\;\mathbf{E}_0, \tag{2.26}$$

where

$$\begin{aligned}\mathbf{G}_i(z) \;&=\; \tfrac{1}{2}\begin{bmatrix}\mathbf{U}_i & \mathbf{0}\\ \mathbf{0} & \mathbf{V}_i\end{bmatrix}\begin{bmatrix}\mathbf{I} & \mathbf{I}\\ \mathbf{I} & -\mathbf{I}\end{bmatrix}\begin{bmatrix}\mathbf{I} & \mathbf{0}\\ \mathbf{0} & z^{-1}\mathbf{I}\end{bmatrix}\begin{bmatrix}\mathbf{I} & \mathbf{I}\\ \mathbf{I} & -\mathbf{I}\end{bmatrix}\\ &\triangleq\; \tfrac{1}{2}\,\mathbf{\Phi}_i\,\mathbf{W}\,\mathbf{\Lambda}(z)\,\mathbf{W},\end{aligned} \tag{2.27}$$

and $\mathbf{E}_0$ has the form in Eq.(2.24). The complete GenLOT's lattice structure is presented in Figure 12 where the initial stage can be chosen to be DCT. Here, all degrees of freedom reside in the rotation angles of the $\frac{M}{2}\times\frac{M}{2}$ orthogonal matrices $\mathbf{U}_i$ and $\mathbf{V}_i$. More importantly, Eq.(2.26) has been proven to be a general factorization that covers all linear phase paraunitary filter banks with even M and filter length $L = KM$ [75],

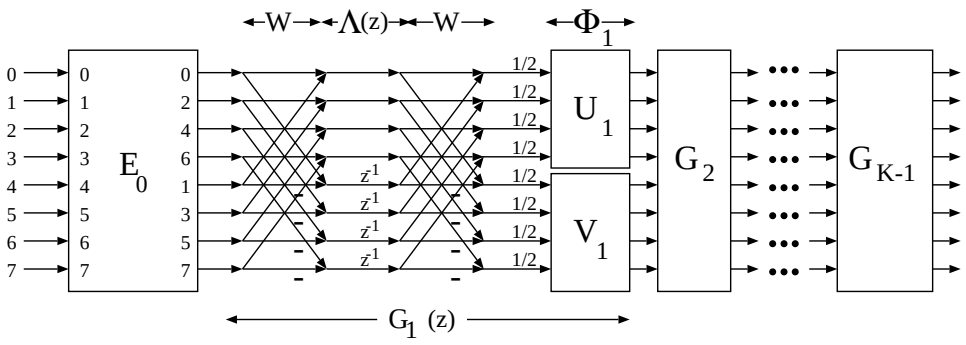

Figure 12: The generalized lapped orthogonal transform.

[62]. The class of GenLOTs, defined this way, allows us to view the DCT and the LOT as special cases – order-0 GenLOT ($K = 1$) and order-1 GenLOT ($K = 2$) respectively. An 8-channel 40-tap GenLOT design example is depicted in Figure 13. The frequency responses of the filters keep on improving at the expense of computational complexity and transform speed.

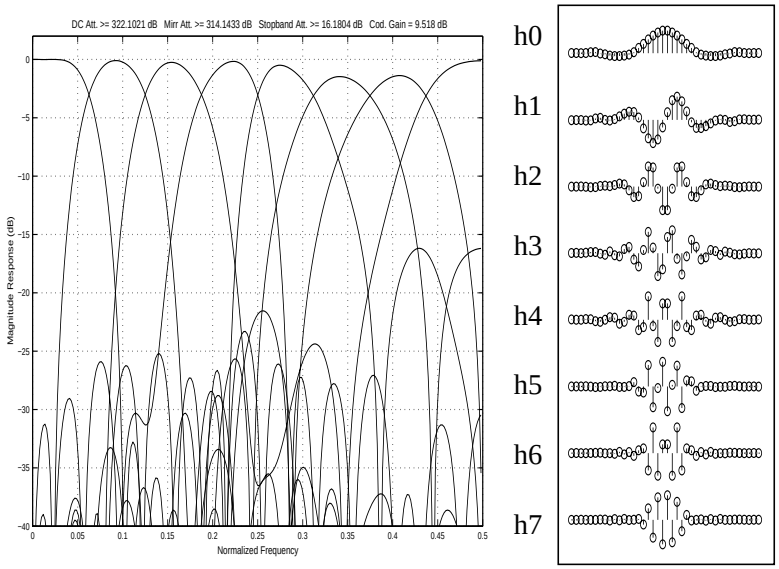

Figure 13: Frequency and impulse response of an 8-channel 40-tap GenLOT.

An M-channel L-tap LPPRFB ($L > M$) can be implemented as an $M \times L$ lapped

transform as demonstrated in Figure 14 [47]. In the 1D direct implementation, the input signal can be blocked into sequences of length L, overlapped by $(L - M)$ samples with adjacent sequences. The M columns of the transform coefficient matrix $\mathbf{P}$ hold the impulse responses of the analysis filters $h_i[n]$. The resulting M subbands $X_i[n]$ can then be quantized, coded, and transmitted to the decoder where the inverse transform is performed to reconstruct the original signal $x[n]$. In the 2D case illustrated in Figure 14(b), the transform coefficients can be evaluated separably: taking the 1D transform along the rows and then along the columns of an image block $\mathbf{x}_i$ of size $L \times L$. The corresponding block $\mathbf{X}_i$ of transform coefficients can be written as $\mathbf{X}_i = \mathbf{P}^T \mathbf{x}_i \mathbf{P}$, and it now has size $M \times M$. The next block of transform coefficients are computed by repeating the process with the spatial window moved away (either vertically or horizontally) by M samples, thus there is an $L \times (L - M)$ overlap in the spatial domain while there is no overlap in the frequency domain. To reiterate, lapped transform provides an elegant solution to the elimination of annoying blocking artifacts in traditional block-transform image coders at a reasonable cost – in both system memory requirement and transform speed. Lapped transform outperforms the popular non-overlapped DCT [67] on two counts: (i) from the analysis viewpoint, it takes into account inter-block correlation, hence, provides better energy compaction; (ii) from the synthesis viewpoint, its basis functions decay asymptotically to zero at the ends, reducing blocking discontinuities drastically.

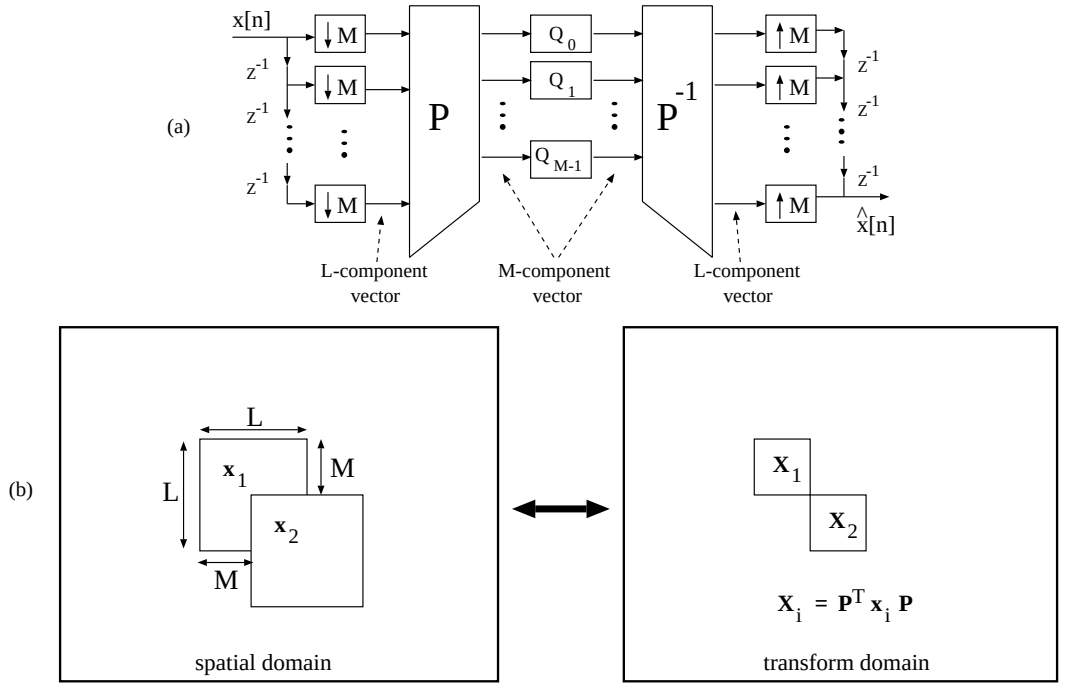

Figure 14: M-channel LPPRFB as lapped transform. (a) Direct implementation in 1D. (b) Illustration in 2D.

2.6.5 M-band Wavelets

Fingerprint, seismic, and many landscape images are usually not predominantly lowpass. Existing textures in these images require finer frequency partitioning than that of the dyadic wavelet transform. In other words, M-band wavelet representations offer higher performance in tiling the frequency plane. This can be advantageous both in terms of energy compaction [77] and in providing hierarchical, multiscale access to information. Applying to the compression of the above types of imagery, 3-band and 4-band wavelets have been shown to outperform 2-band wavelets, particularly with regard to absolute

error measures [76], [22]. Moreover, many applications also utilize tree-structured filter banks (also called *wavelet-packet*) decomposition to obtain a multiscale/nonuniform-frequency representation. For instance, instead of the traditional wavelet transform in Figure 15(a), the FBI's Wavelet Scalar Quantization standard opts for a cascade of 2-channel filter banks to achieve an approximation of 4-channel decomposition as in Figure 15(b).

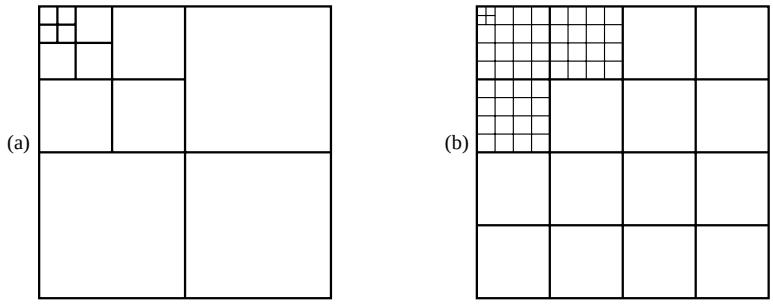

Figure 15: Frequency partitioning. (a) Dyadic wavelet transform. (b) FBI Wavelet Scalar Quantization standard.

Extending the main concept in 2-band wavelets, the N-vanishing wavelet moments condition in M-band can be stated as enforcing N-th order flatness of the lowpass filter at DC, i.e., N zeroes at $\omega = \pi$. It has been shown that GenLOTs with one and two vanishing moments exist and they outperformed the same-order GenLOTs optimized for stopband rejection in image coding experiments [75], [76]. Furthermore, the authors showed that vanishing moments can be enforced directly upon GenLOT's lattice coefficients. The novel FBs presented in this dissertation can generate various orthogonal/biorthogonal M-band wavelets.

2.7 Transform-Based Image Compression

One of the most successful applications of filter banks is in transform-based image compression. Two dominant techniques in the field – block-transform coding and subband coding – are actually the same in principle. A typical transform-based image coder as depicted in Figure 16 operates by *transforming* the data to remove redundancy, then *quantizing* the transform coefficients to reduce the bit rate, and finally *entropy coding* the quantizer's output to achieve even higher compression. Since our focus is at the transform stage, we shall only present very briefly the main concepts in the other two stages.

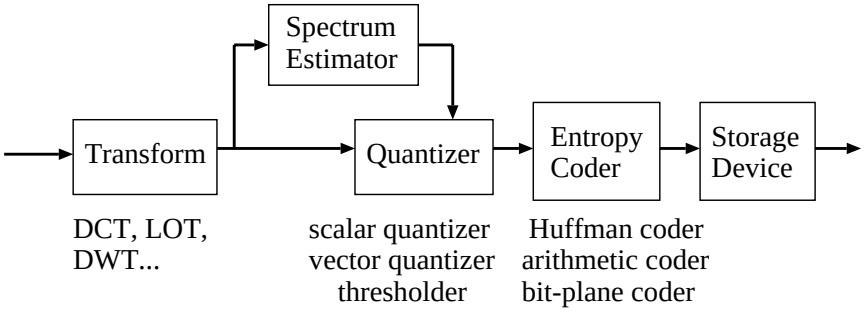

Figure 16: The general paradigm of transform-based coders.

2.7.1 Quantization and Entropy Coding

After the transformation, many transform coefficients are often large floating-point numbers, which may take a lot of bits to represent. In order to achieve compression, we have to map the coefficients into a discrete and finite alphabet. This mapping process is called *quantization*. In this dissertation, we shall utilize the simple scalar quantization scheme

as shown in Figure 17, where each transform coefficient c is independently mapped to its corresponding integer output qc. The scalar quantizer is very popular in practice because of its simplicity and inexpensive implementation. In many image coding schemes [58], [71], [72], [73], [110, 112], scalar quantizer has shown to be very effective. For high-frequency subbands, a scalar quantizer with variable dead-zone (typically the dead-zone range Q_{dz} is twice the stepsize Q_k elsewhere else as shown in Figure 17) can increase compression substantially without much loss of visual quality [17]. This is similar to a combination of thresholding and quantizing.

The *spectrum estimator* block in Figure 16 serve as a bit allocator for the quantizer. The bit allocator solves the classic problem: given a bit budget R, how can one distribute these bits to N transform coefficients so that a certain cost function D (usually the mean square error) is minimized? The bit distribution outputs of the bit allocator decide the quantizer stepsizes Q_k. Note that both thresholding and quantization introduce nonlinearity to the system and result in information loss. If a perfect-reconstruction filter bank is used at the transform stage, quantization/thresholding is the lone lossy step in the entire coding process. Hence, the error analysis can be significantly simplified.

After quantization, entropy coding is used to further compressed the signal. Entropy coding is a reversible process; therefore, the quantized coefficients can be recovered perfectly. The idea is to find another mapping such that the average number of bits per symbol is minimized. This is equivalent to assigning short codes to more probable symbols and reserving longer codes to less probable ones. Most popular entropy coding

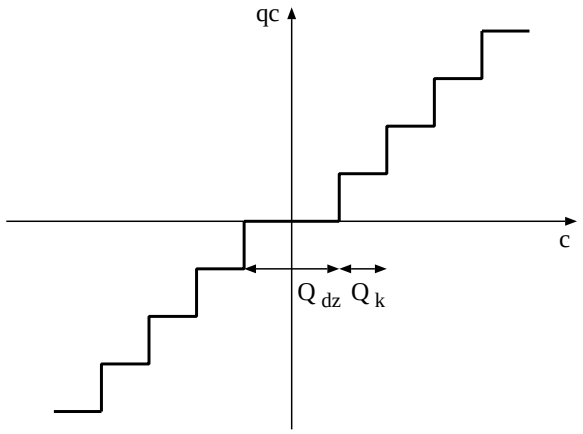

Figure 17: A scalar quantizer with dead-zone.

schemes are Huffman coding and arithmetic coding. Detailed discussions on bit allocation, quantization, and entropy coding can be found in [18], [32] and references therein. Simplistically speaking, the entropy coding step can be thought of as an efficient method to encode the positions and the values of the significant (non-zero) transform coefficients.

2.7.2 Transform Choice and Its Significance

As illustrated in Figure 16, there are many choices in each of the three basic stages in a generic transform-based image coder. However, the last two stages have a very strong correlation to the transformation chosen in the initial step. In other words, the actual transform selected plays a key role in the overall success of the image coder. The transform choice dictates the quantization and entropy coding strategies in the later steps.

The objective of any transform is to decorrelate the image pixels as much as possible by projecting the original image onto its set of basis functions. The resulting coefficients

of the transform serve as the means to store the image. In the analysis stage, the more carefully we choose the basis, the fewer coefficients we need to keep to represent the image accurately and the higher the coder's performance gets. In the synthesis stage, a good basis should result in perceptually-pleasant reconstructed images.

Current popular transforms used in the beginning stage of a transform-based image coder are the DCT, the LT, and the wavelet transform. The JPEG image compression standard [58] is based on the 8×8 DCT. In this algorithm, the input image is broken into 8×8 blocks, each of which is then transformed via a tensor product of two 8-point DCT's as demonstrated in Figure 14 ($M = 8; L = 8$). The transform coefficients from each image block are scalar-quantized, arranged in a zig-zag fashion, and then Huffman coded. So, JPEG chooses to encode coefficients from the same spatial locality together. The JPEG algorithm yields good results for compression ratios around 10:1 and below (on typical 8-bit gray-scale images), but at higher compression ratios the underlying block nature of the transform begins to show through the compressed image. At high compression ratios (24:1 and up), most of the bit budget is spent on the DC (lowest frequency) coefficients, and the input image has been approximated by a set of 8×8 blocks – this is the common *blocking* artifacts.

Subband coding has recently emerged as the leading candidate for standardization in future image compression systems thanks to the development of the wavelet transform. Wavelet representations with implicit overlapping and variable-length basis functions produces smoother and more perceptually pleasant reconstructed images. Early approaches in subband filter design are more concerned with high stopband attenuation

and perfect frequency selectivity. The idea originates from well-known results in information theory: filters with these characteristics produce perfectly decorrelated subband signals which can be encoded independently (coefficients at the same frequency locality are coded together). The performance of such coders approaches optimal coding gain when the number of subbands approaches infinity [32]. However, these approaches result in filters with long impulse responses. At low bit rates, huge quantization noise can be spread out to neighboring smooth image regions, causing *ringing* artifacts.

Latest developments in wavelets and their application in subband coding provoke a different philosophy. Instead of aiming for exceptional decorrelation between subbands, wavelet coders look for other filter properties that still maintain a reasonable level of perceptual quality at low bit rates, and take advantage of the correlation across the subbands by a judicious combination of quantizer and entropy coder. The embedded zerotree coder [73] and its improved variations [71], [72], [110] exploit the redundancy across the scales in the dyadic wavelet transform. The innovation here is to predict the *insignificance* of the transform coefficients (the occurrence of zeros) rather than attempt to predict their *significance* (the occurrence of nonzero values). The zerotree coder also provides a very efficient framework for bit-plane progressive image transmission: ordering the coefficients by magnitude, transmitting the most significant bits first, and repeating the transmission process with lower bit planes until the bit budget is full. State-of-the-art wavelet-based embedded coders yield some of the highest performances in image compression up to date. However, one major drawback from the wavelet basis is the *blurring* artifacts due

to the heavy quantization of image details in high-frequency subbands. In this dissertation, we shall show that the same embedded idea can be applied to encode lapped transform coefficients as well. In fact, if designed and utilized appropriately, uniform-band lapped transforms consistently outperform wavelets on all test images at all bit rates. Our LT-based coders provide a better trade-off in the suppression of blocking, ringing, and blurring artifacts.

Chapter 3

General Theory

3.1 Introduction

This chapter investigates the general theory of M-channel FIR linear phase perfect reconstruction filter banks with analysis and synthesis filters of lengths $L_i = K_i M + \beta$, where $\beta \in \mathcal{Z}, 0 \leq \beta < M$, and $K_i \in \mathcal{Z}^+$. For this large subclass of systems, we first investigate the restriction that the linear phase property imposes on the FB polyphase matrices. The symmetry property of the polyphase matrices leads to various necessary conditions for the existence of linear phase perfect reconstruction filter banks. These fundamental results can be very helpful in restricting the search space of possible solutions and they help greatly in the development of general lattice structures in later chapters.

Note that the most general FIR LP system has filter lengths $L_i = K_i M + \beta_i$. However, it has been proven that all β_i have to be the same if one needs to use symmetric extension in the filter bank's implementation [8].

3.2 Polyphase Matrices of a LPFB

Consider an M-channel filter bank with a set of linear phase analysis filters $H_i(z)$, $i \in \mathcal{Z}$, $0 \leq i \leq M-1$. Let the length of the i-th filter $H_i(z)$ be $L_i = K_i M + \beta$, where $\beta, K_i \in Z$, and $0 \leq \beta < M$, $K_i \geq 1$. Since K_i is arbitrary, the filter length L_i is also arbitrary. The same β is required for all $H_i(z)$ because of the practical usage of symmetric extension in implementation as previously mentioned [8]. The linear phase property of the filters dictates certain symmetry relationships between the components of the FB polyphase matrices $\mathbf{E}(z)$ and $\mathbf{R}(z)$.

First, define $\mathbf{D}$ as a diagonal matrix whose entry is $+1$ when the corresponding filter is symmetric and -1 when the corresponding filter is antisymmetric. Define $\hat{\mathbf{Z}}(z)$ as the diagonal matrix

$$\hat{\mathbf{Z}}(z) \triangleq diag\left[\ z^{-(K_0-1)}\ \ z^{-(K_1-1)}\ \ \ldots\ z^{-(K_{M-1}-1)}\ \right], \tag{3.1}$$

and

$$\hat{\mathbf{J}}(z) \triangleq \begin{bmatrix} z^{-1}\mathbf{J}_\beta & \mathbf{0}_{\beta\times(M-\beta)} \\ \mathbf{0}_{(M-\beta)\times\beta} & \mathbf{J}_{M-\beta} \end{bmatrix}. \tag{3.2}$$

We can derive the following symmetry property of the polyphase matrices $\mathbf{E}(z)$ and $\mathbf{R}(z)$.

Theorem 3.6 *All analysis filters of lengths $L_i = K_i M + \beta$ in an M-channel FB has linear phase if and only if the associated polyphase matrix $\mathbf{E}(z)$ satisfies the following condition*

$$\mathbf{E}(z) \ = \ \mathbf{D}\ \hat{\mathbf{Z}}(z)\ \mathbf{E}(z^{-1})\ \hat{\mathbf{J}}(z). \tag{3.3}$$

Analogously, all synthesis filters of lengths $L_i = K_i M + \beta$ in an M-channel FB has linear phase if and only if the associated polyphase matrix $\mathbf{R}(z)$ has the following form

$$\mathbf{R}(z) \;=\; \hat{\mathbf{J}}(z)\,\mathbf{R}(z^{-1})\,\hat{\mathbf{Z}}(z)\,\mathbf{D}. \tag{3.4}$$

Proof.

In order to see why the form of $\mathbf{E}(z)$ in Eq.(3.3) is equivalent to the LP property of the filters, let us examine the impulse response of an LP filter $h_i[n]$ with length $L = K_i M + \beta$ and the corresponding polyphase components $E_{i0}(z)$, $E_{i1}(z)$, ... , $E_{i(M-1)}(z)$. Since the filter length is a multiple of M plus β, the first β polyphases have one more coefficient than the rest:

$$\begin{cases} E_{i\ell}(z) &= \displaystyle\sum_{k=0}^{K_i} h_i[kM+\ell]\, z^{-k}, \quad \text{for } 0 \;\le\; \ell \;\le\; \beta - 1 \\ E_{i\ell}(z) &= \displaystyle\sum_{k=0}^{K_i - 1} h_i[kM+\ell]\, z^{-k}, \quad \text{for } \beta \;\le\; \ell \;\le\; M-1. \end{cases} \tag{3.5}$$

A careful examination of $E_{i0}(z)$ and $E_{i(\beta-1)}(z)$ shows that they are time-reversed versions (denoted by the $\tilde{}$ notation) of each other:

$$\begin{aligned} \widetilde{E}_{i(\beta-1)}(z) &\triangleq z^{-K_i}\, E_{i(\beta-1)}(z^{-1}) \\ &= h_i[K_iM + \beta - 1] \;+\; h_i[K_iM + \beta - 1 - M]\, z^{-1} \;+\; \cdots \;+\; h_i[\beta-1]\, z^{-K} \\ &= \pm \sum_{k=0}^{K_i} h_i[kM]\, z^{-k} \;=\; \pm\, E_{i0}(z), \end{aligned} \tag{3.6}$$

where we have used the fact that $h_i[n]$ has LP: $h_i(n) = \pm h_i[K_iM + \beta - 1 - n]$. Similarly, $\widetilde{E}_{i(M-1)}(z) \;=\; \pm\, E_{i\beta}(z)$ where the $\pm$ sign is used to denote two separate cases: $h_i[n]$ is either symmetric or antisymmetric. This linear phase property in Eq.(3.6) can be

generalized to the rest of the polyphase components to obtain the following relationships:

$$\begin{cases} E_{i\ell}(z) &= \pm\, \widetilde{E}_{i(\beta-1-\ell)}(z), \qquad \text{for } 0 \le \ell \le \beta-1 \\ E_{i\ell}(z) &= \pm\, \widetilde{E}_{i(M+\beta-1-\ell)}(z), \quad \text{for } \beta \le \ell \le M-1. \end{cases} \tag{3.7}$$

Using Eq.(3.7), one can easily verify the LP-equivalent property of $\mathbf{E}(z)$ in Eq.(3.3), both necessarily and sufficiently.

A similar proof can be constructed for the case of the synthesis bank. The lone difference is the transpositional relationship between $\mathbf{E}(z)$ and $\mathbf{R}(z)$: the synthesis polyphase matrix $\mathbf{R}(z)$ stores the synthesis filters in its columns instead of rows. □

Example. Suppose there exists a 4-channel LPFB with 2 10-tap symmetric filters ($h_0[n]$ and $h_1[n]$) and 2 6-tap antisymmetric analysis filters ($h_2[n]$ and $h_3[n]$). In this example, $\beta = 2$. The LP property of the filters means: $h_0[n] = h_0[9-n]$, $h_1[n] = h_1[9-n]$, $h_2[n] = -h_2[5-n]$, and $h_3[n] = -h_3[5-n]$. Thus, the polyphase matrix $\mathbf{E}(z)$ of this system has a highly symmetrical form – the polyphase components $E_{i0}(z)$ and $E_{i1}(z)$ are time-reversedly related, and so are $E_{i2}(z)$ and $E_{i3}(z)$:

$$\mathbf{E}(z) = \begin{bmatrix} h_0[0] + h_0[4]z^{-1} + h_0[1]z^{-2} & h_0[1] + h_0[4]z^{-1} + h_0[0]z^{-2} & \cdots \\ h_1[0] + h_1[4]z^{-1} + h_1[1]z^{-2} & h_1[1] + h_1[4]z^{-1} + h_1[0]z^{-2} & \cdots \\ h_2[0] - h_2[1]z^{-1} & h_2[1] - h_2[0]z^{-1} & \cdots \\ h_3[0] - h_3[1]z^{-1} & h_3[1] - h_3[0]z^{-1} & \cdots \end{bmatrix}$$

$$\begin{bmatrix} \cdots & h_0[2] + h_0[3]z^{-1} & h_0[3] + h_0[2]z^{-1} \\ \cdots & h_1[2] + h_1[3]z^{-1} & h_1[3] + h_1[2]z^{-1} \\ \cdots & h_2[2] & -h_2[2] \\ \cdots & h_3[2] & -h_3[2] \end{bmatrix}.$$

Pre-multiplying $\mathbf{E}(z^{-1})$ by

$$\mathbf{D} = \begin{bmatrix} 1 & 0 & 0 & 0 \\ 0 & 1 & 0 & 0 \\ 0 & 0 & -1 & 0 \\ 0 & 0 & 0 & -1 \end{bmatrix},$$

post-multiplying by

$$\hat{\mathbf{J}}(z) = \begin{bmatrix} 0 & z^{-1} & 0 & 0 \\ z^{-1} & 0 & 0 & 0 \\ 0 & 0 & 0 & 1 \\ 0 & 0 & 1 & 0 \end{bmatrix},$$

and then pre-multiplying the resulting product by

$$\hat{\mathbf{Z}}(z) = \begin{bmatrix} z^{-1} & 0 & 0 & 0 \\ 0 & z^{-1} & 0 & 0 \\ 0 & 0 & 1 & 0 \\ 0 & 0 & 0 & 1 \end{bmatrix}$$

give us back $\mathbf{E}(z)$ as stated in Theorem 3.6.

Remarks. The matrix $\hat{\mathbf{Z}}(z)$ takes care of the arbitrary lengths of the filters (with different K_i), while $\hat{\mathbf{J}}(z)$ accounts for the fact that the first β polyphase components of

each filter are one order higher than the rest. Secondly, the trace of $\mathbf{D}$ reveals the number of symmetric and antisymmetric filters in the system. Here, the trace is zero, i.e., half of the filters are symmetric, the other half antisymmetric. Thirdly, we have assumed that the impulse response of each causal filter always starts at index 0. In our convention, if for some reasons that a filter is delayed (shifted) by n samples, the n padded zeros are counted as active filter coefficients. Hence, the effective length of the LP filter is now considered to be $L + 2n$ where another n zeros have been padded onto the filter tail to retain symmetry. Finally, Eq.(3.3) and Eq.(3.4) are extensions of the linear phase constraint proposed in [101] and later used extensively in [75] where all analysis and synthesis filters have the same length $L = KM$. In that case, we have the following corollary.

Corollary 3.7 *In the case where all analysis and synthesis filters having the same length $L = KM$, the linear phase property of the filters is equivalent to*

$$\mathbf{E}(z) = z^{-(K-1)}\, \mathbf{D}\, \mathbf{E}(z^{-1})\, \mathbf{J} \tag{3.8}$$

$$\mathbf{R}(z) = z^{-(K-1)}\, \mathbf{J}\, \mathbf{R}(z^{-1})\, \mathbf{D}. \tag{3.9}$$

Proof.

The proof is rather trivial. When $K_i = K$, the $\hat{\mathbf{Z}}(z)$ matrix in Eq.(3.1) reduces to $z^{-(K-1)}\mathbf{I}$. Also, since $\beta = 0$, the $\hat{\mathbf{J}}(z)$ in Eq.(3.2) becomes the z-independent $\mathbf{J}$. Replacing $\hat{\mathbf{Z}}(z)$ and $\hat{\mathbf{J}}(z)$ in Eq.(3.3) and Eq.(3.4) by the appropriate simplification immediately yields the results in Corollary 3.7. □

3.3 Permissible Conditions

Using the symmetrical form of $\mathbf{E}(z)$ from Theorem 3.6, the trace and the determinant of $\mathbf{D}$ can be manipulated to obtain the permissible lengths and symmetry polarity for LPPRFB of arbitrary channels and arbitrary lengths.

Theorem 3.8 *In an M-channel LPPRFB with filter lengths $L_i = K_i M + \beta$,*

- *if M is even and β is even, there are $\frac{M}{2}$ symmetric and $\frac{M}{2}$ antisymmetric filters.*
- *if M is even and β is odd, there are $(\frac{M}{2}+1)$ symmetric and $(\frac{M}{2}-1)$ antisymmetric filters.*
- *if M is odd, there are $(\frac{M+1}{2})$ symmetric and $(\frac{M-1}{2})$ antisymmetric filters.*

Remarks. This theorem provides the most general constraints for linear phase perfect reconstruction filter banks; it holds for both biorthogonal and paraunitary systems. In other words, Theorem 3.8 requires an LPPRFB (with filters satisfying the stated length condition) to have the same number of symmetric and antisymmetric filters when the number of channel M is even and all the filters have even length. If M is even, but all the filters are now odd-length, then the system must have two more symmetric filters. For odd-channel systems, the number of symmetric filters always exceeds the number of antisymmetric filters by one. This is a useful and powerful result. It allows the FB designers to narrow down the search for possible solutions. It expands our knowledge and understanding of LPPRFB by explaining partially why only certain solutions exist. It also lays a foundation on which complete and minimal lattice structures are developed in

the later chapters of the dissertation. Before presenting the formal proof of the theorem, let us first introduce a couple of useful lemmas that appear persistently throughout.

Lemma 3.9

$$tr(\hat{\mathbf{J}}(z)) \;=\; \begin{cases} 0 & \textit{if } M \textit{ is even and } \beta \textit{ is even} \\ 1+z^{-1} & \textit{if } M \textit{ is even and } \beta \textit{ is odd} \\ 1 & \textit{if } M \textit{ is odd and } \beta \textit{ is even} \\ z^{-1} & \textit{if } M \textit{ is odd and } \beta \textit{ is odd.} \end{cases} \tag{3.10}$$

Proof.

From Eq.(3.2), we have

$$tr(\hat{\mathbf{J}}(z)) \;=\; tr\left(\begin{bmatrix} z^{-1}\,\mathbf{J}_{\beta} & \mathbf{0}_{\beta\times(M-\beta)} \\ \mathbf{0}_{(M-\beta)\times\beta} & \mathbf{J}_{M-\beta} \end{bmatrix} \right).$$

There are four cases to consider. When M is even and β is even, $(M-\beta)$ is also even, and all of the diagonal elements of the matrix $\hat{\mathbf{J}}(z)$ are zeros. Thus, its trace is 0. When M is even and β is odd, $(M-\beta)$ is odd. Hence, we now pick up two non-zero elements on the diagonal of $\hat{\mathbf{J}}(z)$: 1 and z^{-1}. When M is odd, β and $(M-\beta)$ cannot be both odd or both even. Therefore, in this case, only one non-zero element can be picked up: either 1 or z^{-1} depending on whether β is even or odd, respectively. □

Lemma 3.10

$$|\hat{\mathbf{J}}(z)| \;=\; \left| \begin{bmatrix} z^{-1}\mathbf{J}_{\beta} & \mathbf{0}_{\beta\times(M-\beta)} \\ \mathbf{0}_{(M-\beta)\times\beta} & \mathbf{J}_{M-\beta} \end{bmatrix} \right| \;=\; \begin{cases} (-1)^{(\frac{M}{2}+\beta)}\, z^{-\beta} & \textit{if } M \textit{ is even} \\ (-1)^{(\frac{M-1}{2})}\, z^{-\beta} & \textit{if } M \textit{ is odd.} \end{cases} \tag{3.11}$$

Proof.

Notice that $\hat{\mathbf{J}}(z)$ is a square block-diagonal matrix, thus its determinant can be factorized as follows [16]:

$$|\hat{\mathbf{J}}(z)| \;=\; |z^{-1}\mathbf{J}_\beta|\,|\mathbf{J}_{M-\beta}| \;=\; z^{-\beta}\,|\mathbf{J}_\beta|\,|\mathbf{J}_{M-\beta}|.$$

With the factorization above, coupling with the facts that $|\mathbf{J}_{4m}| = |\mathbf{J}_{4m+1}| = 1$ and $|\mathbf{J}_{4m+2}| = |\mathbf{J}_{4m+3}| = -1$, $m \in \mathcal{Z}^+$, one can verify that Lemma 3.10 holds by considering four possible cases: $M = 4m, M = 4m+1, M = 4m+2$, and $M = 4m+3$. □

With the help of Lemma 3.9, proving Theorem 3.8 is a trivial task.

Proof of Theorem 3.8.

Since $\mathbf{E}(z)$ is invertible, and $\mathbf{D}^{-1} = \mathbf{D}$, Eq.(3.3) can be rewritten as follows:

$$\mathbf{D} \;=\; \hat{\mathbf{Z}}(z)\,\mathbf{E}(z^{-1})\,\hat{\mathbf{J}}(z)\,\mathbf{E}^{-1}(z). \tag{3.12}$$

Taking the trace of both sides, and using the fact that $tr(\mathbf{A}\,\mathbf{B}) = tr(\mathbf{B}\,\mathbf{A})$, one can obtain

$$tr(\mathbf{D}) \;=\; tr(\hat{\mathbf{Z}}(z)\,\mathbf{E}(z^{-1})\,\hat{\mathbf{J}}(z)\,\mathbf{E}^{-1}(z)) \;=\; tr(\mathbf{E}^{-1}(z)\,\hat{\mathbf{Z}}(z)\,\mathbf{E}(z^{-1})\,\hat{\mathbf{J}}(z)).$$

$Tr(\mathbf{D})$ is a constant, therefore, its value can be obtained by evaluating the right-hand side of the above equation at a specific value of the variable z. Since

$$\mathbf{E}(z^{-1})\,\hat{\mathbf{Z}}(z)\,\mathbf{E}^{-1}(z)|_{z=1} \;=\; \mathbf{E}(1)\,\mathbf{I}\,\mathbf{E}^{-1}(1) \;=\; \mathbf{I},$$

we have

$$tr(\mathbf{D}) \;=\; tr(\mathbf{E}^{-1}(z)\,\hat{\mathbf{Z}}(z)\,\mathbf{E}(z^{-1})\,\hat{\mathbf{J}}(z))\,|_{z=1} \;=\; tr(\hat{\mathbf{J}}(z))\,|_{z=1}. \tag{3.13}$$

Again, there are four possible cases. Recall that $\mathbf{D}$ is a diagonal matrix whose entry is $+1$ when the corresponding filter is symmetric and -1 when the corresponding filter is antisymmetric. When both M and β are even, Lemma 3.9 yields $tr(\mathbf{D}) = tr(\hat{\mathbf{J}}(z))\,|_{z=1} = 0$. Hence, the system must have an equal number of symmetric and antisymmetric filters to satisfy the linear phase and perfect reconstruction properties. When M is even and β is odd, $tr(\mathbf{D}) = (1 + z^{-1})\,|_{z=1} = 2$. Thus, we need two more symmetric filters in this case. The results from the remaining two odd-M cases can be trivially obtained in a similar manner. One can also choose to evaluate Eq.(3.13) at other values of z, say $z = -1$, and arrives at the same result. The proof becomes slightly more tedious. We leave it as an exercise for interested readers. □

In time-domain FB designs [51], [70], the symmetry polarity as stated in Theorem 3.8 is not a narrow enough requirement. The filter lengths are also crucial in achieving perfect reconstruction. If the designer chooses the wrong filter lengths, his optimization routine will not converge. Therefore, besides the necessary LPPR condition for the symmetry polarity, we also have to obtain the necessary restriction on the filter lengths as well (more precisely speaking, the necessary condition for the sum of their lengths).

Theorem 3.11 *In an M-channel LPPRFB with filter lengths $L_i = K_i M + \beta$,*

- *if M is even and β is even, $\sum_{i=0}^{M-1} K_i$ is even.*
- *if M is even and β is odd, $\sum_{i=0}^{M-1} K_i$ is odd.*
- *if M is odd and β is even, $\sum_{i=0}^{M-1} K_i$ is odd.*

- *if M is odd and β is odd, $\sum_{i=0}^{M-1} K_i$ is even.*

Proof.

Case 1: M is even and β is even.

The determinant of $\mathbf{D}$ can also be manipulated in the same manner as its trace to prove Theorem 3.11. Taking the determinant of both sides of Eq.(3.3) gives

$$|\mathbf{E}(z)| \;=\; |\mathbf{D}|\,|\hat{\mathbf{Z}}(z)|\,|\mathbf{E}(z^{-1})|\,|\hat{\mathbf{J}}(z)| \;=\; |\mathbf{D}|\,z^{-(\sum_{i=0}^{M-1}K_i)+M}\,|\mathbf{E}(z^{-1})|\,|\hat{\mathbf{J}}(z)|, \qquad (3.14)$$

where we have used the fact that the determinant of the product of two square matrices is equal to the product of the determinants of the factors [16]. Evaluating Eq.(3.14) at $z = 1$ gives $|\mathbf{D}|\,|\hat{\mathbf{J}}(1)| \;=\; 1$. Using the result from Lemma 3.10 to substitute for $|\hat{\mathbf{J}}(1)|$, one can see that, for even M and even β, this relation must hold:

$$|\mathbf{D}|\,|\hat{\mathbf{J}}(1)| \;=|\mathbf{D}|\,(-1)^{(\frac{M}{2}+\beta)} \;=\; |\mathbf{D}|\,(-1)^{(\frac{M}{2})} \;=\; 1.$$

This is consistent with the derivation from the trace previously. When $\frac{M}{2}$ is odd, $|\mathbf{D}|$ must be -1, i.e., there are an odd number of antisymmetric filters. On the other hand, when $\frac{M}{2}$ is even, $|\mathbf{D}|$ must be $+1$ because now there are an even number of antisymmetric filters.

So, by evaluating the determinant of $\mathbf{D}$ at $z = 1$, nothing is gained, i.e., one can only confirm the validity of result from Theorem 3.8. However, evaluating Eq.(3.14) at $z = -1$ gives

$$(-1)^{-(\sum_{i=0}^{M-1}K_i)+M}\,|\mathbf{D}|\,|\hat{\mathbf{J}}(-1)| \;=\; (-1)^{-(\sum_{i=0}^{M-1}K_i)}\,|\mathbf{D}|\,(-1)^{(\frac{M}{2}+\beta)}\,(-1)^{-\beta} \;=\; 1, \quad (3.15)$$

where the result from Lemma 3.10 is used to substitute for $|\hat{\mathbf{J}}(-1)|$. Note that this is true for all cases with even M. Since β is also even in this case, Eq.(3.15) simplifies to

$$(-1)^{-(\sum_{i=0}^{M-1} K_i)} \, |\mathbf{D}| \, (-1)^{\frac{M}{2}} \;=\; 1.$$

For even M, there are two cases to consider: if $M = 4m$, then $\frac{M}{2}$ is even, and $|\mathbf{D}| = 1$, so the sum $\sum_{i=0}^{M-1} K_i$ has to be even; similarly, if $M = 4m+2$, then $\frac{M}{2}$ is odd, $|\mathbf{D}| = -1$, and $\sum_{i=0}^{M-1} K_i$ must be even. □

Case 2: M is even and β is odd.

At $z = 1$, following the same derivation as in *Case 1*, we get

$$|\mathbf{D}| \, |\hat{\mathbf{J}}(1)| \;= |\mathbf{D}| \, (-1)^{(\frac{M}{2}+\beta)} \;=\; 1,$$

from which the reader can easily verify that $|\mathbf{D}|$ is consistent with result in Theorem 3.8. At $z = -1$, with β odd, Eq.(3.15) simplifies to

$$(-1)^{-(\sum_{i=0}^{M-1} K_i)} \, |\mathbf{D}| \, (-1)^{(\frac{M}{2}+\beta)} \;=\; -1.$$

Again there are two cases to consider: $M = 4m$ and $M = 4m+2$. When $M = 4m$, $\frac{M}{2}$ is even, and the above equation reduces to

$$(-1)^{-(\sum_{i=0}^{M-1} K_i)} \, |\mathbf{D}| \;=\; 1.$$

Also, for $M = 4m$, Theorem 3.8 requires an odd number of antisymmetric filters, implying $|\mathbf{D}| = -1$. Hence, $\sum_{i=0}^{M-1} K_i$ must be odd.

When $M = 4m+2$, $\frac{M}{2}$ is odd, so

$$(-1)^{-(\sum_{i=0}^{M-1} K_i)} \, |\mathbf{D}| \;=\; -1.$$

For $M = 4m + 2$, Theorem 3.8 establishes that there must be an even number of antisymmetric filters (either $2m$ or $2m + 2$), implying $|\mathbf{D}| = 1$. Then, $\sum_{i=0}^{M-1} K_i$ has to be odd. □

Case 3: M is odd and β is even.

Evaluating Eq.(3.14) at $z = -1$, and substituting the result from Lemma 3.10 for $|\hat{\mathbf{J}}(-1)|$, we get

$$(-1)^{-(\sum_{i=0}^{M-1} K_i)+M} |\mathbf{D}| \, |\hat{\mathbf{J}}(-1)| \;=\; (-1)^{-(\sum_{i=0}^{M-1} K_i)+M} |\mathbf{D}| \, (-1)^{(\frac{M-1}{2})} \, (-1)^{-\beta} \;=\; 1, \quad (3.16)$$

Since β is even, Eq.(3.16) simplifies to

$$(-1)^{-(\sum_{i=0}^{M-1} K_i)+M} \, |\mathbf{D}| \, (-1)^{(\frac{M-1}{2})} \;=\; 1. \quad (3.17)$$

For $M = 4m+1$, $\frac{M-1}{2}$ is even. So, $(-1)^{(\frac{M-1}{2})} = 1$. Moreover, the number of antisymmetric filters is also even, implying $|\mathbf{D}| = 1$. Therefore, $(\sum_{i=0}^{M-1} K_i - M)$ must be even for Eq.(3.17) to hold. It follows that $\sum_{i=0}^{M-1} K_i$ has to be odd. For $M = 4m + 3$, $\frac{M-1}{2}$ is odd. Therefore, $|\mathbf{D}| = -1$, $(-1)^{(\frac{M-1}{2})} = -1$, and

$$(-1)^{-(\sum_{i=0}^{M-1} K_i)+M} \, |\mathbf{D}| \, (-1)^{(\frac{M-1}{2})} \;=\; (-1)^{-(\sum_{i=0}^{M-1} K_i)+M} \;=\; 1.$$

This implies that $(\sum_{i=0}^{M-1} K_i - M)$ must be even, and $\sum_{i=0}^{M-1} K_i$ has to be odd. □

Case 4: M is odd and β is odd.

With odd β, Eq.(3.16) can be simplified to

$$(-1)^{-(\sum_{i=0}^{M-1} K_i)+M} \, |\mathbf{D}| \, (-1)^{(\frac{M-1}{2})} \;=\; -1. \quad (3.18)$$

For $M = 4m+1$, $\frac{M-1}{2}$ is even, and $(-1)^{(\frac{M-1}{2})} = 1$. Moreover, the number of antisymmetric filters is also even, implying $|\mathbf{D}| = 1$. Thus, $(\sum_{i=0}^{M-1} K_i - M)$ must be odd for the above

equation to hold. Therefore, $\sum_{i=0}^{M-1} K_i$ is even. For $M = 4m + 3$, $\frac{M-1}{2}$ is odd. Hence, $|\mathbf{D}| = -1$, $(-1)^{(\frac{M-1}{2})} = -1$, and the same result can be obtained: $\sum_{i=0}^{M-1} K_i$ is even. □

From Theorem 3.11, an interesting corollary can be derived on the behavior of the total length of all the filters in a LPPRFB.

Corollary 3.12 *In an M-channel LPPRFB with filter lengths* $L_i = K_i M + \beta$, $m \in \mathcal{Z}^+$,

- *if M is even,* $\sum_{i=0}^{M-1} L_i = 2mM$.
- *if M is odd,* $\sum_{i=0}^{M-1} L_i = (2m+1)M$.

Proof.

Since $L_i = K_i M + \beta$, $\sum_{i=0}^{M-1} L_i = M(\beta + \sum_{i=0}^{M-1} K_i)$. If M is even and β is also even, Theorem 3.11 requires $\sum K_i$ to be even. Hence, $(\beta + \sum_{i=0}^{M-1} K_i)$ is even. In other words, any even-channel LPPRFB in the class being considered has its sum of filter lengths as an even multiple of the number of channels. If β is now odd, then $\sum K_i$ has to be odd, so $(\beta + \sum_{i=0}^{M-1} K_i)$ is even. For odd value of M, using a similar argument, we arrive at the conclusion that the total length of all the filters must be an odd multiple of M. □

The results from Theorem 3.8, Theorem 3.11 and Corollary 3.12 are summarized in Table 2. S stands for the number of symmetric filters; A stands for the number of antisymmetric filters. Note that these results hold true for both sets of analysis and synthesis filters of any LPPR system satisfying Eq.(3.3) or Eq.(3.4) in Theorem 3.6.

To no surprise, the solutions for the well-studied 2-channel LPPRFB agree with our result. There are two systems for 2-channel LPFB. A type A system has even-length filters with different symmetry polarity while a type B system has odd-length filters with

same symmetry [53]. This can be confirmed using Table 2. Type A systems belong to the first row ($M = 2$, and $\beta = 0$). Therefore, there must be one symmetric and one antisymmetric filter. Since they both have even length (and $K_0 + K_1$ is even), the sum of the filter lengths is a multiple of 4. Similarly, Type B systems satisfy all constraints in the second row of the table (it belongs to the even-M, odd-β case with $M = 2$ and $\beta = 1$) [53].

All of the M-channel solutions reported so far also follow the results in our permissible table as well. For example, the 3-channel LPPRFB in [54] has 2 symmetric filters and 1 antisymmetric filter. They have lengths 56, 53, and 56 ($M = 3, \beta = 1$). The sum of the corresponding K_i (18, 17, and 18) is odd. Also, the total length is an odd multiple of 3. Another 3-channel solution reported in [70] has 2 symmetric and 1 antisymmetric filters with lengths 53, 44, and 44 respectively. This system belongs to the case of odd M and even β. Therefore, the number of symmetric filters must exceed the number of antisymmetric ones by one. Moreover, the sum of K_i (17, 14, 14) is odd, which is consistent with the result in Theorem 3.11. Several LP cosine modulated PR FB with filter lengths not equal to KM are reported recently in [41]. All of these FB lengths and polarity symmetry also fall within our constraints (the zero-value coefficients resulted from the optimization process need to be counted as well).

Case	*Symmetry Polarity*	*Length Condition*	*Sum of Lengths*
M even, β even	$\frac{M}{2}$ S & $\frac{M}{2}$ A	$\sum_{i=0}^{M-1} K_i$ even	$2mM$
M even, β odd	$(\frac{M}{2}+1)$ S & $(\frac{M}{2}-1)$ A	$\sum_{i=0}^{M-1} K_i$ odd	$2mM$
M odd, β even	$(\frac{M+1}{2})$ S & $(\frac{M-1}{2})$ A	$\sum_{i=0}^{M-1} K_i$ odd	$(2m+1)M$
M odd, β odd	$(\frac{M+1}{2})$ S & $(\frac{M-1}{2})$ A	$\sum_{i=0}^{M-1} K_i$ even	$(2m+1)M$

Table 2: Possible solutions for M-channel LPPRFBs with filter lengths $L_i = K_i M + \beta$.

3.4 Summary

Several important results in the general theory concerning LPPRFBs with arbitrary number of channels M and filters of arbitrary lengths $L_i = K_i M + \beta$ are presented in this chapter. We first derive the symmetry condition of the polyphase matrices. This condition is pivotal to the development of the general LP-propagating structure presented in the next chapter. Furthermore, the symmetrical property of the polyphase matrices deepens our understanding of LPPRFBs and proves crucial in identifying the possible solutions in terms of filter symmetry polarity and filter lengths. Prior to the start of any actual design, we have already eliminated numerous possibilities. The permissible conditions in Table 2 will be utilized throughout the remaining of the dissertation in constructing complete and minimal lattice structures in later chapters.

Chapter 4

LP-Propagating Biorthogonal Lattice Structures

4.1 Introduction

A lattice structure for LPPRFBs based on the singular value decomposition (SVD) is introduced in this chapter. The lattice can be proven to use a minimal number of delay elements and to completely span a large class of M-channel linear phase perfect reconstruction filter banks: all analysis and synthesis filters have the same FIR length $L = KM$, sharing the same center of symmetry. The lattice also structurally enforces both linear phase and perfect reconstruction properties, is capable of providing fast and efficient implementation, and avoids the costly matrix inversion problem in the optimization process. From a block transform perspective, the new lattice represents the family of generalized lapped biorthogonal transforms (GLBT) with arbitrary number of channels M and arbitrary large overlapping samples KM. The relaxation of the orthogonal constraint allows the GLBT to have significantly different analysis and synthesis basis functions which can then be tailored appropriately to fit a particular application. Several

design examples are presented to confirm the validity of the theory.

4.2 General LP-Propagating Structure

4.2.1 Problem Formulation

Throughout this chapter, the class of M-channel FBs under investigation possesses all of the following properties: (i) the FB has perfect reconstruction as in Eq.(2.6) of Definition 2.2; (ii) all filters (both analysis and synthesis) are FIR as in Eq.(2.7) of Theorem 2.3; (iii) all filters have the same length $L = KM$ where $K \in \mathcal{Z}^+$, i.e., $\mathbf{E}(z)$ and $\mathbf{R}(z)$ have the same order; (iv) all analysis and synthesis filters have real coefficients and linear phase, i.e., they are either symmetric $h[n] = h[L-1-n]$ or antisymmetric $h[n] = -h[L-1-n]$ as discussed in Section 2.3.2.

For this class of LPPRFBs, the problem of permissible conditions on the filter length and symmetry polarity has been solved in the previous chapter; the results are summarized in Table 2. In this chapter, we shall exploit the symmetry property of the polyphase matrices and the necessary conditions for possible LPPR systems to develop the most general LPPR-propagating lattice structure.

4.2.2 General Structure

Recall the essential concept of the lattice structure as illustrated in Figure 4 of Section 2.3.4: $\mathbf{G}(z)$ must be chosen such that both sets of filters $H_{F,i}(z)$ (represented by $\mathbf{F}(z)$)

and $H_{E,i}(z)$ (represented by $\mathbf{E}(z)$) possess the same desirable properties. The following theorem introduces a general structure for $\mathbf{G}(z)$ where the propagating properties are chosen to be LP and PR.

Theorem 4.13 *Suppose there exists an M-channel FIR LPPRFB with all analysis and synthesis filters of length $L = KM$ with the associated polyphase matrix $\mathbf{F}(z)$ of order $(K-1)$. Define the order-$(K+N-1)$ polyphase matrix $\mathbf{E}(z) \triangleq \mathbf{G}(z)\mathbf{F}(z)$ where the propagating structure is the all-zero $\mathbf{G}(z)$ of order N, i.e., $\mathbf{G}(z) = \sum_{i=0}^{N} \mathbf{A}_i z^{-i}$. Then, $\mathbf{E}(z)$ has LP and PR if and only if*

- $\mathbf{G}(z)$ *is FIR invertible.*
- $\mathbf{G}(z)$ *takes the form* $\mathbf{G}(z) = z^{-N}\,\mathbf{D}\,\mathbf{G}(z^{-1})\,\mathbf{D}$.
- $\mathbf{A}_i = \mathbf{D}\,\mathbf{A}_{N-i}\,\mathbf{D}$.

Proof.

First, $\mathbf{E}(z) = \mathbf{G}(z)\mathbf{F}(z)$, hence $|\mathbf{E}(z)| = |\mathbf{G}(z)|\,|\mathbf{F}(z)|$ and $\mathbf{E}^{-1}(z) = \mathbf{F}^{-1}(z)\mathbf{G}^{-1}(z)$. Since $\mathbf{F}(z)$ is FIR invertible, it is clear that $\mathbf{E}^{-1}(z)$ exists and is FIR if and only if $\mathbf{G}(z)$ is FIR invertible. Next, $\mathbf{F}(z)$ represents a LPFB ; therefore, $\mathbf{F}(z)$ and its associated synthesis polyphase matrix $\mathbf{R}(z)$ must satisfy the LP property in Corollary 3.7 of the previous chapter

$$\mathbf{F}(z) = z^{-(K-1)}\,\mathbf{D}\,\mathbf{F}(z^{-1})\,\mathbf{J} \quad \text{(analysis)}$$

$$\mathbf{R}(z) = z^{-(K-1)}\,\mathbf{J}\,\mathbf{R}(z^{-1})\,\mathbf{D} \quad \text{(synthesis)}$$

where $\mathbf{D}$ is the diagonal matrix with entries being $+1$ or -1 depending on the corresponding filter being symmetric or antisymmetric. For clarity of presentation and without any

loss of generality, all symmetric filters are permuted to be on top, i.e.,

$$\mathbf{D} = \begin{bmatrix} \mathbf{I}_S & \mathbf{0} \\ \mathbf{0} & -\mathbf{I}_A \end{bmatrix}$$

where S stands for the number of symmetric filters and A stands for the number of antisymmetric filters. S and A have to satisfy the necessary constraints in Table 2: $S = A = \frac{M}{2}$ if M is even; $S = \frac{M+1}{2}$ and $A = \frac{M-1}{2}$ if M is odd.

Similarly, the LP property of $\mathbf{E}(z)$ is equivalent to

$$\begin{aligned}
& \mathbf{E}(z) &&= z^{-(K+N-1)}\, \mathbf{D}\, \mathbf{E}(z^{-1})\, \mathbf{J} \\
\Longleftrightarrow\ & \mathbf{E}(z) &&= z^{-(K+N-1)}\, \mathbf{D}\, \mathbf{G}(z^{-1})\, \mathbf{F}(z^{-1})\, \mathbf{J} \\
\Longleftrightarrow\ & \mathbf{E}(z) &&= z^{-N}\, \mathbf{D}\, \mathbf{G}(z^{-1})\, z^{-(K-1)}\, \mathbf{F}(z^{-1})\, \mathbf{J} \\
\Longleftrightarrow\ & \mathbf{E}(z) &&= z^{-N}\, \mathbf{D}\, \mathbf{G}(z^{-1})\, \mathbf{D}\, z^{-(K-1)}\, \mathbf{D}\, \mathbf{F}(z^{-1})\, \mathbf{J} \\
\Longleftrightarrow\ & \mathbf{E}(z) &&= z^{-N}\, \mathbf{D}\, \mathbf{G}(z^{-1})\, \mathbf{D}\, \mathbf{F}(z).
\end{aligned}$$

Thus for $\mathbf{E}(z)$ to have LP, it is necessary and sufficient that

$$\mathbf{G}(z) \;=\; z^{-N}\, \mathbf{D}\, \mathbf{G}(z^{-1})\, \mathbf{D}. \tag{4.1}$$

Now, substituting $\mathbf{G}(z) = \sum_{i=0}^{N} \mathbf{A}_i z^{-i}$ into the right-hand side of Eq.(4.1) yields

$$\begin{aligned}
\mathbf{G}(z) \quad &= \quad z^{-N}\mathbf{D}\, (\textstyle\sum_{i=0}^{N} \mathbf{A}_i z^{i})\, \mathbf{D} \;=\; \mathbf{D}\, (\textstyle\sum_{i=0}^{N} \mathbf{A}_i z^{i-N})\, \mathbf{D} \\
&= \quad \mathbf{D}\, (\textstyle\sum_{i=0}^{N} \mathbf{A}_{N-i} z^{-i})\, \mathbf{D} \;=\; \textstyle\sum_{i=0}^{N} (\mathbf{D}\mathbf{A}_{N-i}\mathbf{D})\, z^{-i}. \\
\Longrightarrow\ & \mathbf{A}_i = \mathbf{D}\, \mathbf{A}_{N-i}\, \mathbf{D}.
\end{aligned} \tag{4.2}$$

In other words, the specific form of $\mathbf{G}(z)$ in Eq.(4.1) imposes interesting symmetric constraints on the matrices $\mathbf{A}_i$. □

Remarks. Theorem 4.13 already presents a strong result. It states that the building block $\mathbf{G}(z)$ with the three aforementioned properties is unique when the propagation of LP and PR is concerned – there exists no other solution. The reader should also note that the order N of $\mathbf{G}(z)$ is purposely chosen to be arbitrary so that it can cover all classes of FBs that may not be factorizable with order-1 structures. For example, according to Table 2, odd-channel even-length LPPR system does not exist. Hence, it is not possible to construct a lattice with order-1 building blocks when M is odd. The minimum length increment in this case has to be $2M$, and the simplest possible structure must have order of at least 2. Section 4.3 and Section 4.4 discuss in details more specific cases with order-1 and order-2 LP-propagating structures respectively. Finally, the LP-propagating structure in Theorem 4.13 has taken into account the number of permissible symmetric (or antisymmetric) filters, a crucial element in the existence of LPPR systems, in the form of the diagonal matrix $\mathbf{D}$.

4.3 Lattice Structure for Even-Channel LPPRFB

Let us assume further that M is even. In this case, possible solutions must have $\frac{M}{2}$ symmetric and $\frac{M}{2}$ antisymmetric filters as indicated in Table 2. Furthermore, we know that LPPRFB exists for every integer $K \geq 1$ [75], [62], [80], [48], i.e., these FBs can be factorized by order-1 structure. If $N = 1$ in Eq.(4.2), $\mathbf{A}_1 = \mathbf{D}\mathbf{A}_0\mathbf{D}$. Then, $\mathbf{G}(z)$ takes the general form of $\mathbf{G}(z) = \mathbf{A}_0 + z^{-1}\mathbf{D}\mathbf{A}_0\mathbf{D}$.

Theorem 4.14 $\mathbf{G}(z)$ *in Theorem 4.13 is not FIR invertible if* $\mathbf{A}_0$ *has full rank.*

Proof.

Suppose that $\mathbf{G}(z)$ is FIR invertible, and without loss of generality, let

$$\mathbf{G}^{-1}(z) = \mathbf{B}_0 + z\mathbf{D}\mathbf{B}_0\mathbf{D}$$

(keep in mind that the synthesis filters have LP and the same order as the analysis filters). Since $\mathbf{G}^{-1}(z)\mathbf{G}(z) = \mathbf{I}$, evaluating the equation with like powers of z yields

$$\begin{aligned} \mathbf{B}_0\mathbf{A}_0 + \mathbf{D}\mathbf{B}_0\mathbf{A}_0\mathbf{D} &= \mathbf{I} \\ \mathbf{A}_0\mathbf{B}_0 + \mathbf{D}\mathbf{A}_0\mathbf{B}_0\mathbf{D} &= \mathbf{I} \end{aligned} \tag{4.3}$$

$$\begin{aligned} \mathbf{B}_0\mathbf{D}\mathbf{A}_0 &= \mathbf{0} \\ \mathbf{A}_0\mathbf{D}\mathbf{B}_0 &= \mathbf{0} \end{aligned} \tag{4.4}$$

If $\mathbf{A}_0$ is full-rank, $\mathbf{B}_0 = \mathbf{0}$ and Eq. (4.3) becomes inconsistent. □

Moreover, according to Sylvester's rank theorem [16], one can easily prove that $\rho(\mathbf{A}_0) + \rho(\mathbf{B}_0) \leq M$ from Eq. (4.4). The proof will become clear to the reader later in this section. Our interest is in the most general solution and there should be no bias on a particular bank. Hence, we propose the following solution with $\rho(\mathbf{A}_0) = \rho(\mathbf{B}_0) \leq \frac{M}{2}$:

$$\mathbf{A}_0 = \frac{1}{2}\begin{bmatrix} \mathbf{U} & \mathbf{U} \\ \mathbf{V} & \mathbf{V} \end{bmatrix}, \tag{4.5}$$

where $\mathbf{U}$ and $\mathbf{V}$ are arbitrary $\frac{M}{2} \times \frac{M}{2}$ matrices. We shall later prove that the choice of $\mathbf{A}_0$ in Eq.(4.5) is indeed the most general solution. Now, $\mathbf{G}(z) = \mathbf{A}_0 + z^{-1}\mathbf{D}\mathbf{A}_0\mathbf{D}$ can be factorized as follows

$$\mathbf{G}(z) = \tfrac{1}{2}\begin{bmatrix} \mathbf{U} + z^{-1}\mathbf{U} & \mathbf{U} - z^{-1}\mathbf{U} \\ \mathbf{V} - z^{-1}\mathbf{V} & \mathbf{V} + z^{-1}\mathbf{V} \end{bmatrix} = \tfrac{1}{2}\begin{bmatrix} \mathbf{U} & \mathbf{0} \\ \mathbf{0} & \mathbf{V} \end{bmatrix}\begin{bmatrix} \mathbf{I} & \mathbf{I} \\ \mathbf{I} & -\mathbf{I} \end{bmatrix}\begin{bmatrix} \mathbf{I} & \mathbf{0} \\ \mathbf{0} & z^{-1}\mathbf{I} \end{bmatrix}\begin{bmatrix} \mathbf{I} & \mathbf{I} \\ \mathbf{I} & -\mathbf{I} \end{bmatrix}$$

$$\stackrel{\triangle}{=} \frac{1}{2}\,\mathbf{\Phi}\;\mathbf{W}\;\mathbf{\Lambda}(z)\;\mathbf{W}. \tag{4.6}$$

All of the delays are now contained in $\mathbf{\Lambda}(z)$, while $\mathbf{W}$ resembles the famous "butterfly" matrix in the FFT implementation. Since $\mathbf{W}$ and $\mathbf{\Lambda}(z)$ have orthogonal inverses, $\mathbf{G}(z)$ is invertible if and only if $\mathbf{\Phi}$ is invertible, i.e., $\mathbf{U}$ and $\mathbf{V}$ are invertible. A cascade of $(K-1)$ blocks $\mathbf{G}_i = \frac{1}{2}\mathbf{\Phi}_i\mathbf{W}\mathbf{\Lambda}(z)\mathbf{W}$ and a zero-order initial block $\mathbf{E}_0$ generates the polyphase matrix of an even-channel LPPRFB with filter length $L = KM$:

$$\mathbf{E}(z) \;=\; \mathbf{G}_{K-1}(z)\,\mathbf{G}_{K-2}(z)\,\cdots\,\mathbf{G}_2(z)\,\mathbf{G}_1(z)\,\mathbf{E}_0 \;=\; \prod_{i=K-1}^{1}\mathbf{G}_i(z)\,\mathbf{E}_0. \tag{4.7}$$

The starting block $\mathbf{E}_0$ has no delay element, represents an LPPRFB of length M, and was often chosen to be the DCT [62], [7], [48]. The most general $\mathbf{E}_0$ that satisfies Eq.(3.8) has the following form:

$$\mathbf{E}_0 = \frac{1}{\sqrt{2}}\begin{bmatrix} \mathbf{U}_0 & \mathbf{U}_0\mathbf{J} \\ \mathbf{V}_0\mathbf{J} & -\mathbf{V}_0 \end{bmatrix} = \frac{1}{\sqrt{2}}\begin{bmatrix} \mathbf{U}_0 & \mathbf{0} \\ \mathbf{0} & \mathbf{V}_0 \end{bmatrix}\begin{bmatrix} \mathbf{I} & \mathbf{J} \\ \mathbf{J} & -\mathbf{I} \end{bmatrix}. \tag{4.8}$$

For $\mathbf{E}_0$ to have PR, $\mathbf{U}_0$ and $\mathbf{V}_0$ again have to be invertible. The corresponding causal synthesis polyphase matrix is then

$$\mathbf{R}(z) \;=\; z^{-(K-1)}\mathbf{E}_0^{-1}\mathbf{G}_1^{-1}(z)\mathbf{G}_2^{-1}(z)\cdots\mathbf{G}_{K-2}^{-1}(z)\mathbf{G}_{K-1}^{-1}(z) \;=\; \mathbf{E}_0^{-1}\prod_{i=1}^{K-1} z^{-1}\mathbf{G}_i^{-1}(z). \tag{4.9}$$

The complete lattice for both analysis and synthesis bank is depicted in Figure 18. Results in Eq.(4.6)-(4.9) should not come as a surprise. The factorization is very similar to the GenLOT's lattice structure [62] in the more restrictive case of paraunitary FBs. In that case, the authors obtained PU systems by enforcing orthogonality on $\mathbf{U}_i$ and $\mathbf{V}_i$. Now, we have to show that the proposed factorization does cover all possible solutions in the Problem Formulation of Section 4.2 by proving the converse of the result in Eq.(4.7).

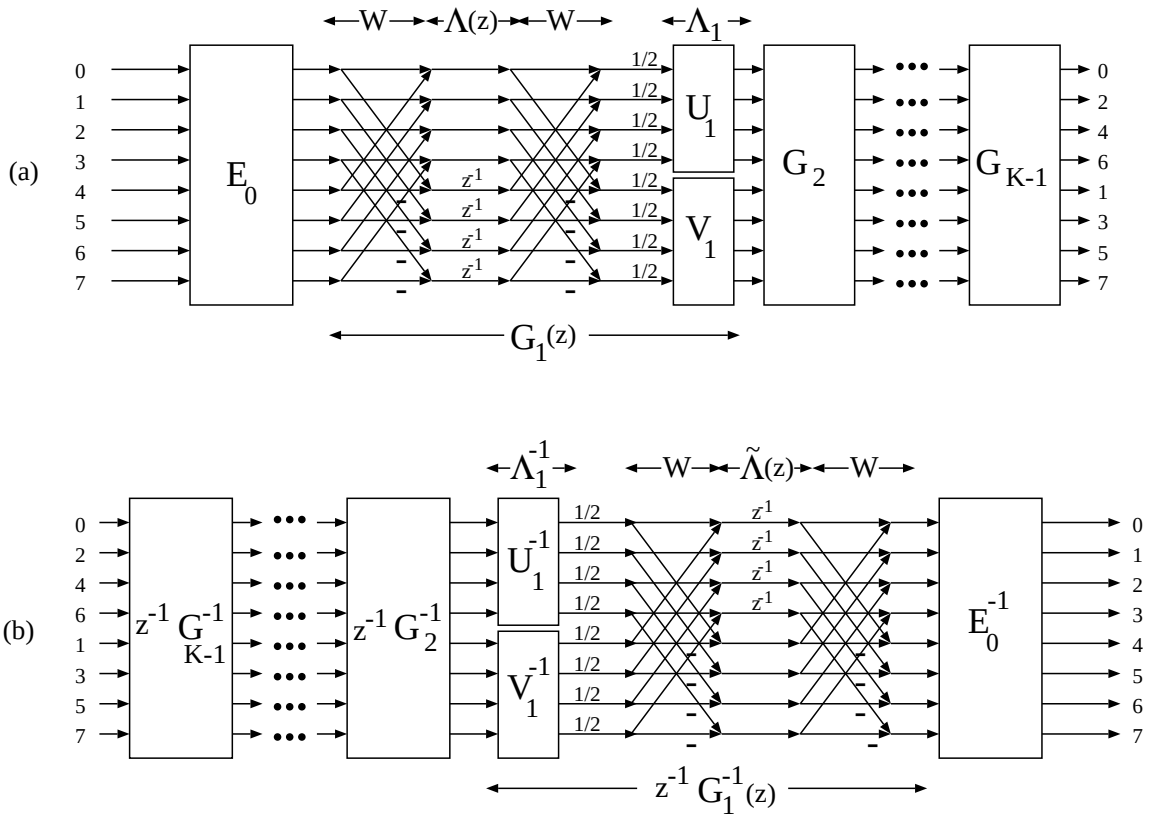

Figure 18: General lattice structure for even-channel LPPRFBs. (a) Analysis bank. (b) Synthesis bank.

Theorem 4.15 *The analysis polyphase matrix* $\mathbf{E}(z)$ *of any even-channel FIR LPPRFB with analysis and synthesis filters of length* $L = KM$ *can always be factored as*

$$\mathbf{E}(z) \;=\; \prod_{i=K-1}^{1} \mathbf{G}_i(z)\, \mathbf{E}_0$$

where $\mathbf{G}_i(z)$ *is as in Eq.(4.6) and* $\mathbf{E}_0$ *is as in Eq.(4.8). The corresponding causal synthesis polyphase matrix is then*

$$\mathbf{R}(z) \;=\; \mathbf{E}_0^{-1} \prod_{i=1}^{K-1} z^{-1}\, \mathbf{G}_i^{-1}(z).$$

The proof of Theorem 4.15 is rather long and extensive. Indifferent readers may proceed without any loss of continuity.

Proof.

The proof is inductive. It keys on the existence of a $\mathbf{G}^{-1}(z)$ matrix that reduces the order of $\mathbf{E}(z)$ by 1 at a time while retaining all of the desirable properties in the reduced-order $\mathbf{F}(z) = \mathbf{G}^{-1}(z)\, \mathbf{E}(z)$. The proof also serves as a guideline for the construction of the lattice given the transform coefficient matrix.

Linear phase: Consider a stage of the lattice in Figure 4. Note that $\mathbf{E}(z)$ and $\mathbf{F}(z)$ now have order $K-1$ and $K-2$ respectively while $\mathbf{G}^{-1}(z)$ is anticausal with order 1. $\mathbf{F}(z)$ can be shown to satisfy the LP property in Eq.(3.8) in a similar manner to the proof of Theorem 4.13:

$$\begin{aligned}
z^{-(K-2)}\, \mathbf{D}\, \mathbf{F}(z^{-1})\, \mathbf{J} \;&=\; z^{-(K-2)}\, \mathbf{D}\, \mathbf{G}^{-1}(z^{-1})\, \mathbf{E}(z^{-1})\, \mathbf{J} \\
&=\; z^{-(K-2)}\, \mathbf{D}\, \mathbf{G}^{-1}(z^{-1})\, z^{(K-1)}\, \mathbf{D}\, \mathbf{E}(z)\, \mathbf{J}\, \mathbf{J} \\
&=\; z\, \mathbf{D}\, \mathbf{G}^{-1}(z^{-1})\, \mathbf{D}\, \mathbf{G}(z)\, \mathbf{F}(z) \\
&=\; z\, \mathbf{D}\, \mathbf{G}^{-1}(z^{-1})\, \mathbf{D}\, z^{-1}\, \mathbf{D}\, \mathbf{G}(z^{-1})\, \mathbf{D}\;\; \mathbf{F}(z) \;=\; \mathbf{F}(z),
\end{aligned}$$

where we have exploited the facts that $\mathbf{E}(z) = z^{-(K-1)}\mathbf{D}\mathbf{E}(z^{-1})\mathbf{J}$ from Eq.(2.6) and $\mathbf{G}(z) = z^{-1}\mathbf{D}\mathbf{G}(z^{-1})\mathbf{D}$ from Theorem 4.13. □

Perfect reconstruction: From Eq.(4.6),

$$\mathbf{F}(z) \;=\; \mathbf{G}^{-1}(z)\,\mathbf{E}(z) \;=\; \tfrac{1}{2}\,\mathbf{W}\,\mathbf{\Lambda}(z^{-1})\,\mathbf{W}\,\mathbf{\Phi}^{-1}\,\mathbf{E}(z). \tag{4.10}$$

Since all matrices on the right-hand side of this equation have FIR inverse, $\mathbf{F}(z)$ is also FIR invertible, i.e., it represents a FIR perfect reconstruction system. □

Causality: The above proofs for $\mathbf{F}(z)$ to have LP and PR are actually expected because we specifically design $\mathbf{G}(z)$ to propagate these properties. Any choice of

$$\mathbf{\Phi} = \begin{bmatrix} \mathbf{U} & \mathbf{0} \\ \mathbf{0} & \mathbf{V} \end{bmatrix}$$

such that it is invertible will suffice. The difficult part is to show that there always exist invertible matrices $\mathbf{U}$ and $\mathbf{V}$ that will produce a causal $\mathbf{F}(z)$ obtained from Eq.(4.10). Let

$$\mathbf{F}(z) \;=\; \sum_{i=0}^{K-2} \mathbf{F}_i\, z^{-i},\;\; \mathbf{F}_{K-2} \neq \mathbf{0} \quad \text{and} \quad \mathbf{E}(z) \;=\; \sum_{i=0}^{K-1} \mathbf{E}_i\, z^{-i},\;\; \mathbf{E}_{K-1} \neq \mathbf{0}. \tag{4.11}$$

From Eq.(4.10), one can derive

$$\begin{aligned} \mathbf{F}(z) \;&=\; \tfrac{1}{2} \begin{bmatrix} \mathbf{I} & \mathbf{I} \\ \mathbf{I} & -\mathbf{I} \end{bmatrix} \begin{bmatrix} \mathbf{I} & \mathbf{0} \\ \mathbf{0} & z\mathbf{I} \end{bmatrix} \begin{bmatrix} \mathbf{I} & \mathbf{I} \\ \mathbf{I} & -\mathbf{I} \end{bmatrix} \begin{bmatrix} \mathbf{U}^{-1} & \mathbf{0} \\ \mathbf{0} & \mathbf{V}^{-1} \end{bmatrix} \mathbf{E}(z) \\ &=\; \tfrac{1}{2} \left(\begin{bmatrix} \mathbf{U}^{-1} & \mathbf{V}^{-1} \\ \mathbf{U}^{-1} & \mathbf{V}^{-1} \end{bmatrix} + z \begin{bmatrix} \mathbf{U}^{-1} & -\mathbf{V}^{-1} \\ -\mathbf{U}^{-1} & \mathbf{V}^{-1} \end{bmatrix} \right) \left(\sum_{i=0}^{K-1} \mathbf{E}_i\, z^{-i} \right). \end{aligned} \tag{4.12}$$

We have to show that it is possible to eliminate the noncausal part in Eq.(4.12) by achieving

$$\begin{bmatrix} \mathbf{U}^{-1} & -\mathbf{V}^{-1} \\ -\mathbf{U}^{-1} & \mathbf{V}^{-1} \end{bmatrix} \mathbf{E}_0 \;=\; \mathbf{0} \tag{4.13}$$

Now, let the polyphase matrix of the corresponding synthesis bank be

$$\mathbf{R}(z) \;=\; \sum_{i=0}^{K-1} \mathbf{R}_i \, z^i, \;\; \mathbf{R}_{K-1} \neq \mathbf{0}, \tag{4.14}$$

where the $z^{-\ell}$ factor in Eq.(2.6) has been absorbed into $\mathbf{R}(z)$ to make it anticausal. The biorthogonal condition is modified to $\mathbf{R}(z)\mathbf{E}(z) = \mathbf{I}$, leading to the following equivalent condition in the time domain:

$$\sum_{i=0}^{K-1-\ell} \mathbf{R}_i \mathbf{E}_{i+\ell} \;=\; \delta[\ell]\,\mathbf{I}, \quad \forall \;\; \ell \;\; \text{s.t. } 0 \leq i+\ell \leq K-1. \tag{4.15}$$

The relationship of interest here is $\mathbf{R}_{K-1}\mathbf{E}_0 = \mathbf{0}$. Next, the LP properties of $\mathbf{E}(z)$ and $\mathbf{R}(z)$ in Eq.(3.8) and Eq.(3.9) yield

$$\begin{aligned} \sum_{i=0}^{K-1} \mathbf{E}_i \, z^{-i} \;&=\; z^{-(K-1)}\, \mathbf{D}\, (\sum_{i=0}^{K-1} \mathbf{E}_i \, z^i)\, \mathbf{J} \\ \sum_{i=0}^{K-1} \mathbf{R}_i \, z^i \;&=\; z^{K-1}\, \mathbf{J}\, (\sum_{i=0}^{K-1} \mathbf{R}_i \, z^{-i})\, \mathbf{D}, \end{aligned}$$

which imply that

$$\mathbf{E}_i \;=\; \mathbf{D}\,\mathbf{E}_{K-i-1}\,\mathbf{J} \quad \text{and} \quad \mathbf{R}_i \;=\; \mathbf{J}\,\mathbf{R}_{K-i-1}\,\mathbf{D}. \tag{4.16}$$

Hence, we can obtain

$$\mathbf{R}_{K-1}\,\mathbf{E}_0 \;=\; \mathbf{J}\,\mathbf{R}_{K-i-1}\,\mathbf{D}\,\mathbf{E}_0 \;=\; \mathbf{R}_0\,\mathbf{D}\,\mathbf{E}_0 = \mathbf{0}.$$

Applying Sylvester's rank inequality [16] to $\mathbf{R}_0\,\mathbf{D}\,\mathbf{E}_0 = \mathbf{0}$ produces

$$\rho(\mathbf{R}_0) \;+\; \rho(\mathbf{D}\,\mathbf{E}_0) \;-\; M \;\leq\; \rho(\mathbf{R}_0\,\mathbf{D}\,\mathbf{E}_0) = 0$$

$$\Longrightarrow \quad \rho(\mathbf{R}_0) \;+\; \rho(\mathbf{E}_0) \;\leq\; M. \tag{4.17}$$

The proof of causality is accomplished if $\rho(\mathbf{E}_0) \leq \frac{M}{2}$, since in that case, the dimension of the null space of $\mathbf{E}_0$ is larger than or equal to $\frac{M}{2}$. Hence, it is possible to choose $\frac{M}{2}$ linearly independent vectors from $\mathbf{E}_0$'s null space to serve as $[\ \mathbf{U}^{-1} \quad -\mathbf{V}^{-1}\ ]$. In the paraunitary case, this can be achieved easily because Eq.(2.9) immediately implies $\rho(\mathbf{R}_0) = \rho(\mathbf{E}_0) \leq \frac{M}{2}$. The biorthogonal case is more troublesome, and we need Lemma 4.16 below, which shows that the condition $\rho(\mathbf{E}_0) > \frac{M}{2}$ (or $\rho(\mathbf{R}_0) > \frac{M}{2}$) leads to asymmetrical systems where the filters of one bank have higher order than the filters of the other. More simply stated, in the case where all analysis and synthesis filters have the same length $L = KM$, it is necessary that

$$\rho(\mathbf{E}_0) \leq \frac{M}{2} \quad \text{and} \quad \rho(\mathbf{R}_0) \leq \frac{M}{2}.$$

□

Order Reduction: It can be easily verified that the structure $\mathbf{G}^{-1}(z)$ in Eq.(4.10) with $\mathbf{U}$ and $\mathbf{V}$ chosen to eliminate noncausality as in Eq.(4.13) also reduces the order of $\mathbf{E}(z)$ by 1. From Eq.(4.12), after one factorization step, the highest-order component of $\mathbf{F}(z) = \mathbf{G}^{-1}(z)\mathbf{E}(z)$ is

$$\begin{bmatrix} \mathbf{U}^{-1} & \mathbf{V}^{-1} \\ \\ \mathbf{U}^{-1} & \mathbf{V}^{-1} \end{bmatrix} \mathbf{E}_{K-1}. \tag{4.18}$$

Substituting $\mathbf{E}_{K-1} = \mathbf{D}\mathbf{E}_0\mathbf{J}$ from Eq.(4.16) into Eq.(4.18) yields

$$\begin{bmatrix} \mathbf{U}^{-1} & \mathbf{V}^{-1} \\ \mathbf{U}^{-1} & \mathbf{V}^{-1} \end{bmatrix} \mathbf{D}\ \mathbf{E}_0\ \mathbf{J} \ = \ \begin{bmatrix} \mathbf{U}^{-1} & -\mathbf{V}^{-1} \\ \mathbf{U}^{-1} & -\mathbf{V}^{-1} \end{bmatrix} \mathbf{E}_0\ \mathbf{J} \ = \ \mathbf{0}\ \mathbf{J} \ = \ \mathbf{0}. \tag{4.19}$$

Therefore, the factorization is guaranteed to terminate after $(K-1)$ steps. □

Lemma 4.16 *If there exist two polyphase matrices*

$$\mathbf{E}(z) = \sum_{i=0}^{K-1} \mathbf{E}_i\, z^{-i} \quad \textit{and} \quad \mathbf{R}(z) = \sum_{i=0}^{K-1} \mathbf{R}_i\, z^{i}$$

representing FIR even-channel LPPRFB with all filters having the same length $L = KM$, then $\rho(\mathbf{E}_0) \leq \frac{M}{2}$ and $\rho(\mathbf{R}_0) \leq \frac{M}{2}$.

Proof.

Note that we consider causal analysis bank and anticausal synthesis bank purely for the clarity of presentation. Eq.(2.6) now simplifies to $\mathbf{R}(z)\mathbf{E}(z) = \mathbf{I}$, whereas $|\mathbf{E}(z)| = z^{-m} = 1/|\mathbf{R}(z)|$ and $|\mathbf{R}(z)| = z^{m}$. Indeed, one can manipulate Eq.(3.8) and Eq.(3.9) to obtain the exact order m of their determinants:

$$|\mathbf{E}(z)| \ = \ |z^{-(K-1)}\mathbf{I}|\ |\mathbf{D}|\ |\mathbf{E}(z^{-1})|\ |\mathbf{J}| \ = \ z^{-M(K-1)}\ \frac{1}{|\mathbf{E}(z)|} \quad \Longrightarrow |\mathbf{E}(z)| = z^{\frac{-M(K-1)}{2}}.$$

We shall complete the proof by contradiction. Suppose that $\rho(\mathbf{E}_0) > \frac{M}{2}$, thus $\rho(\mathbf{R}_0) < \frac{M}{2}$. Consider the possibility of the factorization of the anticausal $\mathbf{R}(z)$. Similarly to the approach described by Eq.(4.12) and Eq.(4.13), we need to obtain

$$\mathbf{R}_0 \begin{bmatrix} \mathbf{U} & -\mathbf{U} \\ -\mathbf{V} & \mathbf{V} \end{bmatrix} \ = \ \mathbf{0} \tag{4.20}$$

to eliminate causality. In this case, $\rho(\mathbf{R}_0) < \frac{M}{2}$, and it is possible to choose $[\ \mathbf{U}\ \ -\mathbf{V}\ ]^T$ from $\frac{M}{2}$ linearly independent vectors from the null space of $\mathbf{R}_0$. In other words, it is possible to write $\mathbf{R}(z)$ as $\mathbf{R}(z) = \mathbf{R}_{K-2}(z)\mathbf{G}^{-1}(z)$ where both factors are anticausal. Now, we have

$$|\mathbf{R}(z)| \ = \ |\mathbf{R}_{K-2}(z)|\ |\mathbf{G}^{-1}(z)|.$$

Since $|\mathbf{G}^{-1}(z)| = z^{\frac{M}{2}}$,

$$|\mathbf{R}_{K-2}(z)| = z^{\frac{M(K-1)}{2}-\frac{M}{2}} = z^{\frac{M(K-2)}{2}}. \tag{4.21}$$

Therefore, it is easy to show that $\mathbf{R}_{K-2}(z)$ represents an FIR LPPR system of order $(K-2)$ as in the proof of Theorem 4.15.

On the other hand,

$$\mathbf{E}(z) \ = \ \mathbf{R}^{-1}(z) \ = \ \mathbf{G}(z)\,\mathbf{R}_{K-2}^{-1}(z).$$

Consider the product

$$\mathbf{G}^{-1}(z)\,\mathbf{E}(z) \ = \ \mathbf{R}_{K-2}^{-1}(z).$$

We can obtain a causal $\mathbf{R}_{K-2}^{-1}(z)$ with determinant $z^{-\frac{M(K-2)}{2}}$ in similar fashion to Eq.(4.9). However, since $\rho(\mathbf{E}_0) > \frac{M}{2}$, the null space of $\mathbf{E}_0$ has dimension less than $\frac{M}{2}$. Therefore, the anticausal part of $\mathbf{G}^{-1}(z)\mathbf{E}(z)$ cannot possibly be suppressed, i.e.,

$$\begin{bmatrix} \mathbf{U}^{-1} & -\mathbf{V}^{-1} \\ -\mathbf{U}^{-1} & \mathbf{V}^{-1} \end{bmatrix} \mathbf{E}_0 \neq \mathbf{0},$$

for any invertible matrices $\mathbf{U}^{-1}$ and $\mathbf{V}^{-1}$. Moreover, the highest order of $\mathbf{G}^{-1}(z)\,\mathbf{E}(z)$ still exists

$$\begin{bmatrix} \mathbf{U}^{-1} & \mathbf{V}^{-1} \\ \mathbf{U}^{-1} & \mathbf{V}^{-1} \end{bmatrix} \mathbf{E}_{K-1} \neq \mathbf{0},$$

because $\rho(\mathbf{E}_{K-1}) = \rho(\mathbf{E}_0) > \frac{M}{2}$. So, a shift of z leads to a causal system with order K, contradicting with the fact that $\mathbf{R}_{K-2}^{-1}(z)$ is causal with order $(K-2)$ as shown in Eq.(4.21). The case of $\rho(\mathbf{R}_0) > \frac{M}{2}$ can be proven in a similar fashion. □

Theorem 4.15 confirms the generality of our solution. Another major concern as mentioned in Section 2.3.4 is the efficiency of the lattice which shall be established by the following theorem.

Theorem 4.17 *The factorization in Eq.(4.7) is minimal, i.e., the resulting lattice structure employs the minimum number of delays in its implementation.*

Proof.

A structure is said to be minimal if the number of delays used is equal to the degree of the transfer function. For the class of systems in consideration, it can be proven [95] that

$$deg(\mathbf{E}(z)) \;=\; deg(|\mathbf{E}(z)|).$$

Using the symmetry property of the polyphase matrix in Eq.(3.8), we have

$$deg(\mathbf{E}(z)) \;=\; deg(|\mathbf{E}(z)|) \;=\; deg(z^{-(K-1)}|\mathbf{D}|\;|\mathbf{E}(z^{-1})|\;|\mathbf{J}|).$$

Therefore,

$$deg(\mathbf{E}(z)) \;=\; M(K-1) - deg(\mathbf{E}(z)),$$

which leads to the conclusion that $deg(\mathbf{E}(z)) = \frac{M(K-1)}{2}$. In our factorization, there are $(K-1)$ building blocks $\mathbf{G}_i(z)$, each employs $\frac{M}{2}$ delays. The total number of delays in use in the lattice is also $\frac{M(K-1)}{2}$. Thus, the factorization is minimal. □

4.4 Lattice Structure for Odd-Channel LPPRFB

Suppose M is now odd. As previously mentioned in Section 4.2, the minimum order of the propagating structure $\mathbf{G}(z)$ is 2, i.e., $\mathbf{G}(z) = \mathbf{A}_0 + \mathbf{A}_1 z^{-1} + \mathbf{A}_2 z^{-2}$. According to Theorem 4.13, the following relationships must hold

$$\mathbf{A}_2 = \mathbf{D}\,\mathbf{A}_0\,\mathbf{D} \tag{4.22}$$

$$\mathbf{A}_1 = \mathbf{D}\,\mathbf{A}_1\,\mathbf{D}, \tag{4.23}$$

where the reader is reminded that in this case

$$\mathbf{D} = \begin{bmatrix} \mathbf{I}_{\frac{M+1}{2}} & \mathbf{0} \\ \mathbf{0} & -\mathbf{I}_{\frac{M-1}{2}} \end{bmatrix}.$$

We expect the factorization to be quite similar to the even-channel case. The main difference is that the system now has one more symmetric filter. So, consider the factorization below

$$\mathbf{G}(z) = \frac{1}{4} \begin{bmatrix} \mathbf{U} & \mathbf{u}_1 & \mathbf{0} \\ \mathbf{u}_2 & u_0 & \mathbf{0} \\ \mathbf{0} & \mathbf{0} & \mathbf{V} \end{bmatrix} \begin{bmatrix} \mathbf{I}+z^{-1}\mathbf{I} & \mathbf{0} & \mathbf{I}-z^{-1}\mathbf{I} \\ \mathbf{0} & 2 & \mathbf{0} \\ \mathbf{I}-z^{-1}\mathbf{I} & \mathbf{0} & \mathbf{I}+z^{-1}\mathbf{I} \end{bmatrix}$$

$$\times \begin{bmatrix} \mathbf{Q} & \mathbf{q}_1 & \mathbf{0} \\ \mathbf{q}_2 & q_0 & \mathbf{0} \\ \mathbf{0} & \mathbf{0} & \mathbf{R} \end{bmatrix} \begin{bmatrix} \mathbf{I}+z^{-1}\mathbf{I} & \mathbf{0} & \mathbf{I}-z^{-1}\mathbf{I} \\ \mathbf{0} & 2z^{-1} & \mathbf{0} \\ \mathbf{I}-z^{-1}\mathbf{I} & \mathbf{0} & \mathbf{I}+z^{-1}\mathbf{I} \end{bmatrix} \tag{4.24}$$

where matrices $\mathbf{U}$, $\mathbf{V}$, $\mathbf{Q}$, $\mathbf{R}$, and $\mathbf{I}$ have size $\frac{M-1}{2} \times \frac{M-1}{2}$; $\mathbf{u}_1$ and $\mathbf{q}_1$ are of size $\frac{M-1}{2} \times 1$; $\mathbf{u}_2$ and $\mathbf{q}_2$ are of size $1 \times \frac{M-1}{2}$; u_0 and q_0 are scalars.

This particular choice of $\mathbf{G}(z)$ results in

$$\mathbf{A}_0 = \frac{1}{4} \begin{bmatrix} \mathbf{UQ}+2\mathbf{u}_1\mathbf{q}_2+\mathbf{UR} & \mathbf{0} & \mathbf{UQ}+2\mathbf{u}_1\mathbf{q}_2+\mathbf{UR} \\ \mathbf{u}_2\mathbf{Q}+2u_0\mathbf{q}_2+\mathbf{u}_2\mathbf{R} & 0 & \mathbf{u}_2\mathbf{Q}+2u_0\mathbf{q}_2+\mathbf{u}_2\mathbf{R} \\ \mathbf{VQ}+\mathbf{VR} & \mathbf{0} & \mathbf{VQ}+\mathbf{VR} \end{bmatrix} \tag{4.25}$$

$$\mathbf{A}_1 = \frac{1}{4} \begin{bmatrix} 2\mathbf{UQ}+2\mathbf{u}_1\mathbf{q}_2-2\mathbf{UR} & 2\mathbf{Uq}_1+4\mathbf{u}_1q_0 & -2\mathbf{u}_1\mathbf{q}_2 \\ 2\mathbf{u}_2\mathbf{Q}+2u_0\mathbf{q}_2-2\mathbf{u}_2\mathbf{R} & 2\mathbf{u}_2\mathbf{q}_1+4u_0q_0 & -2u_0\mathbf{q}_2 \\ \mathbf{0} & 2\mathbf{Vq}_1 & 2\mathbf{VR}-2\mathbf{VQ} \end{bmatrix} \tag{4.26}$$

$$\mathbf{A}_2 = \frac{1}{4} \begin{bmatrix} \mathbf{UQ}+\mathbf{UR} & 2\mathbf{Uq}_1 & -\mathbf{UQ}-\mathbf{UR} \\ \mathbf{u}_2\mathbf{Q}+\mathbf{u}_2\mathbf{R} & 2\mathbf{u}_2\mathbf{q}_1 & -\mathbf{u}_2\mathbf{Q}-\mathbf{u}_2\mathbf{R} \\ -\mathbf{VQ}-\mathbf{VR} & -2\mathbf{Vq}_1 & \mathbf{VQ}+\mathbf{VR} \end{bmatrix}. \tag{4.27}$$

For Eq.(4.22) and Eq.(4.23) to hold simultaneously, the general solution is to set both $\mathbf{q}_1$ and $\mathbf{q}_2$ to $\mathbf{0}$. (Another solution is to choose $\mathbf{q}_1$, $\mathbf{u}_1$, and u_0 to be $\mathbf{0}$. However, annihilating $\mathbf{u}_1$ and u_0 automatically eliminates $\mathbf{q}_2$ from the set of free parameters.)

With $\mathbf{q}_1 = \mathbf{q}_2^T = \mathbf{0}$, the simplified factorization takes the following form

$$\mathbf{G}(z) = \frac{1}{4} \begin{bmatrix} \mathbf{U} & \mathbf{u}_1 & \mathbf{0} \\ \mathbf{u}_2 & u_0 & \mathbf{0} \\ \mathbf{0} & \mathbf{0} & \mathbf{V} \end{bmatrix} \begin{bmatrix} \mathbf{I}+z^{-1}\mathbf{I} & \mathbf{0} & \mathbf{I}-z^{-1}\mathbf{I} \\ \mathbf{0} & 2 & \mathbf{0} \\ \mathbf{I}-z^{-1}\mathbf{I} & \mathbf{0} & \mathbf{I}+z^{-1}\mathbf{I} \end{bmatrix}$$
$$\times \begin{bmatrix} \mathbf{Q} & \mathbf{0} & \mathbf{0} \\ \mathbf{0} & q_0 & \mathbf{0} \\ \mathbf{0} & \mathbf{0} & \mathbf{R} \end{bmatrix} \begin{bmatrix} \mathbf{I}+z^{-1}\mathbf{I} & \mathbf{0} & \mathbf{I}-z^{-1}\mathbf{I} \\ \mathbf{0} & 2z^{-1} & \mathbf{0} \\ \mathbf{I}-z^{-1}\mathbf{I} & \mathbf{0} & \mathbf{I}+z^{-1}\mathbf{I} \end{bmatrix}. \tag{4.28}$$

The two matrices containing delay elements z^{-1} can be factorized further as follows

$$\begin{bmatrix} \mathbf{I}+z^{-1}\mathbf{I} & \mathbf{0} & \mathbf{I}-z^{-1}\mathbf{I} \\ \mathbf{0} & 2 & \mathbf{0} \\ \mathbf{I}-z^{-1}\mathbf{I} & \mathbf{0} & \mathbf{I}+z^{-1}\mathbf{I} \end{bmatrix} = \begin{bmatrix} \mathbf{I} & \mathbf{0} & \mathbf{I} \\ \mathbf{0} & \sqrt{2} & \mathbf{0} \\ \mathbf{I} & \mathbf{0} & -\mathbf{I} \end{bmatrix} \begin{bmatrix} \mathbf{I} & \mathbf{0} & \mathbf{0} \\ \mathbf{0} & 1 & \mathbf{0} \\ \mathbf{0} & \mathbf{0} & z^{-1}\mathbf{I} \end{bmatrix} \begin{bmatrix} \mathbf{I} & \mathbf{0} & \mathbf{I} \\ \mathbf{0} & \sqrt{2} & \mathbf{0} \\ \mathbf{I} & \mathbf{0} & -\mathbf{I} \end{bmatrix}$$
$$\triangleq \mathbf{W}_{\mathrm{O}}\, \mathbf{\Lambda}_0(z)\, \mathbf{W}_{\mathrm{O}} \tag{4.29}$$
$$\begin{bmatrix} \mathbf{I}+z^{-1}\mathbf{I} & \mathbf{0} & \mathbf{I}-z^{-1}\mathbf{I} \\ \mathbf{0} & 2z^{-1} & \mathbf{0} \\ \mathbf{I}-z^{-1}\mathbf{I} & \mathbf{0} & \mathbf{I}+z^{-1}\mathbf{I} \end{bmatrix} = \begin{bmatrix} \mathbf{I} & \mathbf{0} & \mathbf{I} \\ \mathbf{0} & \sqrt{2} & \mathbf{0} \\ \mathbf{I} & \mathbf{0} & -\mathbf{I} \end{bmatrix} \begin{bmatrix} \mathbf{I} & \mathbf{0} & \mathbf{0} \\ \mathbf{0} & z^{-1} & \mathbf{0} \\ \mathbf{0} & \mathbf{0} & z^{-1}\mathbf{I} \end{bmatrix} \begin{bmatrix} \mathbf{I} & \mathbf{0} & \mathbf{I} \\ \mathbf{0} & \sqrt{2} & \mathbf{0} \\ \mathbf{I} & \mathbf{0} & -\mathbf{I} \end{bmatrix}$$
$$\triangleq \mathbf{W}_{\mathrm{O}}\, \mathbf{\Lambda}_1(z)\, \mathbf{W}_{\mathrm{O}}. \tag{4.30}$$

In both Eq.(4.29) and Eq.(4.30), all factors have trivial orthogonal inverses. Hence, further enforcement of the PR property on $\mathbf{G}(z)$ requires $\begin{bmatrix} \mathbf{U} & \mathbf{u}_1 \\ \mathbf{u}_2 & u_0 \end{bmatrix}$, $\mathbf{V}$, $\mathbf{Q}$, and $\mathbf{R}$ to be invertible while q_0 to be a nonzero scalar. Higher order systems can be constructed by cascading more $\mathbf{G}(z)$ stages:

$$\mathbf{E}(z) = \mathbf{G}_{K-1}(z)\, \mathbf{G}_{K-3}(z) \cdots \mathbf{G}_3(z)\, \mathbf{G}_1(z)\, \mathbf{E}_0, \qquad K \text{ odd}, \tag{4.31}$$

and the corresponding synthesis polyphase matrix is given by

$$\mathbf{R}(z) \;=\; \mathbf{E}_0^{-1}\, z^{-2}\mathbf{G}_1^{-1}(z)\, z^{-2}\mathbf{G}_3^{-1}(z)\, \cdots\, z^{-2}\mathbf{G}_{K-3}^{-1}(z)\, z^{-2}\mathbf{G}_{K-1}^{-1}(z). \tag{4.32}$$

Again, the starting block $\mathbf{E}_0$ of the cascade does not contain any delay; it represents the simplest LPPRFB with all filters of length M. The general solution for $\mathbf{E}_0$ is

$$\mathbf{E}_0 = \begin{bmatrix} \mathbf{U}_0 & \mathbf{u}_{01}\sqrt{2} & \mathbf{U}_0\mathbf{J} \\ \mathbf{u}_{02} & u_{00}\sqrt{2} & \mathbf{u}_{02}\mathbf{J} \\ -\mathbf{V}_0\mathbf{J} & \mathbf{0} & \mathbf{V}_0 \end{bmatrix} = \tfrac{1}{\sqrt{2}} \begin{bmatrix} \mathbf{U}_0 & \mathbf{u}_{01} & \mathbf{0} \\ \mathbf{u}_{02} & u_{00} & \mathbf{0} \\ \mathbf{0} & \mathbf{0} & \mathbf{V}_0 \end{bmatrix} \begin{bmatrix} \mathbf{I} & \mathbf{0} & \mathbf{J} \\ \mathbf{0} & \sqrt{2} & \mathbf{0} \\ -\mathbf{J} & \mathbf{0} & \mathbf{I} \end{bmatrix}, \tag{4.33}$$

where $\begin{bmatrix} \mathbf{U}_0 & \mathbf{u}_{01} \\ \mathbf{u}_{02} & u_{00} \end{bmatrix}$ and $\mathbf{V}_0$ need to be invertible. If a fast-computable transform is desired, $\mathbf{E}_0$ can be chosen as the $M \times M$ DCT coefficient matrix.

The full lattice structure for the analysis bank is depicted in Figure 19(a). The synthesis bank in Figure 19(b) is obtained from Eq.(4.32). In contrast to the even-channel case, the odd-channel lattice in Figure 19 is not complete; however, it is still minimal.

Theorem 4.18 *The factorization in Eq.(4.31) is minimal in term of the number of delay elements used in the FB's implementation.*

Proof.

This result comes right from the proof of Theorem 4.17. The degree of $\mathbf{E}(z)$ is $\frac{M(K-1)}{2}$ for both odd and even M. In our odd-channel solution, K is always odd; there are $\frac{K-1}{2}$ "double" building blocks $\mathbf{G}_i(z)$, each employs M delays ($\mathbf{\Lambda}_0(z)$ has $\frac{M-1}{2}$ while $\mathbf{\Lambda}_1(z)$ has

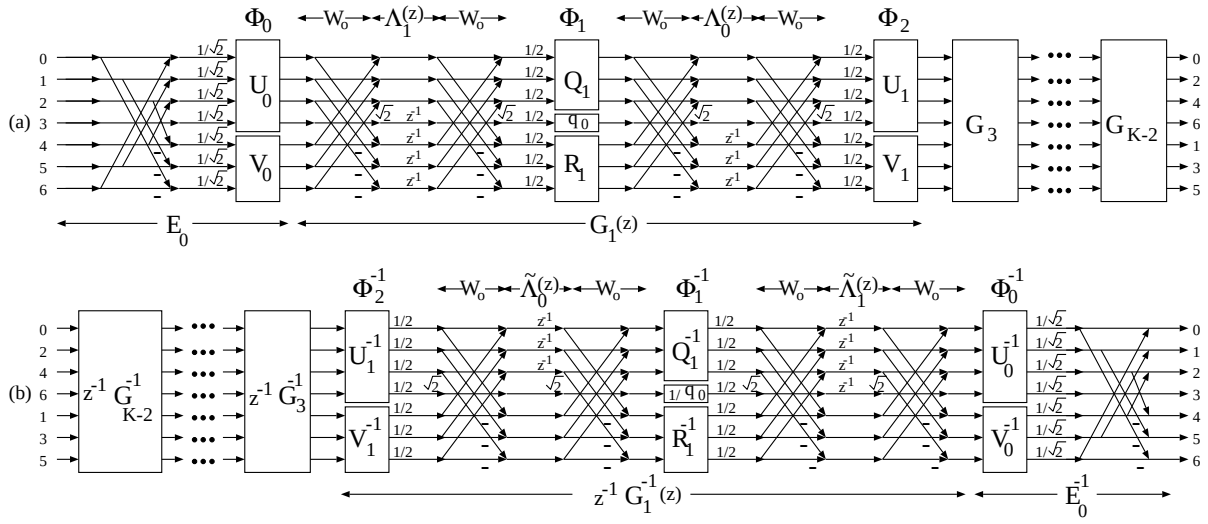

Figure 19: Lattice structure for odd-channel LPPRFBs. (a) Analysis bank. (b) Synthesis bank.

$\frac{M+1}{2}$ delays). Therefore, the total number of delays employed in the implementation is $\frac{M(K-1)}{2}$. □

Remarks. There is a couple of interesting side notes on the lattice in Figure 19. First, to construct odd-channel LPPUFBs (odd-channel GenLOTs), one simply has to choose all free-parameter matrices $\begin{bmatrix} \mathbf{U}_i & \mathbf{u}_{i1} \\ \mathbf{u}_{i2} & u_{i0} \end{bmatrix}$, $\mathbf{V}_i$, $\mathbf{Q}_i$, $\mathbf{R}_i$, and q_i in the propagating stages $\mathbf{G}_i(z)$ and the starting block $\mathbf{E}_0$ to be orthogonal. This choice turns out to be an alternate, but equivalent, form of the factorization presented earlier in [38]. Secondly, the curious readers will immediately ponder: what happens at the middle of the "double" structure? To answer that question, let us consider the simplest case where only half of

stage $\mathbf{G}(z)$ is involved, i.e.,

$$\mathbf{E}(z) = \begin{bmatrix} \mathbf{Q} & \mathbf{0} & \mathbf{0} \\ \mathbf{0} & q_0 & \mathbf{0} \\ \mathbf{0} & \mathbf{0} & \mathbf{R} \end{bmatrix} \begin{bmatrix} \mathbf{I}+z^{-1}\mathbf{I} & \mathbf{0} & \mathbf{I}-z^{-1}\mathbf{I} \\ \mathbf{0} & 2z^{-1} & \mathbf{0} \\ \mathbf{I}-z^{-1}\mathbf{I} & \mathbf{0} & \mathbf{I}+z^{-1}\mathbf{I} \end{bmatrix} \begin{bmatrix} \mathbf{U}_0 & \mathbf{u}_{01}\sqrt{2} & \mathbf{U}_0\mathbf{J} \\ \mathbf{u}_{02} & u_{00}\sqrt{2} & \mathbf{u}_{02}\mathbf{J} \\ -\mathbf{V}_0\mathbf{J} & \mathbf{0} & \mathbf{V}_0 \end{bmatrix} \tag{4.34}$$

The FB's corresponding transposed coefficient matrix ($\mathbf{P}^T$) is then

$$\begin{bmatrix} \mathbf{QU}_0-\mathbf{QV}_0\mathbf{J} & \mathbf{Qu}_{01} & \mathbf{QU}_0\mathbf{J}+\mathbf{QV}_0 & \mathbf{QU}_0+\mathbf{QV}_0\mathbf{J} & \mathbf{Qu}_{01} & \mathbf{QU}_0\mathbf{J}-\mathbf{QV}_0 \\ \mathbf{0} & \mathbf{0} & \mathbf{0} & q_0\mathbf{u}_{02} & q_0u_0 & q_0\mathbf{u}_{02}\mathbf{J} \\ \mathbf{RU}_0-\mathbf{RV}_0\mathbf{J} & \mathbf{Ru}_{01} & \mathbf{RU}_0\mathbf{J}+\mathbf{RV}_0 & -\mathbf{RU}_0-\mathbf{RV}_0\mathbf{J} & -\mathbf{Ru}_{01} & -\mathbf{RU}_0\mathbf{J}+\mathbf{RV}_0 \end{bmatrix}.$$

Interestingly, the FB still has PR because every factor in Eq.(4.34) is invertible. Furthermore, all filters still have LP as $\mathbf{P}^T$ indicates. The only trouble comes from the symmetric filter in the middle which turns out to have only M taps. This type of systems with filters of unequal lengths is outside the class of FB in consideration in this chapter.

4.5 Parameterization of Invertible Matrices

Up until this point, we are still evasive on how to parameterize invertible matrices. In the paraunitary case, each of the $N \times N$ orthogonal matrices $\mathbf{U}_i, \mathbf{V}_i$ containing the free parameters is completely characterized by $\frac{N(N-1)}{2}$ Givens rotations [62] as shown in Figure 6 (drawn for $M = 4$). This parameterization of the FB by rotation angles (called lattice coefficients) structurally enforces the LP and PR properties, i.e., in the lattice representation both LP and PR properties are retained regardless of coefficient quantization. From a design perspective, the lattice structure is a powerful FB design

tool since the lattice coefficients can be varied independently and arbitrarily without affecting the most desirable FB properties. Unconstrained optimization can be applied to obtain secondary features such as coding gain and stopband attenuation. From a practical perspective, the lattice provides a fast, efficient, and robust structure which is perfect for hardware implementation.

The difficulty in the biorthogonal case is obvious: how do we completely characterize a nonsingular square matrix $\mathbf{U}_i$ of size N? One naive solution is to choose $\mathbf{U}_i$'s elements as the lattice coefficients. However, there are many problems with this solution. First of all, it is difficult to guarantee exact reconstruction when the matrix elements are quantized. Secondly, this "parameterization" method does not provide a fast and efficient FB implementation. Furthermore, in order to obtain a high-performance FB, we have to synthesize the lattice by an optimization process to find the set of optimal (may be only local) lattice coefficients. This process typically involves thousands of iterative steps, so we have to face the costly matrix inversion problem. Finally, how can we prevent the optimization process from encountering singular or near-singular matrices?

To solve the aforementioned problems, we propose a parameterization method of invertible matrices by their singular value decompositions (SVD). Recall that every invertible matrix has an SVD representation: $\mathbf{U}_i = \mathbf{U}_{i0}\mathbf{\Gamma}_i\mathbf{U}_{i1}$, where $\mathbf{U}_{i0}$ and $\mathbf{U}_{i1}$ are orthogonal matrices, and $\mathbf{\Gamma}_i$ is a diagonal matrix with positive elements [25]. Thus, $\mathbf{U}_i$ of size N can be completely characterized by $N(N-1)$ rotation angles θ_i (from $\mathbf{U}_{i0}$, $\mathbf{U}_{i1}$) and $\frac{M}{2}$ diagonal multipliers α_i (from $\mathbf{\Gamma}_i$) as illustrated in Figure 20. Invertibility is guaranteed structurally under a mild condition – as long as none of the diagonal coefficients

α_i representing $\mathbf{\Gamma}_i$ is quantized to zero. Moreover, inverting $\mathbf{U}_i$ is now very fast, and singularity can be prevented by a simple cost function in the optimization process where a penalty is assigned whenever a diagonal coefficient (or its inverse) ventures too close to zero.

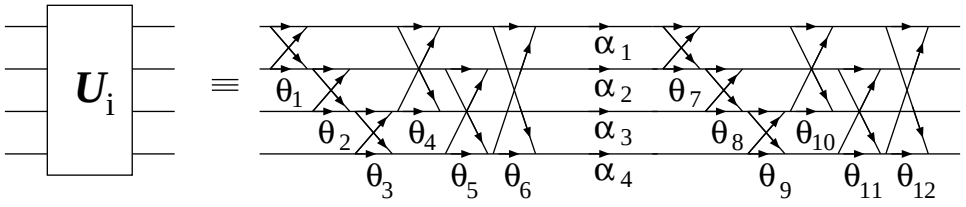

Figure 20: Parameterization of an invertible matrix.

In the even-channel case, under the SVD parameterization, $\mathbf{\Phi}_i$ can be further factorized as

$$\mathbf{\Phi}_i = \begin{bmatrix} \mathbf{U}_{i0} & \mathbf{0} \\ \mathbf{0} & \mathbf{V}_{i0} \end{bmatrix} \begin{bmatrix} \mathbf{\Gamma}_i & \mathbf{0} \\ \mathbf{0} & \mathbf{\Delta}_i \end{bmatrix} \begin{bmatrix} \mathbf{U}_{i1} & \mathbf{0} \\ \mathbf{0} & \mathbf{V}_{i1} \end{bmatrix}. \tag{4.35}$$

Again, the $\frac{M}{2} \times \frac{M}{2}$ orthogonal matrices $\mathbf{U}_{i0}$, $\mathbf{U}_{i1}$, $\mathbf{V}_{i0}$, and $\mathbf{V}_{i1}$ are parameterized by $\frac{M(M-2)}{8}$ rotations each. The diagonal matrices $\mathbf{\Gamma}_i$ and $\mathbf{\Delta}_i$ are characterized by $\frac{M}{2}$ positive parameters each. The detailed even-channel lattice structure is shown in Figure 21 (drawn for $M = 8$). Each of the K cascading blocks in the lattice (including $\mathbf{E}_0$) has $\frac{M^2}{2}$ degrees of freedom. Thus, the most general M-channel LPPRFB with filter length $L = KM$ (i.e., $M \times L$ GLBT) can be parameterized by $\frac{KM^2}{2} = \frac{LM}{2}$ parameters as expected from the most general LP systems. The classical trade-off between the FB's speed and performance can be elegantly carried out by setting some of the diagonal multipliers to 1 or some of the rotation angles to 0.

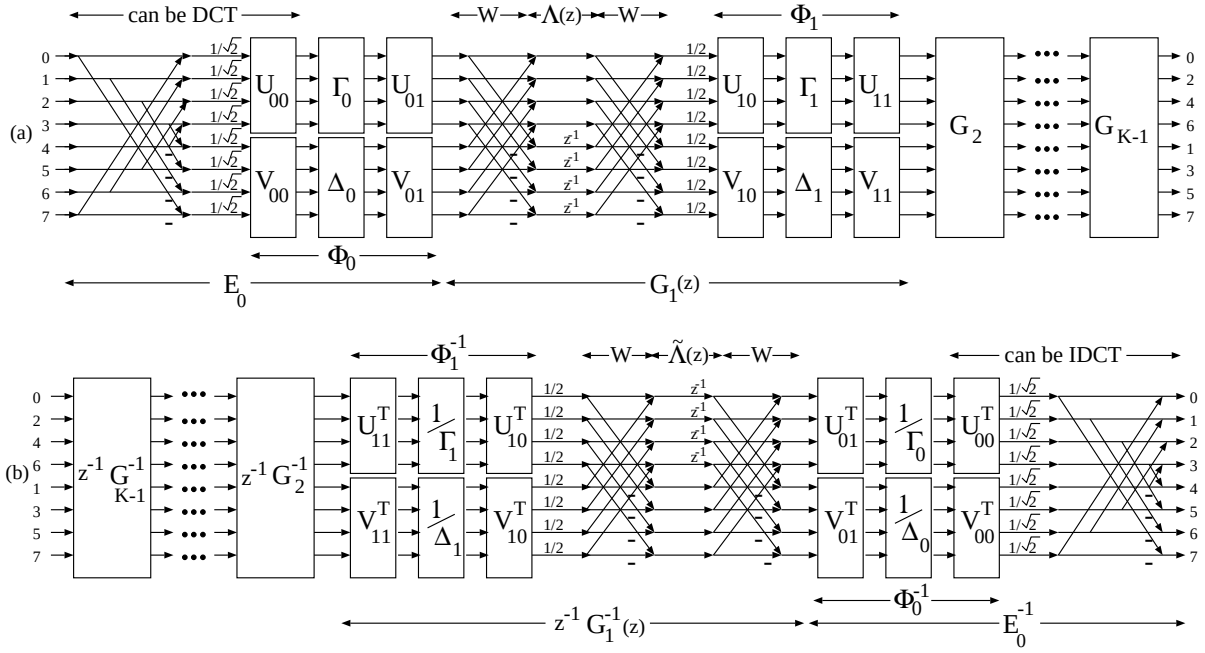

Figure 21: Detailed lattice structure for even-channel LPPRFBs. (a) Analysis bank. (b) Synthesis bank.

It is also very interesting to verify that all previously reported even-channel LPPRFB's lattice structures are special cases of the new lattice. For examples, the GLT design example in [7] has $M = 8, K = 2$, $\mathbf{U}_{00}$ and $\mathbf{V}_{00}$ from the DCT; $\mathbf{U}_{01} = \mathbf{V}_{01} = \mathbf{\Gamma}_0 = \mathbf{\Delta}_0 = \mathbf{I}$; $\mathbf{U}_1$ and $\mathbf{V}_1$ parameterized as a cascade of block diagonal matrices. The LBT in [48] has $M = 8, K = 2$, $\mathbf{U}_{00}$ and $\mathbf{V}_{00}$ from the DCT, $\mathbf{U}_{01} = \mathbf{V}_{01} = \mathbf{\Gamma}_0 = \mathbf{I}$, $\mathbf{\Delta}_0 = diag[\sqrt{2}\ \ 1\ \ 1\ \ 1]$, and $\mathbf{U}_1$, $\mathbf{V}_1$ orthogonal. When orthogonality is imposed, we get back GenLOT [62]. The popular case of $M = 2$ that leads to biorthogonal wavelets deserves more attention in Section 4.6.

Needless to mention, the odd-channel case is much more complicated. An order-2 stage $\mathbf{G}_i(z)$ contains $(\frac{M+1}{2})^2 + 3(\frac{M-1}{2})^2 + 1 = (M^2 - M + 2)$ free parameters whereas

$\mathbf{E}_0$ has $(\frac{M+1}{2})^2 + (\frac{M-1}{2})^2 = \frac{M^2+1}{2}$. Since there are $\frac{M+1}{2}$ symmetric filters, $\frac{M-1}{2}$ antisymmetric filters, and all of them have LP, the most general solution is expected to have $(\frac{M+1}{2})(\frac{KM+1}{2}) + (\frac{M-1}{2})(\frac{KM-1}{2}) = \frac{KM^2+1}{2}$ free parameters. Subtracting $\frac{M^2+1}{2}$ parameters which belong to the initial stage $\mathbf{E}_0$, each stage $\mathbf{G}_i(z)$ (there are $\frac{K-1}{2}$ of them) should possess M^2 degrees of freedom. In our proposed solution in the previous section, each stage is off by $(M-2)$ parameters.

4.6 2-Channel LPPRFB Revisited

When $M = 2$, the orthogonal matrices $\mathbf{U}_{i0}$, $\mathbf{V}_{i0}$ degenerate to singleton 1 or -1. The only free parameters come from the diagonal elements α_{i0} and α_{i1} from $\mathbf{\Gamma}_i$ and $\mathbf{\Delta}_i$. The resulting lattice for 2-channel LPPRFB is presented in Figure 22.

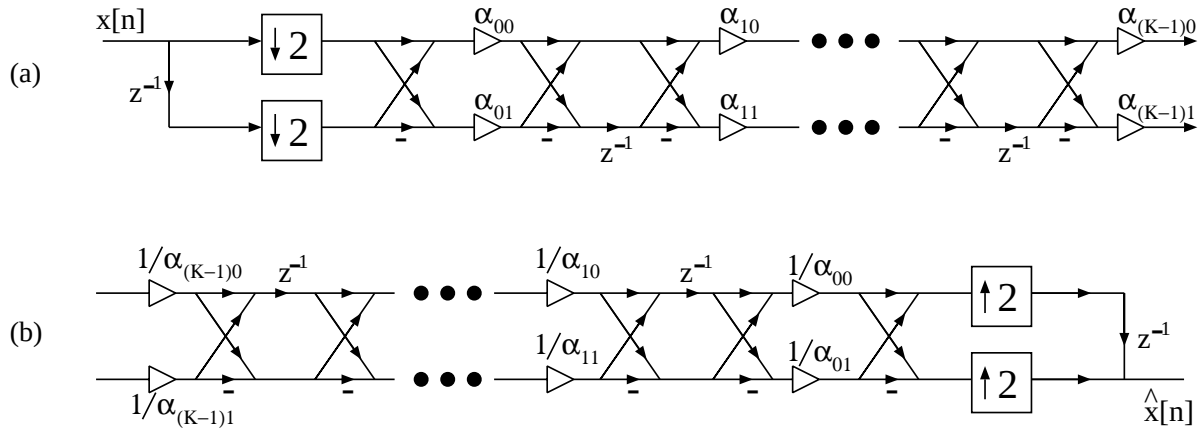

Figure 22: Lattice structure for 2-channel LPPRFBs. (a) Analysis bank. (b) Synthesis bank.

It is a nice, simple exercise to show that the lattice in Figure 22 is a modular and slightly more general form of the famous Type-A system lattice introduced by Nguyen

and Vaidyanathan [53]. The propagating property is now linear phase instead of time-reversal. The coefficients k_i in the type-A lattice can be shown to be simply $\frac{\alpha_{i0} - \alpha_{i1}}{\alpha_{i0} + \alpha_{i1}}$. Moreover, the authors of [53] have chosen to normalize their lattice by enforcing the condition $\alpha_{i0} + \alpha_{i1} = 1$.

From a casual glance, the four filters $H_0(z)$, $H_1(z)$, $F_0(z)$, and $F_1(z)$ seem not to follow the classical "alternating sign" properties: $F_0(z) = H_1(-z)$ and $F_1(z) = -H_0(-z)$. However, a more careful examination shows that $F_0(z)$ and $H_1(-z)$, $F_1(z)$ and $-H_0(-z)$ are only off by a scaling parameter. Hence, the aliasing cancellation condition in Eq.(2.14) and the distortion elimination condition in Eq.(2.15) are still satisfied. In fact, it can be shown that the scaling disappears when we enforce the following condition on the lattice coefficients: $\prod_{i=1}^{K-1} \alpha_{i0}\, \alpha_{i1} = 1$.

The elegant lattice in Figure 22 lends itself nicely to various practical constraints. For instance, a nice feature that generates a lot of research interests is that the FB coefficients are dyadic rationals [78], [77], [6]. Such FBs can be implemented by pure shift-and-add operations, leading to low-power, multiplierless systems in VLSI. Furthermore, these transform can map integers to integers, a crucial requirement for lossless image coding. Obtaining dyadic-rational coefficients from the 2-channel lattice in Figure 22 is trivial. We simply have to pick the lattice coefficients $\{ \alpha_{i0}, \alpha_{i1} \}$ from the set of powers of two $\{ 2^i, i \in \mathcal{Z} \}$. More generally, the lattice can realize rational-coefficient LPPRFBs by restricting $\{ \alpha_{i0}, \alpha_{i1} \}$ as rational numbers.

As another example, arbitrary degrees of regularity (vanishing moments) can be enforced directly upon the set of of lattice coefficients. This is the novel concept of *regularity*

robustness, i.e., wavelets in the lattice representation still retains the smoothness of its scaling and wavelet functions regardless of coefficient quantization. To illustrate the idea, let us consider a 2-channel LPPRFB where all filters have length 4. From Figure 22, one can easily (but tediously) arrive at the following filter coefficients in close forms:

$$\begin{aligned}
h_0[n] &= \tfrac{1}{2\sqrt{2}}\,[\alpha_{10}(\alpha_{00}-\alpha_{01})\ \ \alpha_{10}(\alpha_{00}+\alpha_{01})\ \ \alpha_{10}(\alpha_{00}+\alpha_{01})\ \ \alpha_{10}(\alpha_{00}-\alpha_{01})] \\
h_1[n] &= \tfrac{1}{2\sqrt{2}}\,[-\alpha_{11}(\alpha_{00}-\alpha_{01})\ \ -\alpha_{11}(\alpha_{00}+\alpha_{01})\ \ \alpha_{11}(\alpha_{00}+\alpha_{01})\ \ \alpha_{11}(\alpha_{00}-\alpha_{01})] \\
f_0[n] &= \tfrac{1}{2\sqrt{2}}\,[\tfrac{1}{\alpha_{10}}(\tfrac{1}{\alpha_{00}}-\tfrac{1}{\alpha_{01}})\ \ \tfrac{1}{\alpha_{10}}(\tfrac{1}{\alpha_{00}}+\tfrac{1}{\alpha_{01}})\ \ \tfrac{1}{\alpha_{10}}(\tfrac{1}{\alpha_{00}}+\tfrac{1}{\alpha_{01}})\ \ \tfrac{1}{\alpha_{10}}(\tfrac{1}{\alpha_{00}}-\tfrac{1}{\alpha_{01}})] \\
f_1[n] &= \tfrac{1}{2\sqrt{2}}\,[\tfrac{1}{\alpha_{11}}(\tfrac{1}{\alpha_{00}}-\tfrac{1}{\alpha_{01}})\ \ \tfrac{1}{\alpha_{11}}(\tfrac{1}{\alpha_{00}}+\tfrac{1}{\alpha_{01}})\ \ -\tfrac{1}{\alpha_{11}}(\tfrac{1}{\alpha_{00}}+\tfrac{1}{\alpha_{01}})\ \ -\tfrac{1}{\alpha_{11}}(\tfrac{1}{\alpha_{00}}-\tfrac{1}{\alpha_{01}})].
\end{aligned} \tag{4.36}$$

Enforcing three vanishing moments as described in Eq.(2.18) onto the synthesis lowpass filter $f_0[n]$ leads to the constraint $\alpha_{01} = 2\alpha_{00}$. The filters in Eq.(4.36) then become

$$\begin{aligned}
h_0[n] &= \tfrac{1}{2\sqrt{2}}\,[-\alpha_{10}\alpha_{00}\ \ 3\alpha_{10}\alpha_{00}\ \ 3\alpha_{10}\alpha_{00}\ \ -\alpha_{10}\alpha_{00}] \\
h_1[n] &= \tfrac{1}{2\sqrt{2}}\,[\alpha_{11}\alpha_{00}\ \ -3\alpha_{11}\alpha_{00}\ \ 3\alpha_{11}\alpha_{00}\ \ -\alpha_{11}\alpha_{00}] \\
f_0[n] &= \tfrac{1}{2\sqrt{2}}\,[\tfrac{1}{2\alpha_{10}\alpha_{00}}\ \ \tfrac{3}{2\alpha_{10}\alpha_{00}}\ \ \tfrac{3}{2\alpha_{10}\alpha_{00}}\ \ \tfrac{1}{2\alpha_{10}\alpha_{00}}] \\
f_1[n] &= \tfrac{1}{2\sqrt{2}}\,[\tfrac{1}{2\alpha_{11}\alpha_{00}}\ \ \tfrac{3}{2\alpha_{11}\alpha_{00}}\ \ -\tfrac{3}{2\alpha_{11}\alpha_{00}}\ \ -\tfrac{1}{2\alpha_{11}\alpha_{00}}].
\end{aligned} \tag{4.37}$$

The synthesis scaling function has three vanishing moments independent of the values of α_{00}, α_{10}, and α_{11} (as long as they are not zeros or infinity). These three lattice coefficients can be chosen as dyadic rationals to realize nice integer-coefficient transforms. This section once again confirms the tremendous flexibility and generality of the SVD-based lattice in Figure 21.

4.7 Design

4.7.1 Filter Bank Optimization

Any realization of the lattice coefficient set $\{\theta_i, \alpha_i\}$ in the previous two sections results in an LPPR system. However, for the FB to have high practical value, several other properties are also needed. High-performance FBs can be obtained using unconstrained nonlinear optimization where the lattice coefficients are the free parameters. Some of the popular criteria in FB optimization are: coding gain, DC leakage, attenuation around mirror frequencies, and stopband attenuation. In the particular field of image compression, all of these criteria are well-known desired properties in yielding the best reconstructed image quality [77], [66]. The cost function in the optimization process can be a weighted linear combination of these measures as follows

$$\begin{aligned} C_{\text{overall}} &= \alpha_1 C_{\text{coding gain}} + \alpha_2 C_{\text{DC}} + \alpha_3 C_{\text{mirror}} \\ &\quad + \alpha_4 C_{\text{analysis stopband}} + \alpha_5 C_{\text{synthesis stopband}}. \end{aligned} \tag{4.38}$$

Coding Gain

The coding gain of a transform is defined as the reduction in transform coding mean-square error over pulse-code modulation (PCM) which simply quantizes the samples of the signal with the desired number of bits per sample. Define σ_x^2 as the variance of the input signal $x[n]$, $\sigma_{x_i}^2$ as the variance of the i-th subband, and $||f_i||^2$ as the $\mathcal{L}^2$ norm of the i-th synthesis filter. With several assumptions including scalar quantization and a

sufficient large bit rate, the generalized coding gain can be formulated as [34], [32]:

$$C_{\text{coding gain}} = 10 \log_{10} \frac{\sigma_x^2}{\left(\prod_{i=0}^{M-1} \sigma_{x_i}^2 ||f_i||^2 \right)^{\frac{1}{M}}}. \tag{4.39}$$

The signal $x[n]$ is the commonly-used AR(1) process with intersample autocorrelation coefficient $\rho = 0.95$ [47]. The coding gain can be thought of as an approximate measure of the transform's energy compaction capability. Among the listed criteria, higher coding gain correlates most consistently with higher objective performance (measured in MSE or PSNR). Transforms with higher coding gain compact more energy into a fewer number of coefficients, and the more significant bits of those coefficients always get transmitted first in the progressive transmission framework employed in Chapter 7.

Low DC Leakage

The DC leakage cost function measures the amount of DC energy that leaks out to the bandpass and highpass subbands. The main idea is to concentrate all signal energy at DC into the DC coefficients. This proves to be advantageous in both signal decorrelation and in the prevention of discontinuities in the reconstructed signals. Low DC leakage can prevent the annoying checkerboard artifact that usually occurs when high frequency bands are severely quantized [77]. This problem is more troublesome in traditional block transform coders because high frequency bands are usually more coarsely quantized. The DC cost function is defined as

$$C_{\text{DC}} = \sum_{i=1}^{M-1} \sum_{n=0}^{L-1} h_i[n]. \tag{4.40}$$

The readers should note that all antisymmetric filters have a zero at DC. Therefore, the above formula only needs to apply to symmetric filters to reduce the complexity of the optimization process.

Attenuation at mirror frequencies

The mirror frequency cost function is a generalization of $C_{\rm DC}$. The concern is now at every aliasing frequencies $\omega_m = \frac{2\pi m}{M},\ m \in \mathcal{Z},\ 1 \leq m \leq \frac{M}{2}$. Ramstad *et al* show that frequency attenuation at mirror frequencies are very important in the further reduction of blocking artifacts: the filter responses should be small at these mirror frequencies as well [66]. The corresponding cost function is:

$$C_{\rm mirror} = \sum_{i=0}^{M-1} |H_i(e^{j\omega_m})|^2, \quad \omega_m = \frac{2\pi m}{M}, \quad 1 \leq m \leq \frac{M}{2}. \tag{4.41}$$

Low DC leakage and high attenuation near the mirror frequencies are not as essential to the coder's objective performance as coding gain. However, they do improve the visual quality of the reconstructed image significantly.

Stopband Attenuation

Stopband attenuation of the filters is a classical performance criterion in filter design. In this dissertation, the stopband attenuation criterion measures the sum of all of the filters' energy outside the designated passbands:

$$C_{\rm analysis\ stopband} = \sum_{i=0}^{M-1} \int_{\omega \in \Omega_{stopband}} W_i^a(e^{j\omega})\ |H_i(e^{j\omega})|^2 d\omega \tag{4.42}$$

$$C_{\rm synthesis\ stopband} = \sum_{i=0}^{M-1} \int_{\omega \in \Omega_{stopband}} W_i^s(e^{j\omega})\ |F_i(e^{j\omega})|^2 d\omega. \tag{4.43}$$

In the analysis bank, the stopband attenuation cost helps in improving the signal decorrelation and decreasing the amount of aliasing. In meaningful images, we know *a priori* that most of the energy is concentrated in low frequency region. Hence, high stopband attenuation in this part of the frequency spectrum becomes extremely desirable. In the synthesis bank, the reverse is true. Synthesis filters covering low-frequency bands need to have high stopband attenuation near and/or at $\omega = \pi$ to enhance their smoothness. The biased weighting can be enforced using two simple functions $W_i^a(e^{j\omega})$ and $W_i^a(e^{j\omega})$ as shown in Eq.(4.43).

Initialization

All design examples presented in this dissertation are obtained from the multi-variable nonlinear optimization routine *simplex* [52] in Matlab. To initialize the lattice, we set the matrices containing the free parameters ($\mathbf{U}_i$ and $\mathbf{V}_i$) to either $\mathbf{I}$ or $-\mathbf{I}$. More specifically, the rotation angles θ_i are initialized to either 0 or π, whereas the diagonal multipliers α_i are all initialized to 1.

4.7.2 Design Examples

Figure 23 – 29 present several design examples obtained from nonlinear optimization of the new lattice coefficients with various cost functions. Depicted in Figure 23 is design example I with 4 channels and 8-tap filters. Figure 24 shows design example II, an 8-channel LPPRFB with 16-tap filters (8×16 GLBT). In Figure 25 is design example III with 16 channels and filter length of 32 (16×32 GLBT). All three FBs are DCT-based

and are obtained from a combinatorial cost function where the coding gain is given the highest priority. Design examples I–III illustrate the tremendous degree of flexibility that the new biorthogonal class of LTs enjoys over its orthogonal relatives in previous works [62], [75], [80]. The analysis bank is designed to maximize coding gain, minimize the DC leakage, and minimize the stopband attenuation in low frequency bands where there is usually a high concentration of image energy. On the other hand, the synthesis bank is designed to have its filters decaying asymptotically to zero to completely eliminate blocking artifacts. Furthermore, the stopband attenuation in high frequency synthesis bands is also minimized so that the resulting synthesis filters are generally smooth, leading to more visually-pleasant reconstructed images.

The 8×16 GLBT in design example II, if optimized for pure coding gain, can attain 9.63 dB which equals the coding gain reported on optimal biorthogonal systems in [1]. However, the 8×16 LBT in [1] was obtained by a direct constrained optimization on the filter coefficients, so it might only be near-PR and it certainly does not have a fast, efficient, and robust implementation. In design example II, 0.01 dB of coding gain has been sacrificed for high attenuation at DC, near DC, and at mirror frequencies to ensure a high level of perceptual performance in image coding. In the 16×32 case, our GLBT in Figure 25 achieves an impressive coding gain of 9.96 dB.

GLBT design examples with longer filter length are shown in Figure 26 and Figure 27. While increasing the GLBT length only improves the coding gain marginally (see design example IV in Figure 26), it helps tremendously in the case of stopband attenuation (where longer filters are always beneficial) as testified by design example V in Figure 27.

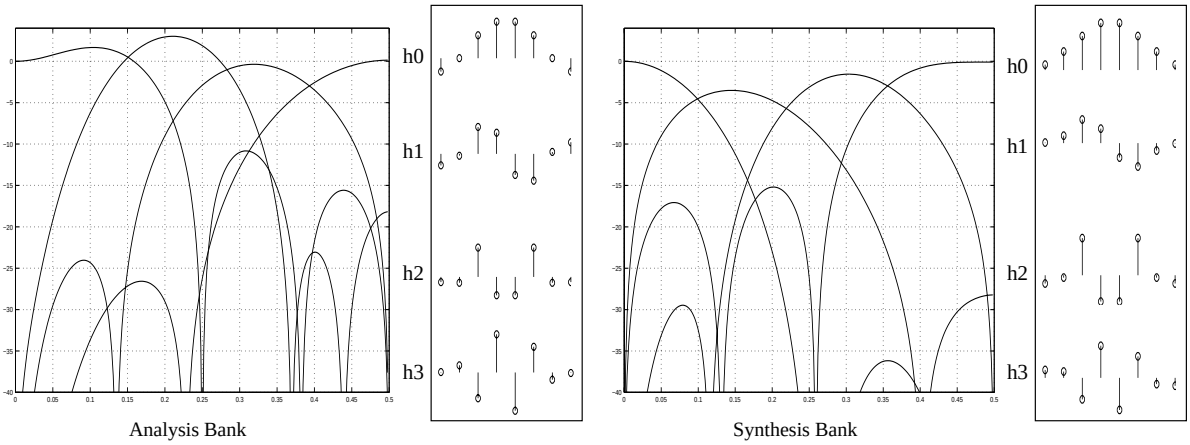

Figure 23: Design example I: $M = 4$ $L = 8$ optimized for coding gain, DC attenuation, mirror frequency attenuation, and stopband attenuation.

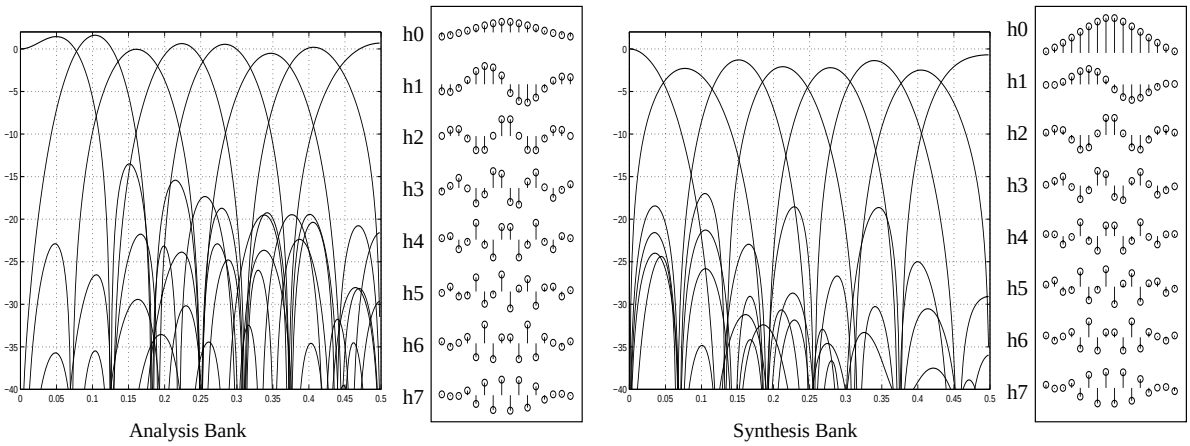

Figure 24: Design example II: $M = 8$ $L = 16$ optimized for coding gain, DC attenuation, mirror frequency attenuation, and stopband attenuation.

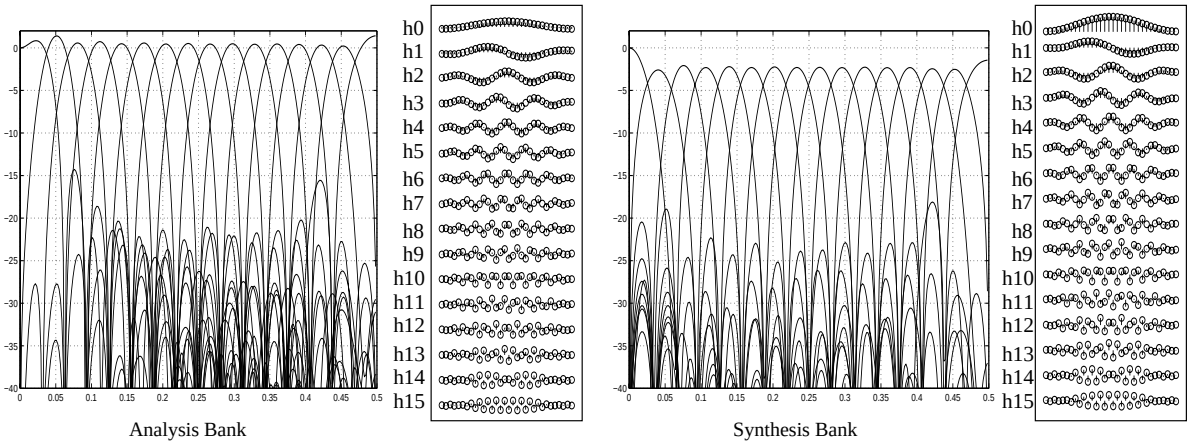

Figure 25: Design example III: $M = 16$ $L = 32$ optimized for coding gain, DC attenuation, mirror frequency attenuation, and stopband attenuation.

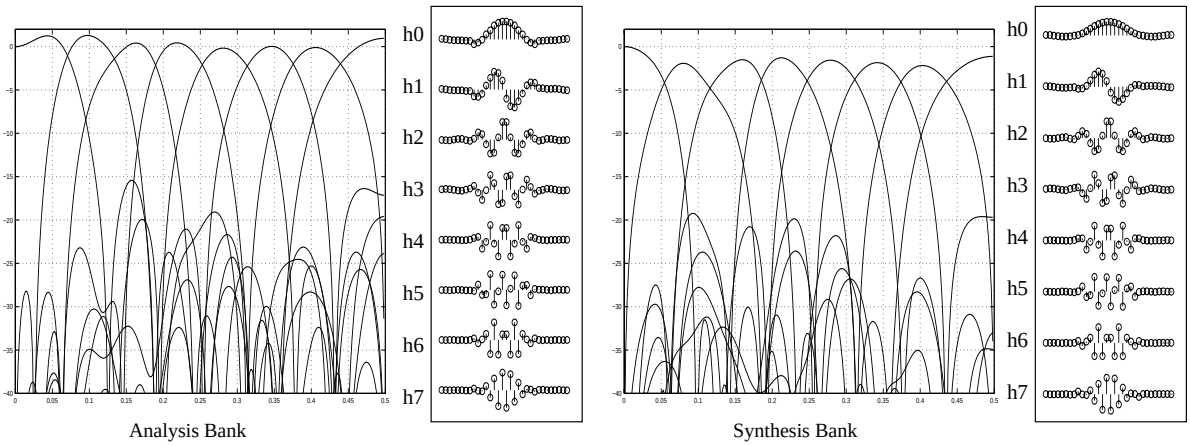

Figure 26: Design example IV: $M = 8$ $L = 32$ optimized for coding gain, DC attenuation, mirror frequency attenuation, and stopband attenuation.

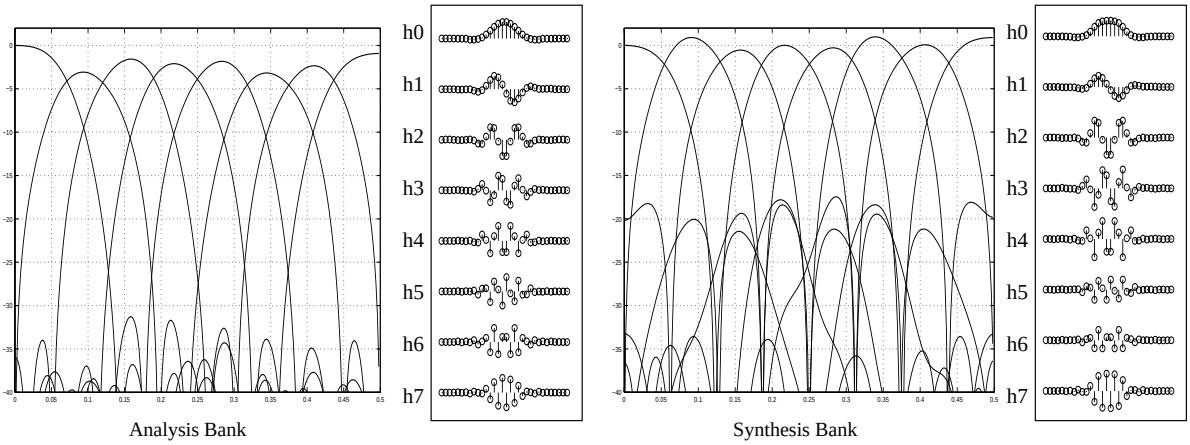

Figure 27: Design example V: $M = 8 \quad L = 32$ optimized for stopband attenuation of analysis bank only.

Two odd-channel FBs are presented in Figure 28 and Figure 29. Design example VI in Figure 28 is a 7-channel 21-tap LPPRFB optimized for maximum coding gain and high stopband attenuation near DC for the analysis bank and near π for the synthesis bank. Hence, the synthesis basis functions are much smoother than the analysis. Design example VII in Figure 29 has 5 channels and filters of 15 taps, optimized for coding gain and DC attenuation. Important properties of several high-performance design examples are compiled in Table 3; the DCT [67], the LOT [47], and the 8×40 GenLOT [89] are included for comparison purposes.

Transform Property	Transform							
	8x8 DCT	8x16 LOT	8x40 GenLOT	8x16 GLBT (II)	16x32 GLBT (III)	8x32 GLBT (IV)	8x32 GLBT (V)	7x21 GLBT (VI)
Coding Gain (dB)	8.83	9.22	9.52	9.62	9.96	9.63	9.33	9.50
DC Attenuation (-dB)	310.62	312.56	322.10	327.40	303.32	327.57	35.92	37.94
Stopband Attenuation (-dB)	9.96	19.38	16.18	13.50	14.28	15.43	31.27	11.97
Mirror Freq. Attenuation (-dB)	322.10	317.24	317.24	55.54	302.35	43.84	23.83	16.45

Table 3: Comparison of transform properties ($L = KM$).

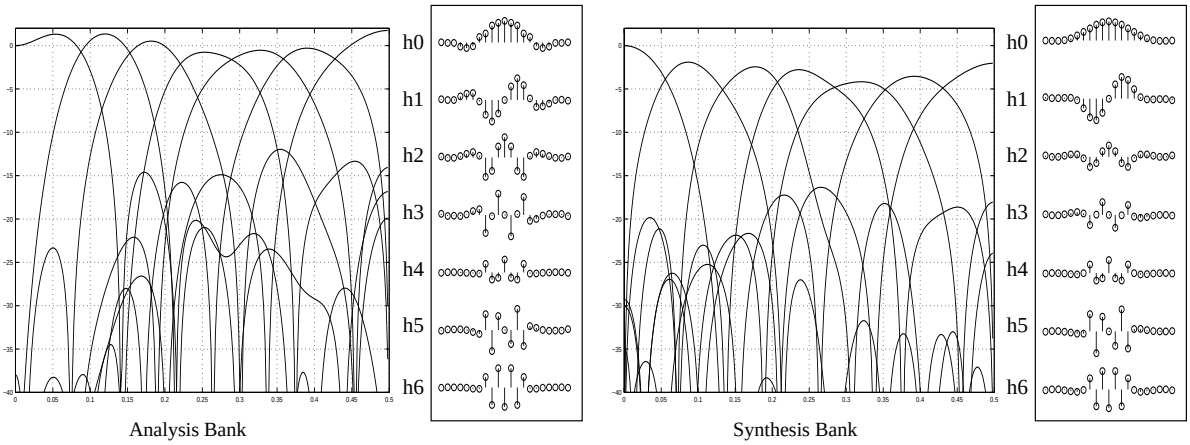

Figure 28: Design example VI: $M = 7 \;\; L = 21$ optimized for coding gain and stopband attenuation.

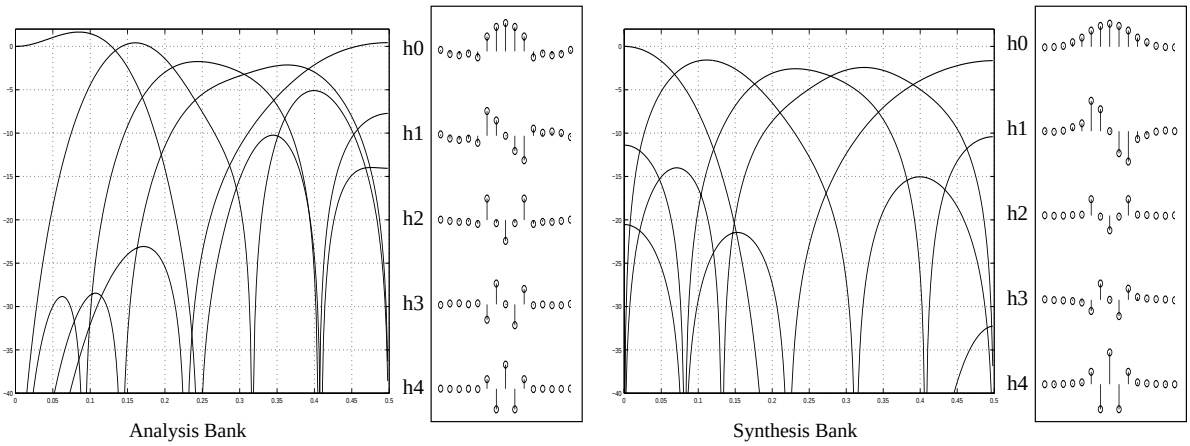

Figure 29: Design example VII: $M = 5 \;\; L = 15$ optimized for coding gain and DC attenuation.

4.8 Summary

We have presented in this chapter general lattice structures for M-channel LPPRFBs with all analysis and synthesis filters of the same length $L = KM$. The novel lattices based on the SVD provide fast, robust, modular implementations and a friendly design procedure for all LP lapped transforms with arbitrary integer overlapping factor K. In the popular even-channel case, the lattice is proven to completely span the set of all possible solutions. We also prove that the proposed lattice structures are minimal in term of the number of delays employed in its implementation for both even and odd number of channels. The relaxation of the orthogonal constraint gives the novel biorthogonal LPFB a whole new dimension of flexibility: the analysis and the synthesis bank can now be tailored appropriately to fit a particular application. Especially in image compression application, the analysis bank can be optimized for maximum energy compaction while the synthesis filters are designed to have a high degree of smoothness. In the progressive image coding example presented later in Chapter 7, we shall demonstrate that the M-channel LPPRFBs presented in this chapter offer the highest coding performances up to date.

Chapter 5

Lapped Transforms of Arbitrary Block Size

5.1 Introduction

In Chapter 4, the term "generalized" in the GLBT is somewhat of a misnomer. The elegant lattices in Figure 18 and Figure 19 can only realize systems with filter length KM. They are certainly not as general as claimed. This length restriction may confine to some extent the flexibility in the system design and implementation. Extending the filter length from KM to $KM + \beta$ provides more degrees of freedom in fine-tuning the filters to meet certain design specification, stopband attenuation for instance, with the lowest level of transform complexity. In all of the previous work on lapped transforms [45], [46], [47], [75], [62] and even in Chapter 4, the step size in increasing the filter length is at least M. Hence, the number of overlapping samples is always a multiple of the number of channels. It is quite natural to ponder whether this is a necessary and/or a reasonable requirement. What happens if one would like to overlap the blocking window by one, two, or any arbitrary number of samples?

The KM length restriction is also not very convenient when the number of channels M is large (say, 16 or 32). From a design point of view, a large increase in length means a higher-dimension non-linear parameter space to be searched and the optimization program tends to be more easily trapped in local minima. From an implementation point of view, a large increase in filter length translates to a much higher computational complexity. This calls for the development of LPPRFBs with arbitrary-length filters, or LTs of arbitrary block size.

A step towards designing the most general LT is taken in this chapter. In other words, M-channel LPPRFBs with filter length $L = KM + \beta$, $\beta \in \mathcal{Z}$, $0 \leq \beta < M-1$, are studied in depth. Similarly to the approach in Chapter 4, we shall first confirm the generality of the LP-propagation structure $\mathbf{G}(z)$ in Theorem 4.13 for the subclass of LPPRFB in consideration. Exploiting this result, we next derive a complete and minimal factorization for all even-channel solutions. This is the most general LT ever reported in the literature. Several design examples obtained from the novel lattice structure are presented. They are compared to the GenLOT [62] and the GLBT [83] in Chapter 4 (both are special cases when $\beta = 0$) in coding gain, stopband attenuation, and attenuation at DC as well as around mirror frequencies.

5.2 Existence conditions

Throughout this chapter, the class of M-channel FB under investigation still possesses all of the properties in the Problem Formulation section of Chapter 4. The only difference

is that all of the filters now have length $L = KM + \beta$ instead of $L = KM$. Most of the results in this chapter are limited to the popular even-channel case. Before deriving any lattice structure, let us first investigate the possible existence of the solutions.

Theorem 5.19 *Even-channel odd-length LPPRFB does not exist. Odd-channel even-length LPPRFB does not exist.*

Proof.

The proof is readily obtained from the permissible conditions in Table 2. If M is even and all filters have the same odd length L, then β is odd and $K_i = K$. Hence, $\sum_{i=0}^{M-1} K_i = MK$, which has to be even, contradicting the requirement that $\sum_{i=0}^{M-1} K_i$ is odd. We can also use the result of Corollary 3.12 directly: the sum of all filter lengths ML is an odd multiple of M, contradicting with the necessary restriction that the sum of length must be an even multiple of the number of channels for even-channel systems. Therefore, even-channel LPPRFBs with filters having the same length $L = KM + \beta$ only exist if the filter length is even. The length increment must be at least two taps at a time. In the LT language, the number of overlapping samples must be even.

Similarly, for odd-channel LPPRFBs, if all filters have the same even length, the sum of length cannot be odd as required. Odd-channel LPPRFBs with filters having the same length $L = KM + \beta$ only exist if the filter length is odd. □

5.3 General Lattice Structure

It can easily be shown that the same approach in Chapter 4 (propagating the LP and PR properties) can be applied to the new class of LPPRFB to obtain a similar factorization of the polyphase matrices.

Theorem 5.20 *Suppose there exists an M-channel FIR LPPRFB with all analysis and synthesis filters of length* $L = KM + \beta$ *with the associated polyphase matrix* $\mathbf{F}(z)$. *Define* $\mathbf{E}(z) \triangleq \mathbf{G}(z)\mathbf{F}(z)$ *where the propagating structure is* $\mathbf{G}(z)$ *of order* N, *i.e.,* $\mathbf{G}(z) = \sum_{i=0}^{N} \mathbf{A}_i z^{-i}$. *Then,* $\mathbf{E}(z)$ *has LP and PR if and only if*

- $\mathbf{G}(z)$ *is FIR invertible.*
- $\mathbf{G}(z)$ *takes the form* $\mathbf{G}(z) = z^{-N}\,\mathbf{D}\,\mathbf{G}(z^{-1})\,\mathbf{D}$.
- $\mathbf{A}_i = \mathbf{D}\,\mathbf{A}_{N-i}\,\mathbf{D}$.

Proof.

Theorem 5.20 is a straightforward extension of Theorem 4.13. The condition that $\mathbf{G}(z)$ is FIR invertible can be easily and immediately established. The lone difference between the two theorems lies at the altered form of the polyphase matrices. With the extra β taps in length, the LP property of $\mathbf{F}(z)$ and $\mathbf{E}(z)$ in Eq.(3.3) becomes

$$\begin{aligned} \mathbf{F}(z) &= z^{-(K-1)}\,\mathbf{D}\,\mathbf{F}(z^{-1})\,\hat{\mathbf{J}}(z) \\ \mathbf{E}(z) &= z^{-(K+N-1)}\,\mathbf{D}\,\mathbf{E}(z^{-1})\,\hat{\mathbf{J}}(z), \end{aligned}$$

where

$$\hat{\mathbf{J}}(z) \;=\; \begin{bmatrix} z^{-1}\mathbf{J}_{\beta} & \mathbf{0}_{\beta\times(M-\beta)} \\ \mathbf{0}_{(M-\beta)\times\beta} & \mathbf{J}_{M-\beta} \end{bmatrix}.$$

However, $\hat{\mathbf{J}}(z)$ does not affect the form of $\mathbf{G}(z)$ in Theorem 4.13 as far as propagating the LP property is concerned

$$\begin{aligned}
& \mathbf{E}(z) \;=\; z^{-(K+N-1)}\,\mathbf{D}\,\mathbf{E}(z^{-1})\,\hat{\mathbf{J}}(z) \\
\Longleftrightarrow\quad & \mathbf{E}(z) \;=\; z^{-(K+N-1)}\,\mathbf{D}\,\mathbf{G}(z^{-1})\,\mathbf{F}(z^{-1})\,\hat{\mathbf{J}}(z) \\
\Longleftrightarrow\quad & \mathbf{E}(z) \;=\; z^{-N}\,\mathbf{D}\,\mathbf{G}(z^{-1})\,z^{-(K-1)}\,\mathbf{F}(z^{-1})\,\hat{\mathbf{J}}(z) \\
\Longleftrightarrow\quad & \mathbf{E}(z) \;=\; z^{-N}\,\mathbf{D}\,\mathbf{G}(z^{-1})\,\mathbf{D}\,z^{-(K-1)}\,\mathbf{D}\,\mathbf{F}(z^{-1})\,\hat{\mathbf{J}}(z) \\
\Longleftrightarrow\quad & \mathbf{E}(z) \;=\; z^{-N}\,\mathbf{D}\,\mathbf{G}(z^{-1})\,\mathbf{D}\,\mathbf{F}(z).
\end{aligned}$$

Therefore, similarly to what we have discovered in the previous chapter, it is necessary and sufficient that $\mathbf{G}(z) = z^{-N}\,\mathbf{D}\,\mathbf{G}(z^{-1})\,\mathbf{D}$ for $\mathbf{E}(z)$ to have LP. The last condition on the symmetry of $\mathbf{A}_i$ follows trivially from the above form of $\mathbf{G}(z)$. □

With the result from Theorem 5.20, we can construct high-order even-channel LP-PRFBs analogously to the cascade structure in Eq.(4.7). The polyphase matrix of the analysis bank is

$$\mathbf{E}(z) \;=\; \mathbf{G}_{K-1}(z)\,\mathbf{G}_{K-2}(z)\,\cdots\,\mathbf{G}_{2}(z)\,\mathbf{G}_{1}(z)\,\mathbf{E}_{0}(z) \;=\; \prod_{i=K-1}^{1}\mathbf{G}_{i}(z)\,\mathbf{E}_{0}(z), \qquad (5.1)$$

where each $\mathbf{G}_i(z)$ building block has the familiar form in Eq.(4.6)

$$\mathbf{G}_{i}(z) = \tfrac{1}{2}\begin{bmatrix} \mathbf{U}_i & \mathbf{0} \\ \mathbf{0} & \mathbf{V}_i \end{bmatrix}\begin{bmatrix} \mathbf{I} & \mathbf{I} \\ \mathbf{I} & -\mathbf{I} \end{bmatrix}\begin{bmatrix} \mathbf{I} & \mathbf{0} \\ \mathbf{0} & z^{-1}\mathbf{I} \end{bmatrix}\begin{bmatrix} \mathbf{I} & \mathbf{I} \\ \mathbf{I} & -\mathbf{I} \end{bmatrix}.$$

The corresponding polyphase matrix of the synthesis bank is then

$$\mathbf{R}(z) \;=\; z^{-(K+\beta-1)}\,\mathbf{E}_0^{-1}(z)\,\mathbf{G}_1^{-1}(z)\,\cdots\,\mathbf{G}_{K-1}^{-1}(z) \;=\; z^{-\beta}\,\mathbf{E}_0^{-1}(z)\prod_{i=1}^{K-1} z^{-1}\,\mathbf{G}_i^{-1}(z). \quad (5.2)$$

The general lattice structure for the analysis bank of an LT of arbitrary block size is shown in Figure 30. To obtain LPPU systems, the free-parameter matrices in $\mathbf{G}_i(z)$ ($\mathbf{U}_i$ and $\mathbf{V}_i$) and $\mathbf{E}_i(z)$ are chosen to be orthogonal. To obtain LPPR systems, $\mathbf{G}_i(z)$ and $\mathbf{E}_0(z)$ are chosen invertible. With each stage $\mathbf{G}_i(z)$ added in or peeled out, the filter length is increased or decreased by M because of the structure of $\mathbf{\Lambda}(z)$. In order to end up with the final length $L = KM + \beta$, we have to take care of the "extra" β coefficients in $\mathbf{E}_0(z)$, i.e., $\mathbf{E}_0(z)$ is the polyphase matrix of a LPPR system with filters' length $(M+\beta)$. Of course, the "extra" β coefficients can be taken care of at the final stage of the factorization in Eq.(5.1) too. However, such structures will not be as modular. The development of the initial stage $\mathbf{E}_0(z)$ is not trivial; it deserves a complete section.

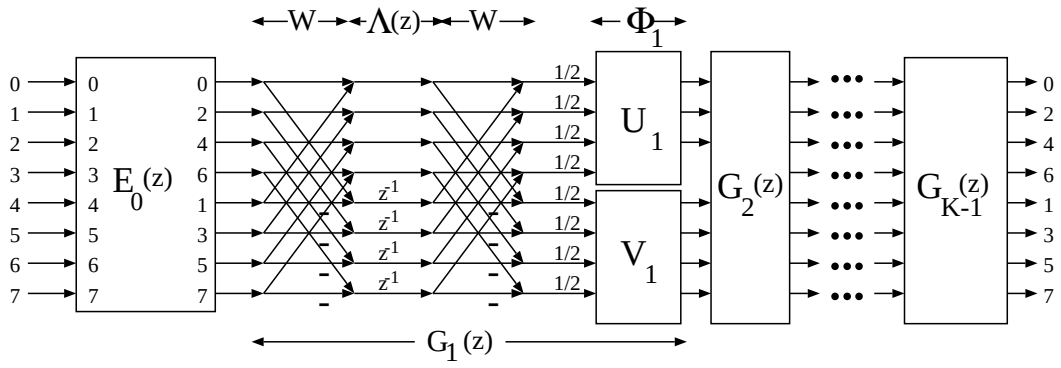

Figure 30: General lattice structure for LTs of arbitrary block size.

5.4 The initial stage $\mathbf{E}_0(z)$

We shall first present the orthogonal (PU) solution, and then generalize to the biorthogonal case by employing the SVD parameterization presented in Chapter 4.

5.4.1 Orthogonal Case

Since $\mathbf{E}_0(z)$ must contain $\frac{M}{2}$ symmetric and $\frac{M}{2}$ antisymmetric filters as stated in Table 2, $\mathbf{E}_0(z)$ has the following form:

$$\mathbf{E}_0(z) \;=\; \tfrac{1}{\sqrt{2}} \begin{bmatrix} \mathbf{S}_{00} + z^{-1}\,\mathbf{S}_{00}\,\mathbf{J} & \mathbf{S}_{01} & \mathbf{S}_{01}\,\mathbf{J} \\ \mathbf{A}_{00}\,\mathbf{J} - z^{-1}\,\mathbf{A}_{00} & \mathbf{A}_{01}\,\mathbf{J} & -\mathbf{A}_{01} \end{bmatrix}, \tag{5.3}$$

where sub-matrices $\mathbf{S}_{00}$ and $\mathbf{A}_{00}$ have size $\frac{M}{2} \times \beta$ while $\mathbf{S}_{01}$ and $\mathbf{A}_{01}$ have size $\frac{M}{2} \times \frac{M-\beta}{2}$. It can be verified that this form of $\mathbf{E}_0(z)$ allows the first β polyphase components to have one order more than the remaining $M-\beta$ polyphases, and $\mathbf{E}_0(z)$ satisfies the LP-equivalent condition in Theorem 3.6. The corresponding coefficient matrix $\mathbf{P}_0$ with each filter's impulse response arranged row-wise is:

$$\mathbf{P}_0 \;=\; \tfrac{1}{\sqrt{2}} \begin{bmatrix} \mathbf{S}_{00} & \mathbf{S}_{01} & \mathbf{S}_{01}\mathbf{J} & \mathbf{S}_{00}\mathbf{J} \\ \mathbf{A}_{00}\mathbf{J} & \mathbf{A}_{01}\mathbf{J} & -\mathbf{A}_{01} & -\mathbf{A}_{00} \end{bmatrix}. \tag{5.4}$$

In order for $\mathbf{E}_0(z)$ to be PU, $\mathbf{P}_0$ has to satisfy the time-domain constraint [95] previously mention in Chapter 2, with $h_i[n]$ being its rows:

$$\sum_{n=-\infty}^{\infty} h_j[n]\, h_k^T[n-\ell M] \;=\; \delta[\ell]\,\delta[j-k], \quad \ell \in \mathcal{Z}.$$

In matrix notation, it is equivalent to $\mathbf{E}_0(z)\,\mathbf{E}_0^T(z^{-1}) = \mathbf{I}$, i.e.,

$$\begin{cases} \mathbf{S}_{00}\,\mathbf{S}_{00}^T \;+\; \mathbf{S}_{01}\,\mathbf{S}_{01}^T \;=\; \frac{1}{2}\,\mathbf{I} \\ \mathbf{A}_{00}\,\mathbf{A}_{00}^T \;+\; \mathbf{A}_{01}\,\mathbf{A}_{01}^T \;=\; \frac{1}{2}\,\mathbf{I} \end{cases} \tag{5.5}$$

$$\begin{cases} \mathbf{S}_{00}\,\mathbf{J}\,\mathbf{S}_{00}^T \;=\; \mathbf{0} \\ \mathbf{A}_{00}\,\mathbf{J}\,\mathbf{A}_{00}^T \;=\; \mathbf{0} \\ \mathbf{S}_{00}\,\mathbf{A}_{00}^T \;=\; \mathbf{0}. \end{cases} \tag{5.6}$$

The first two equations are referred to as the orthogonality conditions; the remaining three are referred to as the shift-orthogonality conditions. A simple solution for Eq.(5.5) and Eq.(5.6) was proposed in [86] – choosing any arbitrary $\frac{M}{2} \times \frac{M}{2}$ orthogonal matrix $\mathbf{U}_0$ and then inserting $\frac{\beta}{2}$ zero column(s) intermittently between the columns of $\mathbf{U}_0$ to form the $\frac{M}{2} \times \frac{M+\beta}{2}$ matrix $[\,\mathbf{S}_{00} \quad \mathbf{S}_{01}\,]$ in Eq.(5.4). The same procedure can be repeated to obtain $[\,\mathbf{A}_{00}\mathbf{J} \quad \mathbf{A}_{01}\mathbf{J}\,]$. More clearly, starting with an $\frac{M}{2} \times \frac{M}{2}$ orthogonal matrix $\mathbf{U}_0$ with columns $\mathbf{u}_{i\cdot}$: $\mathbf{U}_0 \;=\; [\,\mathbf{u}_{1\cdot} \quad \mathbf{u}_{2\cdot} \quad \cdots \quad \mathbf{u}_{\frac{M}{2}\cdot}\,]$, we can insert $\frac{\beta}{2}$ zero columns alternately as following to obtain $[\,\mathbf{S}_{00} \quad \mathbf{S}_{01}\,] \;=\; [\,\mathbf{u}_{1\cdot} \quad \mathbf{0} \quad \mathbf{u}_{2\cdot} \quad \mathbf{0} \quad \cdots \quad \mathbf{u}_{\frac{M}{2}\cdot}\,]$. This solution is demonstrated in Figure 31.

It can be easily verified that the zero-column-inserting method yields four matrices $\mathbf{S}_{00}$, $\mathbf{S}_{01}$, $\mathbf{A}_{00}$, and $\mathbf{A}_{01}$ that satisfy both orthogonality in Eq.(5.5) and shift-orthogonality in Eq.(5.6). However, this solution can only be proven to be general for the case when $\beta = 2$. Let $\mathbf{U}_{00}$ be an arbitrary matrix of size $\frac{M}{2} \times \frac{\beta}{2}$. A more general solution for shift-orthogonality in Eq.(5.6) is $\mathbf{S}_{00} = [\,\mathbf{U}_{00}\,\mathbf{T}_p \quad \mathbf{U}_{00}\,\mathbf{T}_m\,]$, with $\mathbf{T}_p \;\triangleq\; (\mathbf{T}_0 + \mathbf{T}_1\,\mathbf{J})$ and $\mathbf{T}_m \;\triangleq\; (\mathbf{T}_0\,\mathbf{J} - \mathbf{T}_1)$ where $\mathbf{T}_0$, $\mathbf{T}_1$ are any two orthogonal matrices of size $\frac{\beta}{2}$. With the

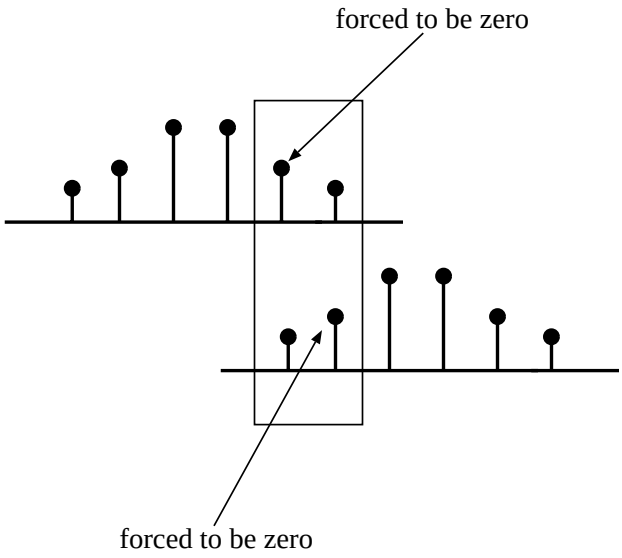

Figure 31: Demonstration of the simple zero-inserting solution.

above form of $\mathbf{S}_{00}$, we can show that shift-orthogonality is achieved, i.e., $\mathbf{S}_{00}\,\mathbf{J}\,\mathbf{S}_{00}^T = \mathbf{0}$:

$$\begin{aligned}
\mathbf{S}_{00}\,\mathbf{J}\,\mathbf{S}_{00}^T &= [\ \mathbf{U}_{00}\,\mathbf{T}_p \quad \mathbf{U}_{00}\,\mathbf{T}_m\ ]\,\mathbf{J}\begin{bmatrix} \mathbf{T}_p^T\,\mathbf{U}_{00}^T \\ \mathbf{T}_m^T\,\mathbf{U}_{00}^T \end{bmatrix} \\
&= [\ \mathbf{U}_{00}\,(\mathbf{T}_0 + \mathbf{T}_1\,\mathbf{J}) \quad \mathbf{U}_{00}\,(\mathbf{T}_0\,\mathbf{J} - \mathbf{T}_1)\ ]\begin{bmatrix} \mathbf{J}\,(\mathbf{J}\,\mathbf{T}_0^T - \mathbf{T}_1^T)\,\mathbf{U}_{00}^T \\ \mathbf{J}\,(\mathbf{T}_0^T + \mathbf{J}\,\mathbf{T}_1^T)\,\mathbf{U}_{00}^T \end{bmatrix} \\
&= \mathbf{U}_{00}\,[\ (\mathbf{T}_0 + \mathbf{T}_1\,\mathbf{J})\,(\mathbf{T}_0^T - \mathbf{J}\,\mathbf{T}_1^T) + (\mathbf{T}_0\,\mathbf{J} - \mathbf{T}_1)\,(\mathbf{J}\,\mathbf{T}_0^T + \mathbf{T}_1^T)\ ]\,\mathbf{U}_{00}^T \\
&= \mathbf{U}_{00}\,[\ \mathbf{T}_0\,\mathbf{T}_0^T - \mathbf{T}_0\,\mathbf{J}\,\mathbf{T}_1^T + \mathbf{T}_1\,\mathbf{J}\,\mathbf{T}_0^T - \mathbf{T}_1\,\mathbf{T}_1^T \\
&\qquad + \mathbf{T}_0\,\mathbf{T}_0^T + \mathbf{T}_0\,\mathbf{J}\,\mathbf{T}_1^T - \mathbf{T}_1\,\mathbf{J}\,\mathbf{T}_0^T - \mathbf{T}_1\,\mathbf{T}_1^T\ ]\,\mathbf{U}_{00}^T \\
&= \mathbf{U}_{00}\,\mathbf{0}\,\mathbf{U}_{00}^T = \mathbf{0}. \qquad (5.7)
\end{aligned}$$

The remaining shift-orthogonality conditions can be obtained similarly. In particular, by choosing $\mathbf{A}_{00} = [\ \mathbf{V}_{00}\,\mathbf{J}\,\mathbf{T}_p \quad \mathbf{V}_{00}\,\mathbf{J}\,\mathbf{T}_m\ ]$, we can easily show that the remaining two shift-orthogonal equations in Eq.(5.6) also hold. For any arbitrary $\frac{M}{2} \times \frac{\beta}{2}$ matrix $\mathbf{U}_{00}$ and

any arbitrary $\frac{M}{2} \times \frac{M-\beta}{2}$ matrix $\mathbf{U}_{01}$ (these matrix sizes guarantee the first β polyphase components to have an extra order), the proposed solutions above lead to the following factorization of $\mathbf{E}_0(z)$ as follows

$$
\begin{aligned}
\mathbf{E}_0(z) &= \frac{1}{\sqrt{2}} \begin{bmatrix} \mathbf{U}_{00}\mathbf{T}_p + z^{-1}\mathbf{U}_{00}\mathbf{T}_m\mathbf{J} & \mathbf{U}_{00}\mathbf{T}_m + z^{-1}\mathbf{U}_{00}\mathbf{T}_p\mathbf{J} & \mathbf{U}_{01} & \mathbf{U}_{01}\mathbf{J} \\ \mathbf{V}_{00}\mathbf{J}\mathbf{T}_p - z^{-1}\mathbf{V}_{00}\mathbf{J}\mathbf{T}_m\mathbf{J} & \mathbf{V}_{00}\mathbf{J}\mathbf{T}_m - z^{-1}\mathbf{V}_{00}\mathbf{J}\mathbf{T}_p\mathbf{J} & \mathbf{V}_{01}\mathbf{J} & -\mathbf{V}_{01} \end{bmatrix} \\
&= \frac{1}{\sqrt{2}} \begin{bmatrix} \mathbf{U}_{00} & \mathbf{U}_{01} & \mathbf{U}_{01}\,\mathbf{J} & z^{-1}\,\mathbf{U}_{00} \\ \mathbf{V}_{00}\,\mathbf{J} & \mathbf{V}_{01}\,\mathbf{J} & -\mathbf{V}_{01} & -z^{-1}\,\mathbf{V}_{00}\,\mathbf{J} \end{bmatrix} \begin{bmatrix} \mathbf{T}_p & \mathbf{T}_m & \mathbf{0} & \mathbf{0} \\ \mathbf{0} & \mathbf{0} & \mathbf{I}_{\frac{M-\beta}{2}} & \mathbf{0} \\ \mathbf{0} & \mathbf{0} & \mathbf{0} & \mathbf{I}_{\frac{M-\beta}{2}} \\ \mathbf{T}_m\,\mathbf{J} & \mathbf{T}_p\,\mathbf{J} & \mathbf{0} & \mathbf{0} \end{bmatrix} \\
&= \frac{1}{\sqrt{2}} \begin{bmatrix} \mathbf{U}_{00} & \mathbf{U}_{01} & \mathbf{U}_{01}\,\mathbf{J} & \mathbf{U}_{00} \\ \mathbf{V}_{00}\,\mathbf{J} & \mathbf{V}_{01}\,\mathbf{J} & -\mathbf{V}_{01} & -\mathbf{V}_{00}\,\mathbf{J} \end{bmatrix} \begin{bmatrix} \mathbf{I}_{\frac{\beta}{2}} & \mathbf{0} & \mathbf{0} & \mathbf{0} \\ \mathbf{0} & \mathbf{I}_{\frac{M-\beta}{2}} & \mathbf{0} & \mathbf{0} \\ \mathbf{0} & \mathbf{0} & \mathbf{I}_{\frac{M-\beta}{2}} & \mathbf{0} \\ \mathbf{0} & \mathbf{0} & \mathbf{0} & z^{-1}\,\mathbf{I}_{\frac{\beta}{2}} \end{bmatrix} \\
&\quad \times \begin{bmatrix} \mathbf{T}_p & \mathbf{T}_m & \mathbf{0} & \mathbf{0} \\ \mathbf{0} & \mathbf{0} & \mathbf{I}_{\frac{M-\beta}{2}} & \\ \mathbf{0} & \mathbf{0} & \mathbf{0} & \mathbf{I}_{\frac{M-\beta}{2}} \\ \mathbf{T}_m\,\mathbf{J} & \mathbf{T}_p\,\mathbf{J} & \mathbf{0} & \mathbf{0} \end{bmatrix} \\
&\triangleq \mathbf{\Phi}_0\,\mathbf{\Lambda}_0(z)\,\mathbf{T}. \qquad (5.8)
\end{aligned}
$$

At this point, our proposed factorization has only guaranteed shift-orthogonality. In order for $\mathbf{E}_0(z)$ to be paraunitary, orthogonality needs to be imposed on $\mathbf{\Phi}_0$ and $\mathbf{T}$ as well. (Note that $\mathbf{\Lambda}_0(z)$ is already paraunitary). First of all, notice that $\mathbf{\Phi}_0$ resembles the

first block of the GLBT in the previous chapter; it can be factorized further as

$$\begin{aligned}
\mathbf{\Phi}_0 &= \frac{1}{\sqrt{2}} \begin{bmatrix} \mathbf{U}_{00} & \mathbf{U}_{01} & \mathbf{U}_{01}\mathbf{J} & \mathbf{U}_{00} \\ \mathbf{V}_{00}\mathbf{J} & \mathbf{V}_{01}\mathbf{J} & -\mathbf{V}_{01} & -\mathbf{V}_{00}\mathbf{J} \end{bmatrix} \\
&= \frac{1}{\sqrt{2}} \begin{bmatrix} \mathbf{U}_{00} & \mathbf{U}_{01} & \mathbf{U}_{01}\mathbf{J} & \mathbf{U}_{00}\mathbf{J} \\ \mathbf{V}_{00}\mathbf{J} & \mathbf{V}_{01}\mathbf{J} & -\mathbf{V}_{01} & \mathbf{V}_{00} \end{bmatrix} \begin{bmatrix} \mathbf{I}_{\frac{\beta}{2}} & \mathbf{0} & \mathbf{0} & \mathbf{0} \\ \mathbf{0} & \mathbf{I}_{\frac{M-\beta}{2}} & \mathbf{0} & \mathbf{0} \\ \mathbf{0} & \mathbf{0} & \mathbf{I}_{\frac{M-\beta}{2}} & \mathbf{0} \\ \mathbf{0} & \mathbf{0} & \mathbf{0} & \mathbf{J}_{\frac{\beta}{2}} \end{bmatrix} \\
&= \frac{1}{\sqrt{2}} \begin{bmatrix} \mathbf{U}_0 & \mathbf{0} \\ \mathbf{0} & \mathbf{V}_0 \end{bmatrix} \begin{bmatrix} \mathbf{I}_{\frac{M}{2}} & \mathbf{J}_{\frac{M}{2}} \\ \mathbf{J}_{\frac{M}{2}} & -\mathbf{I}_{\frac{M}{2}} \end{bmatrix} \begin{bmatrix} \mathbf{I}_{M-\frac{\beta}{2}} & \mathbf{0} \\ \mathbf{0} & \mathbf{J}_{\frac{\beta}{2}} \end{bmatrix}, \qquad (5.9)
\end{aligned}$$

where we have defined $\mathbf{U}_0 \triangleq [\,\mathbf{U}_{00} \quad \mathbf{U}_{01}\,]$ and $\mathbf{V}_0 \triangleq [\,\mathbf{V}_{01} \quad \mathbf{V}_{00}\,]$. Thus, it is clear that $\mathbf{\Phi}_0$ is orthogonal if and only if $\mathbf{U}_0$ and $\mathbf{V}_0$ are orthogonal.

Next, for clarity of presentation, we permute $\mathbf{T}$ into

$$\widetilde{\mathbf{T}} = \begin{bmatrix} \mathbf{T}_p & \mathbf{T}_m & \mathbf{0} \\ \mathbf{T}_m\mathbf{J} & \mathbf{T}_p\mathbf{J} & \mathbf{0} \\ \mathbf{0} & \mathbf{0} & \mathbf{I}_{M-\beta} \end{bmatrix} = \begin{bmatrix} \mathbf{T}_0 + \mathbf{T}_1\mathbf{J} & \mathbf{T}_0\mathbf{J} - \mathbf{T}_1 & \mathbf{0} \\ \mathbf{T}_0 - \mathbf{T}_1\mathbf{J} & \mathbf{T}_0\mathbf{J} + \mathbf{T}_1 & \mathbf{0} \\ \mathbf{0} & \mathbf{0} & \mathbf{I}_{M-\beta} \end{bmatrix}.$$

Then, $\widetilde{\mathbf{T}}$ can be further factorized as

$$\widetilde{\mathbf{T}} = \begin{bmatrix} \mathbf{I}_{\frac{\beta}{2}} & \mathbf{I}_{\frac{\beta}{2}} & \mathbf{0} \\ \mathbf{I}_{\frac{\beta}{2}} & -\mathbf{I}_{\frac{\beta}{2}} & \mathbf{0} \\ \mathbf{0} & \mathbf{0} & \mathbf{I}_{M-\beta} \end{bmatrix} \begin{bmatrix} \mathbf{T}_0 & \mathbf{0} & \mathbf{0} \\ \mathbf{0} & \mathbf{T}_1 & \mathbf{0} \\ \mathbf{0} & \mathbf{0} & \mathbf{I}_{M-\beta} \end{bmatrix} \begin{bmatrix} \mathbf{I}_{\frac{\beta}{2}} & \mathbf{J}_{\frac{\beta}{2}} & \mathbf{0} \\ \mathbf{J}_{\frac{\beta}{2}} & -\mathbf{I}_{\frac{\beta}{2}} & \mathbf{0} \\ \mathbf{0} & \mathbf{0} & \mathbf{I}_{M-\beta} \end{bmatrix}. \qquad (5.10)$$

Again, $\widetilde{\mathbf{T}}$ is orthogonal as long as $\mathbf{T}_0$ and $\mathbf{T}_1$ are chosen orthogonal. Combining Eq.(5.8), Eq.(5.9), and Eq.(5.10), we have a factorization for the paraunitary initial stage $\mathbf{E}_0(z)$.

The corresponding coefficient matrix $\hat{\mathbf{P}}_0$ can be shown to be:

$$\hat{\mathbf{P}}_0 = \frac{1}{\sqrt{2}} \begin{bmatrix} \mathbf{U}_{00}\,\mathbf{T}_p & \mathbf{U}_{00}\,\mathbf{T}_m & \mathbf{U}_{01} & \mathbf{U}_{01}\,\mathbf{J} & \mathbf{U}_{00}\,\mathbf{T}_m\,\mathbf{J} & \mathbf{U}_{00}\,\mathbf{T}_p\,\mathbf{J} \\ \mathbf{V}_{00}\,\mathbf{J}\,\mathbf{T}_p & \mathbf{V}_{00}\,\mathbf{J}\,\mathbf{T}_m & \mathbf{V}_{01}\,\mathbf{J} & -\mathbf{V}_{01} & -\mathbf{V}_{00}\,\mathbf{J}\,\mathbf{T}_m\,\mathbf{J} & -\mathbf{V}_{00}\,\mathbf{J}\,\mathbf{T}_p\,\mathbf{J} \end{bmatrix}. \tag{5.11}$$

By inspection, $\mathbf{E}_0(z)$ produces a linear phase system. Furthermore, since all factors in Eq.(5.8) are orthogonal, $\mathbf{E}_0(z)$ is paraunitary. Thus, the complete system $\mathbf{E}(z)$ in Eq.(5.1) is LPPU. The detailed structure of the initial $\mathbf{E}_0(z)$ block is depicted in Figure 32 (drawn for $M = 8$ and $\beta = 4$). The degrees of freedom reside in the four matrices $\mathbf{T}_0$, $\mathbf{T}_1$, $\mathbf{U}_0$, and $\mathbf{V}_0$. The first two $\frac{\beta}{2} \times \frac{\beta}{2}$ orthogonal matrices are parameterized by $\frac{\beta(\beta-2)}{8}$ rotation angles each, whereas each of the latter two $\frac{M}{2} \times \frac{M}{2}$ orthogonal matrices is parameterized by $\frac{M(M-2)}{8}$ rotation angles. For an even faster implementation, the transfer function matrix

$$\frac{1}{\sqrt{2}} \begin{bmatrix} \mathbf{U}_0 & \mathbf{0} \\ \mathbf{0} & \mathbf{V}_0 \end{bmatrix} \begin{bmatrix} \mathbf{I}_{\frac{M}{2}} & \mathbf{J}_{\frac{M}{2}} \\ \mathbf{J}_{\frac{M}{2}} & -\mathbf{I}_{\frac{M}{2}} \end{bmatrix}$$

can be chosen to be the $M \times M$ DCT.

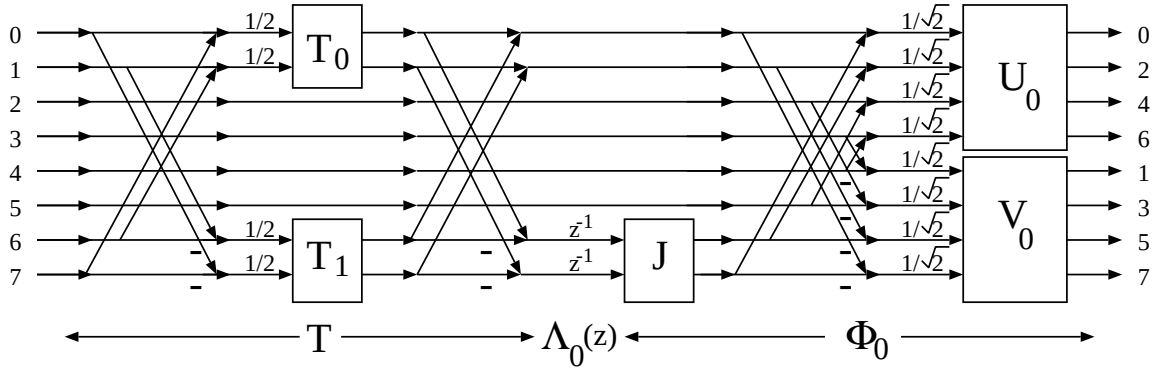

Figure 32: The initial stage $\mathbf{E}_0(z)$ in details.

Remarks. When β decreases to zero, the transfer function from the beginning of $\mathbf{E}_0(z)$ to the matrix

$$\begin{bmatrix} \mathbf{I}_{\frac{M}{2}} & \mathbf{J}_{\frac{M}{2}} \\ \mathbf{J}_{\frac{M}{2}} & -\mathbf{I}_{\frac{M}{2}} \end{bmatrix}$$

in $\mathbf{\Phi}_0$ disappears, and we are left with the familiar zero-order $\mathbf{E}_0$ in Eq.(2.24), i.e., the simple lattice reduces to the traditional DCT form. On the other hand, when β increases to M, $\mathbf{T}_0$ and $\mathbf{T}_1$ become $\frac{M}{2} \times \frac{M}{2}$ orthogonal matrices, the two "butterflies" to their left and to their right become full-grown, $\mathbf{\Lambda}_0(z)$ extends to $\mathbf{\Lambda}(z)$ in Eq.(2.27), and

$$\begin{bmatrix} \mathbf{I}_{\frac{M}{2}} & \mathbf{J}_{\frac{M}{2}} \\ \mathbf{J}_{\frac{M}{2}} & -\mathbf{I}_{\frac{M}{2}} \end{bmatrix} \begin{bmatrix} \mathbf{I}_{M-\frac{\beta}{2}} & \mathbf{0} \\ \mathbf{0} & \mathbf{J}_{\frac{\beta}{2}} \end{bmatrix} \longrightarrow \begin{bmatrix} \mathbf{I}_{\frac{M}{2}} & \mathbf{J}_{\frac{M}{2}} \\ \mathbf{J}_{\frac{M}{2}} & -\mathbf{I}_{\frac{M}{2}} \end{bmatrix} \begin{bmatrix} \mathbf{I}_{\frac{M}{2}} & \mathbf{0} \\ \mathbf{0} & \mathbf{J}_{\frac{M}{2}} \end{bmatrix} = \begin{bmatrix} \mathbf{I}_{\frac{M}{2}} & \mathbf{I}_{\frac{M}{2}} \\ \mathbf{I}_{\frac{M}{2}} & -\mathbf{I}_{\frac{M}{2}} \end{bmatrix}.$$

The initial stage $\mathbf{E}_0(z)$ now grows to the complete LOT lattice in Eq.(2.25). Finally, when $\beta = 2$, there is no degree of freedom: $\mathbf{T}_0$ and $\mathbf{T}_1$ degenerate to singleton 1's. This confirms the comment we have made earlier that inserting two columns of zeros into the $\mathbf{E}_0$ matrix is the only solution in the case $\beta = 2$.

5.4.2 Biorthogonal Case

The extension to the biorthogonal solution is straightforward. As one may have observed from the main results in in Chapter 4, biorthogonal transform can be obtained from its orthogonal relative by simply relaxing the orthogonal constraint on the matrices containing the free parameters. More specifically, if we now choose $\mathbf{T}_0$, $\mathbf{T}_1$, $\mathbf{U}_0$, and $\mathbf{V}_1$ to be invertible (instead of orthogonal), $\mathbf{E}_0(z)$ can be easily verified to satisfy biorthogonality

as defined in Definition 2.5. The four aforementioned matrices can be completely parameterized by the SVD decomposition as described in Section 4.5. When β decreases to zero or increases to M, our proposed initial stage $\mathbf{E}_0(z)$ reduces to $\mathbf{E}_0$ in Eq.(4.8) or extends to a full GLBT of order 2 as shown in Figure 21.

5.5 Completeness and Minimality

The full lattice structure covering M-channel LPPRFB with filter length $L = KM + \beta$ is shown in Figure 33 (drawn for $M = 8$ and $\beta = 4$ here). In the orthogonal case, the lattice coefficients are the rotation angles of the orthogonal matrices $\mathbf{T}_0$, $\mathbf{T}_1$, $\mathbf{U}_i$, and $\mathbf{V}_i$, $i = 0, 1, \ldots, K-1$. Hence, the total number of lattice coefficients (free parameters to fine-tune the transform) is $\frac{KM(M-2)}{4} + \frac{\beta(\beta-2)}{4}$. When β decreases to 0 or increases to M, the number of parameters changes consistently with those previously reported [62], [75] (peeling out a stage or adding in a stage, respectively).

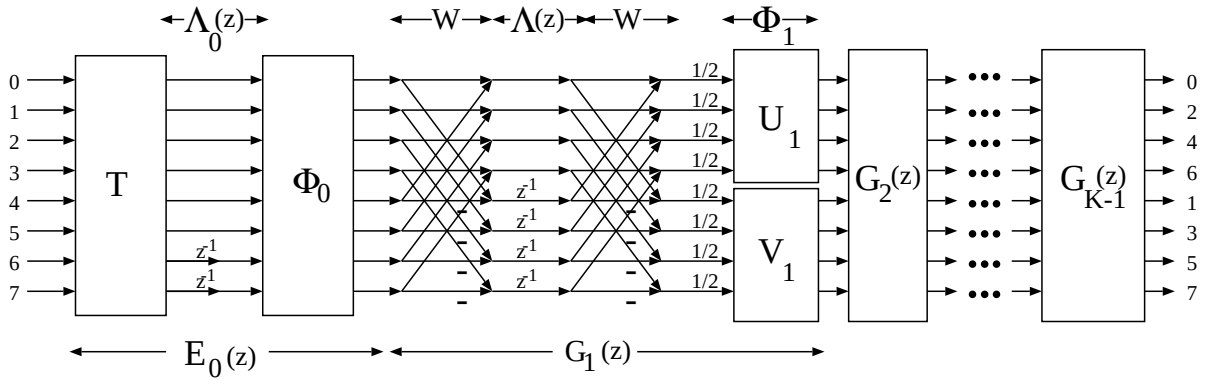

Figure 33: Complete lattice structure for LTs of arbitrary block size.

In the biorthogonal case, the lattice coefficients reside in the invertible matrices $\mathbf{T}_0$,

$\mathbf{T}_1$, $\mathbf{U}_i$, and $\mathbf{V}_i$, $i = 0, 1, \ldots, K-1$. The total number of free parameters now increases to $p = \frac{KM^2}{2} + \frac{\beta^2}{2}$. Again, p varies consistently with the degrees of freedom stated in Section 4.5, i.e., when $\beta \longrightarrow 0$, $p \longrightarrow \frac{KM^2}{2}$; when $\beta \longrightarrow M$, $p \longrightarrow \frac{(K+1)M^2}{2}$. As a reminder, we have shown in Section 5.2 that solutions only exist when β is even: it is not possible to design any even-channel odd-length LPPRFB.

To guarantee that no solution can be missed using this cascade design procedure, the converse of this result, stated in the following theorem, has to be proven. In other words, the proposed solution does cover *all* even-channel LPPRFBs with filter length $L = KM + \beta$.

Theorem 5.21 *The polyphase matrix $\mathbf{E}(z)$ of any even-channel LPPRFB with filter length $L = KM + \beta$ can always be factored as Eq.(5.1) where its factors are given by Eq.(4.6) and Eq.(5.8).*

Proof.

Theorem 5.21 can be rephrased as following: suppose there exists an arbitrary FIR LPPRFB with the associated analysis polyphase matrix $\mathbf{E}(z)$ satisfying Eq.(3.3) then:

- $\mathbf{E}(z)$ can always be factored as in Eq.(5.1).
- $\mathbf{E}_0(z)$ can always be factored as in Eq.(5.8).

The former is achieved by performing the *order reduction* process resembling the procedure presented in the proof of Theorem 4.15. In a straightforward similar manner, we can always construct an order-1 structure, namely $\mathbf{G}(z)$ in Eq.(4.6), such that the

the linear phase property, the perfect reconstruction property, and the causal property are all retained. Furthermore, the order of $\mathbf{E}(z)$ is reduced by 1 after each stage $\mathbf{G}(z)$ is peeled off. Given a polyphase matrix with filters of length $L = KM + \beta$, after $K-1$ reduction steps performed by $\mathbf{G}_i(z), i = 1, 2, \ldots, K-1$, the remainder is the LPPRFB $\mathbf{E}_0(z)$ as shown in Eq.(5.3). Now, all what is left to prove is the latter part of the lemma: $\mathbf{E}_0(z)$ can always be factored as in Eq.(5.8).

We shall first present the proof for the paraunitary case since the notations are simplified significantly. Given an LPPU starting block $\mathbf{E}_0(z)$ as in Eq.(5.3), Eq.(5.4) shows that the corresponding coefficient matrix $\mathbf{P}_0$ will take the form in Eq.(5.4) where $\mathbf{S}_{00}$, $\mathbf{S}_{01}$, $\mathbf{A}_{00}$, and $\mathbf{A}_{01}$ must satisfy the shift-orthogonality and orthogonality condition in Eq.(5.5). respectively. On the other hand, from the proposed factorization of $\mathbf{E}_0(z)$, the corresponding coefficient matrix $\hat{\mathbf{P}}_0$ takes the form in Eq.(5.11).

We have to prove that there exists orthogonal matrices $\mathbf{U}_0 \stackrel{\triangle}{=} [\mathbf{U}_{00} \quad \mathbf{U}_{01}]$, $\mathbf{V}_0 \stackrel{\triangle}{=} [\mathbf{V}_{00} \quad \mathbf{V}_{01}]$ of size $\frac{M}{2} \times \frac{M}{2}$, and $\mathbf{T}_0$, $\mathbf{T}_1$ of size $\frac{\beta}{2} \times \frac{\beta}{2}$ such that:

$$\mathbf{U}_{01} \;=\; \mathbf{S}_{01}, \qquad [\mathbf{U}_{00}\,(\mathbf{T}_0 + \mathbf{T}_1\,\mathbf{J}) \quad \mathbf{U}_{00}\,(\mathbf{T}_0\,\mathbf{J} - \mathbf{T}_1)] \;=\; \mathbf{S}_{00},$$

and similarly,

$$\mathbf{V}_{01} \;=\; \mathbf{A}_{01}, \qquad [\mathbf{V}_{00}\,(\mathbf{T}_0 + \mathbf{T}_1\,\mathbf{J}) \quad \mathbf{V}_{00}\,(\mathbf{T}_0\,\mathbf{J} - \mathbf{T}_1)] \;=\; \mathbf{A}_{00}.$$

The proof for existence of $\mathbf{U}_{01}$ and $\mathbf{V}_{01}$ is not difficult. By imposing the paraunitary constraint on $\mathbf{E}_0(z)$ in Eq.(5.3): $\mathbf{E}_0^T(z)\,\mathbf{E}_0(z) = \mathbf{I}$, it can be shown that the columns of $\mathbf{S}_{01}$ must be orthonormal, i.e., $\mathbf{S}_{01}^T\,\mathbf{S}_{01} = \mathbf{I}_{\frac{M-\beta}{2}}$. Since $\mathbf{U}_{01}$ includes $\frac{M-\beta}{2}$ columns of an

arbitrary orthogonal $\frac{M}{2} \times \frac{M}{2}$ matrix $\mathbf{U}_0$, $\mathbf{U}_{01}$ surely spans the space of all possible $\mathbf{S}_{01}$. In other words, we can obtain $\mathbf{U}_{01}$ from the columns of the given matrix $\mathbf{S}_{01}$. Similar procedures can be carried out in the construction of $\mathbf{V}_{01}$ from $\mathbf{A}_{01}$.

The proof of existence for the remaining building blocks is a little more tricky. We have to show that $[\mathbf{U}_{00}\,(\mathbf{T}_0 + \mathbf{T}_1\,\mathbf{J}) \quad \mathbf{U}_{00}\,(\mathbf{T}_0\,\mathbf{J} - \mathbf{T}_1)]$ spans the space of all possible $\mathbf{S}_{00}$. Since

$$\mathbf{S}_{00}\,\mathbf{S}_{00}^T \;+\; \mathbf{S}_{01}\,\mathbf{S}_{01}^T \;=\; \tfrac{1}{2}\,\mathbf{I}_{\frac{M}{2}},$$

$[\mathbf{S}_{00}\ \mathbf{S}_{01}]$ has rank $\frac{M}{2}$, i.e., the matrix has $\frac{M}{2}$ independent columns out of its $\frac{M+\beta}{2}$ columns. Moreover, shift-orthogonality must also be satisfied, i.e., $\mathbf{S}_{00}\,\mathbf{J}\,\mathbf{S}_{00}^T \;=\; \mathbf{0}_{\frac{M}{2}}$. This means that the columns of $\mathbf{J}\,\mathbf{S}_{00}^T$ lie in the nullspace of $\mathbf{S}_{00}$. Moreover,

$$\rho(\mathbf{J}\,\mathbf{S}_{00}^T) \;=\; \rho(\mathbf{S}_{00}^T) \;=\; \rho(\mathbf{S}_{00}) \;=\; \text{dimension of nullspace of } \mathbf{S}_{00}.$$

Also, for any $\frac{M}{2} \times \beta$ matrix $\mathbf{S}_{00}$,

$$\text{dimension of column space} + \text{dimension of nullspace} \;=\; \beta.$$

Hence, the dimension of the column space of $\mathbf{S}_{00}$ must be $\frac{\beta}{2}$, or in other words, $\mathbf{S}_{00}$ must have $\frac{\beta}{2}$ independent columns. As a result, all $\frac{M-\beta}{2}$ columns of $\mathbf{S}_{01}$ must be independent. This agrees with our result. Recall that $\mathbf{U}_0 \stackrel{\triangle}{=} [\mathbf{U}_{00}\ \ \mathbf{U}_{01}]$ is an $\frac{M}{2} \times \frac{M}{2}$ orthogonal matrix with $\mathbf{U}_{00}$ containing the first $\frac{\beta}{2}$ columns and $\mathbf{U}_{01}$ containing the last $\frac{M-\beta}{2}$ columns. Since the columns of any orthogonal matrix are independent,

$$\rho(\mathbf{U}_{01}) \;=\; \frac{M-\beta}{2} \;=\; \rho(\mathbf{S}_{01}),$$

or $\mathbf{U}_{01}$ spans the space of all possible $\mathbf{S}_{01}$. Similarly, since $\rho(\mathbf{U}_{00}) = \frac{\beta}{2}$,

$$\rho([\,\mathbf{U}_{00}\,(\mathbf{T}_0 + \mathbf{T}_1\,\mathbf{J}) \quad \mathbf{U}_{00}\,(\mathbf{T}_0\,\mathbf{J} - \mathbf{T}_1)\,]) = \frac{\beta}{2} = \rho(\mathbf{S}_{00}),$$

leading to the same conclusion that $[\,\mathbf{U}_{00}\,(\mathbf{T}_0 + \mathbf{T}_1\,\mathbf{J}) \quad \mathbf{U}_{00}\,(\mathbf{T}_0\,\mathbf{J} - \mathbf{T}_1)\,]$ spans the space of all possible $\mathbf{S}_{00}$. It is always possible to construct $\mathbf{U}_{00}$, $\mathbf{T}_0$, and $\mathbf{T}_1$ from the $\frac{\beta}{2}$ linearly-independent columns of $\mathbf{S}_{00}$. The same proof can be conducted for the case involved $\mathbf{V}_0$, $\mathbf{A}_{00}$, and $\mathbf{A}_{01}$.

The generalization to biorthogonality is straightforward: the relationship between the analysis and the synthesis bank is no longer transpositional. We now have two coefficient matrices: $\mathbf{P}_A$ for the analysis bank and $\mathbf{P}_S$ for the synthesis bank. Their relationship is dictated by the following time-domain constraint for biorthogonal systems [77]

$$\sum_{n=-\infty}^{\infty} h_j[n]\, g_k^T[n - \ell M] = \delta[\ell]\,\delta[j-k], \quad \ell \in \mathcal{Z}.$$

where $g_k[n]$ stands for the impulse response of the k-th synthesis filter. The so-called orthogonal and shift-orthogonal constraint in Eq.(5.5) and Eq.(5.6) are still true if the matrices in transposed format are replaced by the appropriate matrices representing the synthesis bank.

From this observation, it is easy to show that the theorem still holds when orthogonal matrices in the proof of the orthogonal case above are replaced by invertible ones (the synthesis bank is not identical to the analysis bank anymore), and orthogonal columns (or rows) are replaced by linearly independent ones. In other words, the elements of $\mathbf{P}_A$ can always be used to construct the matrices $\mathbf{T}_0$, $\mathbf{T}_1$, $\mathbf{U}_0$, and $\mathbf{V}_0$, whereas $\mathbf{T}_0^{-1}$, $\mathbf{T}_1^{-1}$, $\mathbf{U}_0^{-1}$, and $\mathbf{V}_0^{-1}$ can always be constructed from $\mathbf{P}_S$. □

Next, we should establish the minimality of the resulting lattice structure from Eq.(5.1).

Theorem 5.22 *The proposed factorization of* $\mathbf{E}(z)$ *as in Eq.(5.1), where* $\mathbf{E}_0(z)$ *is given as in Eq.(5.8), is minimal, i.e., it employs the fewest number of delays in the implementation of the polyphase matrix.*

Proof.

Similarly to the proof of Theorem 4.17, we have to prove that the number of delays employed should not exceed the degree of the transfer function, or equivalently, the degree of the transfer function's determinant in lossless systems.

Using the symmetry property of the polyphase matrix in Eq.(3.3) of Theorem 3.6, we have

$$deg(\mathbf{E}(z)) \;=\; deg(|\mathbf{E}(z)|) \;=\; deg(|\mathbf{D}|\;|z^{-(K-1)}|\;|\mathbf{E}(z^{-1})|\;|\hat{\mathbf{J}}(z)|).$$

Therefore,

$$deg(\mathbf{E}(z)) \;=\; M(K-1) - deg(\mathbf{E}(z)) + \beta,$$

which leads to $deg(\mathbf{E}(z)) = \frac{M(K-1)+\beta}{2}$. In our factorization, we use $\frac{M}{2}$ delays for each propagation block $\mathbf{G}_i(z)$ and $\frac{\beta}{2}$ delays for the starting block $\mathbf{E}_0(z)$, totaling the same number of $\frac{M(K-1)+\beta}{2}$ delays. Hence, the factorization is minimal. □

5.6 Design Examples

The lattice structure described in the previous sections provides a familiar design procedure because it fits perfectly in the GLBT framework in Chapter 4. The lone difference is in the implementation of the initial stage $\mathbf{E}_0(z)$. The optimization process and its various cost functions in Section 4.7 can be applied directly in the design of the new LTs without any changes. As described in Section 4.7.1, all matrices containing the lattice coefficients are initialized to either $\mathbf{I}$ or $-\mathbf{I}$.

Figure 34(a) shows design example I: a 6-channel LPPUFB with all filters having length 14 ($K = 2,\ \beta = 2$, or 6×14 GenLOT) optimized for stopband attenuation. Design example II in Figure 34(b) is an 8-channel LPPUFB with all filters having length 12 ($K = 1,\ \beta = 4$, or 8×12 GenLOT). The polyphase matrix is simply the initial stage $\mathbf{E}_0(z)$. Refer to Figure 32 for the implementation of this system. As previously advertised, this novel FB can be thought of as a GenLOT with non-integer overlap; in design example II, we have an overlap factor of $\frac{1}{2}$ (or half-block overlap). Interestingly enough, with only two more parameters to optimize and two more delays in the implementation, we are able to obtain a much improved transform comparing to the DCT.

Several other orthogonal design examples are presented in Figure 35 and Figure 36. Both of these examples presented are obtained with a general initial stage. If employing the DCT is desired, the number of parameters is reduced by $\frac{M(M-2)}{4}$, leading to narrower searches and more convenient implementations, but possibly sub-optimal systems.

Two biorthogonal design examples are presented in Figure 37 and Figure 38 where

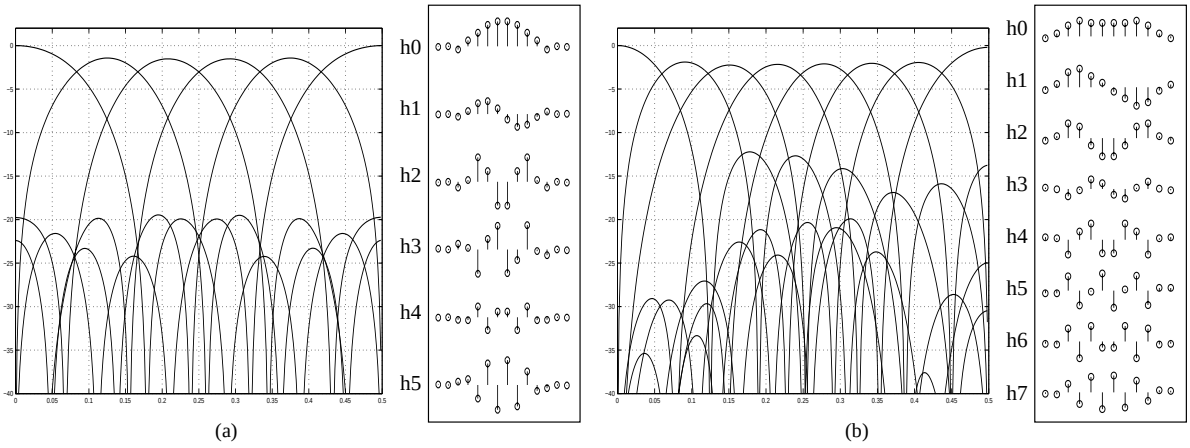

Figure 34: GenLOTs of arbitrary block size. (a) Design example I: $M = 6 \quad L = 14$ optimized for stopband attenuation. (b) Design example II: $M = 8 \quad L = 12$ optimized for coding gain, DC attenuation, mirror frequency attenuation, and stopband attenuation.

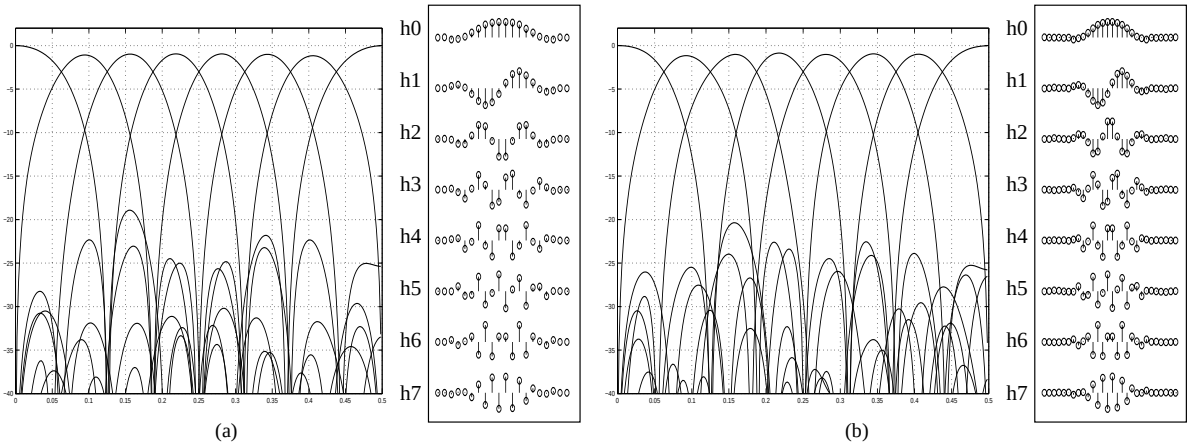

Figure 35: GenLOTs of arbitrary block size. (a) Design example III: $M = 8 \quad L = 20$ optimized for coding gain, DC attenuation, mirror frequency attenuation, and stopband attenuation. (b) Design example IV: $M = 8 \quad L = 28$ optimized for stopband attenuation, coding gain, and mirror frequency attenuation.

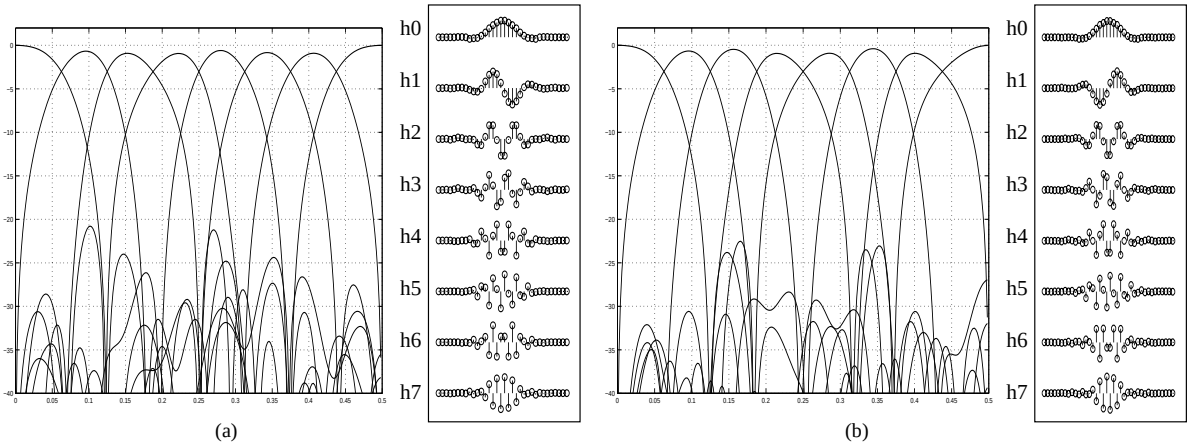

Figure 36: GenLOTs of arbitrary block size. (a) Design example V: $M = 8 \quad L = 34$ optimized for coding gain, DC attenuation, mirror frequency attenuation, and stopband attenuation. (b) Design example VI: $M = 8 \quad L = 38$ optimized for coding gain, DC attenuation, mirror frequency attenuation, and stopband attenuation.

both analysis and synthesis bank are shown. Design example VII is an 8-channel 12-tap LPPRFB (8×12 GLBT) optimized for coding gain and attenuation at DC frequency. Design example VIII is also an 8×12 GLBT; however, it is optimized to have low stopband attenuation in the analysis bank only. This FB is intended to show the new dimension of flexibility that biorthogonal systems possess over orthogonal ones. Several important properties of selective transforms are tabulated in Table 4. Again, the DCT [67] and the LOT [47] are included to serve as benchmarks.

5.7 Summary

In this chapter, the theory, structure, design, and implementation of lapped transforms with arbitrary block size are presented. These new transforms are LPPRFBs where all

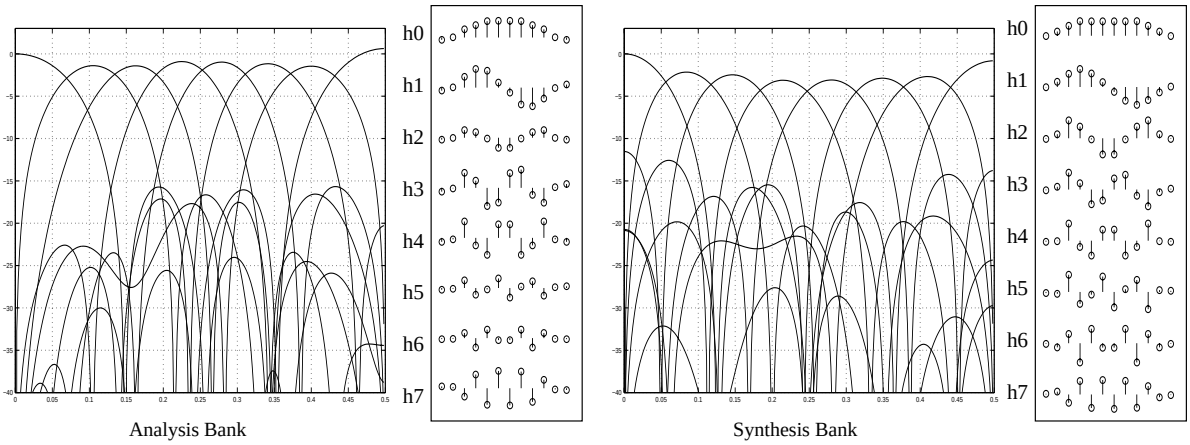

Figure 37: GLBTs of arbitrary block size. Design example VII: $M = 8$ $L = 12$ optimized for coding gain and DC attenuation.

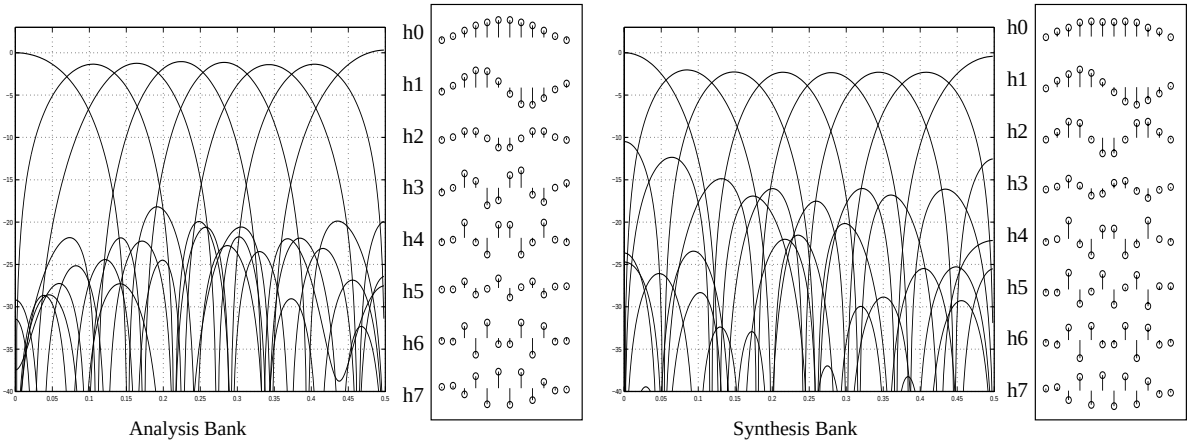

Figure 38: GLBTs of arbitrary block size. Design example VIII: $M = 8$ $L = 12$ optimized for stopband attenuation of analysis bank.

Transform Property	Transform							
	8x8 DCT	8x16 LOT	8x12 GenLOT (II)	8x20 GenLOT (III)	8x34 GenLOT (V)	8x38 GenLOT (VI)	8x12 GLBT (VII)	8x12 GLBT (VIII)
Coding Gain (dB)	8.83	9.22	9.02	9.23	9.31	9.36	9.11	8.99
DC Attenuation (-dB)	310.62	312.56	318.58	322.10	324.60	328.12	190.32	29.19
Stopband Attenuation (-dB)	9.96	19.38	12.22	18.92	20.78	22.52	16.38	18.19
Mirror Freq. Attenuation (-dB)	322.10	317.24	311.86	317.24	316.08	314.14	14.17	13.53

Table 4: Comparison of transform properties ($L = KM + \beta$).

filters have length $L = KM+\beta$. Section 5.2 restricts the search space of possible solutions. Section 5.3 then shows that the same LPPR-propagating building block $\mathbf{G}(z)$ in Chapter 4 can be employed in the derivation of a modular lattice structure for the more general class of LPPRFBs. The subtle generalization lies at the cascade's initial stage $\mathbf{E}_0(z)$ whose derivation is described in details in Section 5.4. The resulting lattice structure is proven to cover all possible even-channel linear phase paraunitary filter banks , i.e., any even-channel linear phase paraunitary systems can be realized by some combination of these lattice coefficients. We also prove that the proposed structure is minimal in term of the number of delays used in the FB implementation.

The lattice is then generalized further to covers biorthogonal systems by the parameterization of the free-parameter invertible matrices by their SVD representations. This is the true generalized lapped transform where the amount of overlap is not constrained to be a multiple of the number of channels. The permissible length constraint presented earlier in the dissertation also yields an elegant proof that the overlap has to be an even number of samples, i.e., odd-length even-channel LT does not exist. The design examples are comparable in term of FB performance with those in previous works [75], [62] and the GLBT in Chapter 4, i.e., the proposed cascade structure can provide as good FBs as those reported previously in the literature. The novel modular lattice in this chapter still guarantees linear phase and perfect reconstruction properties inherently as its predecessos: the systems still have LPPR in spite of the quantization of the lattice coefficients (the rotation angles of the orthogonal matrices and the multipliers in the diagonal matrices).

Chapter 6

Linear Phase Perfect Reconstruction Filter Banks with Variable-Length Filters

6.1 Introduction

This chapter is devoted to the theory, structure, design, and implementation of M-channel FIR linear phase perfect reconstruction filter banks with filters of different length. This class of LPPRFBs can be viewed as the generalized lapped orthogonal/biorthogonal transform with variable-length basis functions that we label VLLOT and VLGLBT respectively. The main motivation of the new transform is its application in block-transform-based image coding. Besides having all of the attractive properties of other FBs presented earlier, the new transform takes advantage of its long basis functions to represent smooth signal and to reduce blocking artifacts, while reserves its short basis functions to represent high-frequency signal components like edges and texture to reduce ringing artifacts. Two design methods are presented, each with its own set of advantages:

the first is based on a direct lattice factorization and the second enforces certain relationships between the lattice coefficients to obtain variable length filters. Various necessary conditions for the existence of meaningful solutions are derived and discussed in both cases. Many design examples are presented.

There are numerous motivations in studying FBs with filters of variable length. First of all, it is quite natural to represent slowly-changing signals by long basis functions. On the other hand, fast-changing, high-frequency components such as edges and textures in images are better captured by short basis functions. The wavelet transform serves as a wonderful illustration of this intuitive concept. Back to the GLBT in Chapter 4 and 5, the GLBT lattice structure imposes a very strict restriction on both analysis and synthesis filters: all of them must have the same length $L = KM + \beta$. The length constraint should be relaxed further to $L_i = K_i M + \beta$. This is the most general class of practical FIR LPPRFBs whose theory has been studied in depth in Chapter 3.

From a lapped transform perspective, it is advantageous for the transforms to have a set of VL bases. Long basis functions mean larger overlaps of input data and smoother impulse responses, leading to a reduction of blocking artifacts in the reconstructed images. Unfortunately, long basis functions are also the main contributors to severe ringing around strong edges, where huge quantization errors are spread out to smoother neighborhood regions. The remedy to this situation is obvious: developing a class of lapped transforms with basis functions of variable length. The longer basis functions help prevent blocking, while the remaining of the basis functions have shorter length to help minimize ringing.

Viewed from another practical angle, blocking is most noticeable in smooth image regions. Therefore, in order to reduce blocking artifacts, high-frequency filters do not need long overlap windows. In fact, they may not have to be overlapped at all. Careful examination of the impulse responses of the high-frequency bandpass filters in the design examples in Figure 23 – 29 and Figure 34 – 38 confirms this statement: the tail-end coefficients of these filters are rather small in magnitude. If the filter length is restricted mathematically, i.e., these coefficients are structurally enforced to exact zeros, the complexity of the resulting FB can be reduced significantly. As in the previous chapters, paraunitary solution is considered first, followed closely by the direct extension to biorthogonality.

6.2 Lattice Structure

6.2.1 Problem Formulation and Existence Conditions

Let us first consider the simplest multi-band LPPRFB with variable-length filters: a system with N long filters of length MK and $(M-N)$ short filters of length $M(K-1)$. The following theorem describes the class of possible solutions in terms of the FB's symmetry polarity and filter length.

Theorem 6.23 *For the class of linear phase perfect reconstruction filter banks described above where M is even, the number of long filters N and the number of short filters $(M-N)$ must both be even.*

Proof.

The sum of all the lengths of the filters is

$$\begin{aligned}\sum_{i=0}^{M-1} L_i &= NMK + (M-N)M(K-1) \\ &= M(NK + MK - NK - M + N) \\ &= M(MK - M + N).\end{aligned}$$

From Table 2, for even M, $(MK-M+N)$ has to be even. Since M is even, $MK-M$ is even for any K. Therefore, N has to be even, and so is $(M-N)$, i.e., there are an even number of long, as well as short, filters. □

Remarks. First of all, Theorem 6.23 holds for both orthogonal and biorthogonal systems. Secondly, it can be easily derived that, with the further assumption that K is odd, Theorem 6.23 holds true for odd-channel systems as well. Thirdly, recall that the long filters have M extra taps only. In the case where N of the filters are arbitrarily longer, the theorem becomes inconclusive. In fact, if the long filters have $2M$ extra taps, it will be clear later in the chapter that we can easily construct a system with an odd number of long filters by combining the lattices in Figure 18 and Figure 19.

Theorem 6.24 *In an M-channel linear phase paraunitary filter bank with M even, N filters of length MK and $(M-N)$ filters of length $M(K-1)$, half of the long filters are symmetric, and half of the short filters are symmetric.*

Proof.

Let $\mathbf{E}_L(z)$ be the $N \times M$ polyphase matrix of order $(K-1)$, representing the longer filters, and $\mathbf{E}_S(z)$ be the $(M-N) \times M$ polyphase matrix of order $(K-2)$, representing

the shorter filters. Without any loss of generality, the long filters are permuted to be on top. Since $\mathbf{E}(z)$ is paraunitary, we can obtain directly from Definition 2.4 the following results

$$\begin{aligned}\mathbf{E}(z)\mathbf{E}^T(z^{-1}) &= \begin{bmatrix} \mathbf{E}_L(z) \\ \\ \mathbf{E}_S(z) \end{bmatrix} \begin{bmatrix} \mathbf{E}_L^T(z^{-1}) & \mathbf{E}_S^T(z^{-1}) \end{bmatrix} \\ &= \begin{bmatrix} \mathbf{E}_L(z)\mathbf{E}_L^T(z^{-1}) & \mathbf{E}_L(z)\mathbf{E}_S^T(z^{-1}) \\ \\ \mathbf{E}_S(z)\mathbf{E}_L^T(z^{-1}) & \mathbf{E}_S(z)\mathbf{E}_S^T(z^{-1}) \end{bmatrix} = \mathbf{I_M}, \end{aligned} \tag{6.1}$$

and

$$\begin{aligned}\mathbf{E}^T(z^{-1})\mathbf{E}(z) &= \begin{bmatrix} \mathbf{E}_L^T(z^{-1}) & \mathbf{E}_S^T(z^{-1}) \end{bmatrix} \begin{bmatrix} \mathbf{E}_L(z) \\ \\ \mathbf{E}_S(z) \end{bmatrix} \\ &= \mathbf{E}_L^T(z^{-1})\mathbf{E}_L(z) + \mathbf{E}_S^T(z^{-1})\mathbf{E}_S(z) = \mathbf{I_M}. \end{aligned} \tag{6.2}$$

Furthermore, $\mathbf{E}(z)$ also has to satisfy the LP property in Eq.(3.8) of Corollary 3.7

$$\begin{bmatrix} \mathbf{E}_L(z) \\ \\ \mathbf{E}_S(z) \end{bmatrix} = \begin{bmatrix} z^{-(K-1)}\mathbf{I}_N & \mathbf{0} \\ \\ \mathbf{0} & z^{-(K-2)}\mathbf{I}_{M-N} \end{bmatrix} \begin{bmatrix} \mathbf{D}_L & \mathbf{0} \\ \\ \mathbf{0} & \mathbf{D}_S \end{bmatrix} \begin{bmatrix} \mathbf{E}_L(z^{-1}) \\ \\ \mathbf{E}_S(z^{-1}) \end{bmatrix} \begin{bmatrix} \mathbf{0} & \mathbf{J} \\ \\ \mathbf{J} & \mathbf{0} \end{bmatrix}, \tag{6.3}$$

where $N \times N$ $\mathbf{D}_L$ and $(M-N) \times (M-N)$ $\mathbf{D}_S$ are diagonal matrices whose entry is $+1$ when the corresponding filter is symmetric and -1 when the corresponding filter is antisymmetric. The traces of these two matrices hold the key to the number of long (as well as short) symmetric and antisymmetric filters.

From Eq.(6.3), we can obtain the following relationships

$$\begin{cases} \mathbf{E}_L(z) &= z^{-(K-1)}\, \mathbf{D}_L\, \mathbf{E}_L(z^{-1})\, \mathbf{J}_M \\ \\ \mathbf{E}_S(z) &= z^{-(K-2)}\, \mathbf{D}_S\, \mathbf{E}_S(z^{-1})\, \mathbf{J}_M. \end{cases} \tag{6.4}$$

Since $\mathbf{E}_L(z)\mathbf{E}_L^T(z^{-1}) = \mathbf{I}_N$ and $\mathbf{E}_S(z)\mathbf{E}_S^T(z^{-1}) = \mathbf{I}_{M-N}$ from Eq.(6.1), solving for $\mathbf{D}_L$ and $\mathbf{D}_S$ yields

$$\begin{cases} \mathbf{D}_L &= z^{-(K-1)}\ \mathbf{E}_L(z^{-1})\ \mathbf{J}_M\ \mathbf{E}_L^T(z^{-1}) \\ \mathbf{D}_S &= z^{-(K-2)}\ \mathbf{E}_S(z^{-1})\ \mathbf{J}_M\ \mathbf{E}_S^T(z^{-1}). \end{cases} \tag{6.5}$$

Taking the trace of both sides and using the fact that $tr(\mathbf{AB}) = tr(\mathbf{BA})$, we have

$$\begin{cases} tr(\mathbf{D}_L) &= tr(z^{-(K-1)}\mathbf{E}_L(z^{-1})\mathbf{J}_M\mathbf{E}_L^T(z^{-1})) &= tr(z^{-(K-1)}\mathbf{E}_L^T(z^{-1})\mathbf{E}_L(z^{-1})\mathbf{J}_M) \\ tr(\mathbf{D}_S) &= tr(z^{-(K-2)}\mathbf{E}_S(z^{-1})\mathbf{J}_M\mathbf{E}_S^T(z^{-1})) &= tr(z^{-(K-2)}\mathbf{E}_S^T(z^{-1})\mathbf{E}_S(z^{-1})\mathbf{J}_M). \end{cases} \tag{6.6}$$

$Tr(\mathbf{D}_L)$ and $tr(\mathbf{D}_S)$ are constants, therefore, their values can be obtained by evaluating the right-hand sides of the above equation at any specific value of z. First, let us consider the case of even K. Evaluating Eq.(6.6) at $z = 1$ yields

$$\begin{cases} tr(\mathbf{D}_L) &= tr(\mathbf{E}_L^T(1)\ \mathbf{E}_L(1)\ \mathbf{J}_M) \\ tr(\mathbf{D}_S) &= tr(\mathbf{E}_S^T(1)\ \mathbf{E}_S(1)\ \mathbf{J}_M). \end{cases} \tag{6.7}$$

On the other hand, evaluating Eq.(6.6) at $z = -1$ yields

$$\begin{cases} tr(\mathbf{D}_L) &= -\ tr(\mathbf{E}_L^T(-1)\ \mathbf{E}_L(-1)\ \mathbf{J}_M) \\ tr(\mathbf{D}_S) &= \quad tr(\mathbf{E}_S^T(-1)\ \mathbf{E}_S(-1)\ \mathbf{J}_M). \end{cases} \tag{6.8}$$

From Eq.(6.2), we also have

$$\begin{cases} \mathbf{E}_L^T(1)\ \mathbf{E}_L(1)\ \mathbf{J}_M + \mathbf{E}_S^T(1)\ \mathbf{E}_S(1)\ \mathbf{J}_M &= \mathbf{J}_M \\ \mathbf{E}_L^T(-1)\ \mathbf{E}_L(-1)\ \mathbf{J}_M + \mathbf{E}_S^T(-1)\ \mathbf{E}_S(-1)\ \mathbf{J}_M &= \mathbf{J}_M. \end{cases} \tag{6.9}$$

Hence, since $tr(\mathbf{J}_M) = 0$, Eq.(6.7) and Eq.(6.9) provide

$$\begin{aligned} tr(\mathbf{D}_L) &= tr(\mathbf{E}_L^T(1)\ \mathbf{E}_L(1)\ \mathbf{J}_M) = tr(\mathbf{J}_M - \mathbf{E}_S^T(1)\ \mathbf{E}_S(1)\ \mathbf{J}_M) \\ &= tr(\mathbf{J}_M) - tr(\mathbf{E}_S^T(1)\ \mathbf{E}_S(1)\ \mathbf{J}_M) = -\ tr(\mathbf{E}_S^T(1)\ \mathbf{E}_S(1)\ \mathbf{J}_M). \end{aligned}$$

Also, from Eq.(6.8) and Eq.(6.9),

$$\begin{aligned} tr(\mathbf{D}_L) &= -tr(\mathbf{E}_L^T(-1)\,\mathbf{E}_L(-1)\,\mathbf{J}_M) = -tr(\mathbf{J}_M - \mathbf{E}_S^T(-1)\,\mathbf{E}_S(-1)\,\mathbf{J}_M) \\ &= -tr(\mathbf{J}_M) + tr(\mathbf{E}_S^T(-1)\,\mathbf{E}_S(-1)\,\mathbf{J}_M) = tr(\mathbf{E}_S^T(1)\,\mathbf{E}_S(1)\,\mathbf{J}_M). \end{aligned}$$

Therefore, $tr(\mathbf{E}_S^T(1)\,\mathbf{E}_S(1)\,\mathbf{J}_M) = 0$, leading to the desired result that

$$tr(\mathbf{D}_L) = 0 \quad \text{and} \quad tr(\mathbf{D}_S) = 0.$$

In other words, half of the longer filters are symmetric while the remaining half are antisymmetric. Similarly, half of the short filters are symmetric, the rest are antisymmetric. It is a simple exercise to verify that the same conclusion can be reached for the case of odd K. □

Theorem 6.25 *In an M-channel linear phase perfect reconstruction filter bank with M even, N filters of length MK, $(M-N)$ filters of length $M(K-1)$, each analysis filter $h_i[n]$ and the corresponding synthesis filter $f_i[n]$ have the same length $L_i, 0 \le i \le M-1$, then half of the long analysis filters are symmetric, and half of the short analysis filters are symmetric. So are the synthesis filters.*

Proof.

The proof of Theorem 6.25 can be modeled closely after the proof of Theorem 6.24. The polyphase matrix of the synthesis bank $\mathbf{R}(z)$ is no longer the delayed transpose of the analysis bank's polyphase matrix $\mathbf{E}(z)$. As in Theorem 4.15 and Lemma 4.16, we consider a causal $\mathbf{E}(z)$ and an anticausal $\mathbf{R}(z^{-1})$ for clarity of presentation only. The

relationship between the two polyphase matrices now becomes

$$\mathbf{R}(z^{-1})\,\mathbf{E}(z) \;=\; \mathbf{E}(z)\,\mathbf{R}(z^{-1}) \;=\; \mathbf{I}.$$

Now, let $\mathbf{E}_L(z)$ be the $\alpha \times M$ polyphase matrix of order $(K-1)$, representing the long analysis filters, and $\mathbf{E}_S(z)$ be the $(M-\alpha) \times M$ polyphase matrix of order $(K-2)$, representing the shorter analysis filters. Similarly, let $\mathbf{R}_L(z)$ and $\mathbf{R}_S(z)$ represent the long and the short synthesis filters respectively. Without any loss of generality, the long analysis filters are permuted to be on top. Consequently, all long synthesis filters are permuted to the left because $h_i[n]$ and $f_i[n]$ have the same length L_i. We can now obtain

$$\begin{aligned}
\mathbf{E}(z)\,\mathbf{R}(z^{-1}) &= \begin{bmatrix} \mathbf{E}_L(z) \\ \mathbf{E}_S(z) \end{bmatrix} \begin{bmatrix} \mathbf{R}_L(z^{-1}) & \mathbf{R}_S(z^{-1}) \end{bmatrix} \\
&= \begin{bmatrix} \mathbf{E}_L(z)\mathbf{R}_L(z^{-1}) & \mathbf{E}_L(z)\mathbf{R}_S(z^{-1}) \\ \mathbf{E}_S(z)\mathbf{R}_L(z^{-1}) & \mathbf{E}_S(z)\mathbf{R}_S(z^{-1}) \end{bmatrix} = \mathbf{I}, \qquad (6.10)
\end{aligned}$$

and

$$\begin{aligned}
\mathbf{R}(z^{-1})\,\mathbf{E}(z) &= \begin{bmatrix} \mathbf{R}_L(z^{-1}) & \mathbf{R}_S(z^{-1}) \end{bmatrix} \begin{bmatrix} \mathbf{E}_L(z) \\ \mathbf{E}_S(z) \end{bmatrix} \\
&= \mathbf{R}_L(z^{-1})\mathbf{E}_L(z) + \mathbf{R}_S(z^{-1})\mathbf{E}_S(z) = \mathbf{I}. \qquad (6.11)
\end{aligned}$$

From here on, the remainder of the proof is identical to the counterpart in Theorem 6.24 by replacing $\mathbf{E}_L^T(z)$ and $\mathbf{E}_S^T(z)$ by $\mathbf{R}_L(z^{-1})$ and $\mathbf{R}_S(z^{-1})$, respectively. □

6.2.2 Orthogonal Lattice Structure

From Theorem 6.24, there are $\frac{N}{2}$ long symmetric filters and $\frac{N}{2}$ long antisymmetric filters. If the long symmetric filters are permuted to be on top, i.e.,

$$\mathbf{D}_L = \begin{bmatrix} \mathbf{I}_{\frac{N}{2}} & \mathbf{0}_{\frac{N}{2}} \\ \mathbf{0}_{\frac{N}{2}} & -\mathbf{I}_{\frac{N}{2}} \end{bmatrix},$$

they now form a remarkably similar system to an N-channel LPPUFB where all filters have the same length KM

$$\mathbf{E}_L(z) = z^{-(K-1)}\mathbf{D}_L\mathbf{E}_L(z^{-1})\mathbf{J}_M \tag{6.12}$$

From [62] (and the more general results in Chapter 4), there exists a factorization similar to the one shown in Eq.(2.26) that reduces the order of the polyphase matrix $\mathbf{E}_L(z)$ by one. Hence, the VLLOT's polyphase matrix $\mathbf{E}(z)$ can always be factorized as follows

$$\mathbf{E}(z) \;=\; \hat{\mathbf{G}}_0(z)\,\mathbf{E}_{K-2}(z) \;=\; \hat{\mathbf{\Phi}}_0\,\hat{\mathbf{W}}\,\hat{\mathbf{\Lambda}}(z)\,\hat{\mathbf{W}}\,\hat{\mathbf{P}}_0\,\mathbf{E}_{K-2}(z), \tag{6.13}$$

where

$$\hat{\mathbf{W}} \;=\; \begin{bmatrix} \mathbf{I}_{\frac{N}{2}} & \mathbf{I}_{\frac{N}{2}} & \mathbf{0} \\ \mathbf{I}_{\frac{N}{2}} & -\mathbf{I}_{\frac{N}{2}} & \mathbf{0} \\ \mathbf{0} & \mathbf{0} & \mathbf{I}_{M-N} \end{bmatrix}, \quad \hat{\mathbf{\Lambda}}(z) \;=\; \begin{bmatrix} \mathbf{I}_{\frac{N}{2}} & \mathbf{0} & \mathbf{0} \\ \mathbf{0} & z^{-1}\mathbf{I}_{\frac{N}{2}} & \mathbf{0} \\ \mathbf{0} & \mathbf{0} & \mathbf{I}_{M-N} \end{bmatrix}, \tag{6.14}$$

and

$$\hat{\mathbf{\Phi}}_0 \;=\; \begin{bmatrix} \hat{\mathbf{U}}_0 & \mathbf{0} & \mathbf{0} \\ \mathbf{0} & \hat{\mathbf{V}}_0 & \mathbf{0} \\ \mathbf{0} & \mathbf{0} & \mathbf{I}_{M-N} \end{bmatrix}. \tag{6.15}$$

$\hat{\mathbf{P}}_0$ is the permutation matrix that arranges the longer filters on top, i.e.,

$$\hat{\mathbf{P}}_0 \;=\; \begin{bmatrix} \mathbf{I}_{\frac{N}{2}} & \mathbf{0} & \mathbf{0} & \mathbf{0} \\ \mathbf{0} & \mathbf{0} & \mathbf{I}_{\frac{N}{2}} & \mathbf{0} \\ \mathbf{0} & \mathbf{I}_{\frac{(M-N)}{2}} & \mathbf{0} & \mathbf{0} \\ \mathbf{0} & \mathbf{0} & \mathbf{0} & \mathbf{I}_{\frac{(M-N)}{2}} \end{bmatrix};$$

and it is added to simplify the presentation only. The reader should note that the above factorization leaves $\mathbf{E}_S(z)$ untouched, it reduces the length of the longer filters by M, so all filters now have the same length of $M(K-1)$. $\mathbf{E}_{K-2}(z)$ is the familiar polyphase matrix of an order-$(K-2)$ GenLOT. The rotation angles of $\frac{N}{2} \times \frac{N}{2}$ orthogonal matrices $\hat{\mathbf{U}}_0$ and $\hat{\mathbf{V}}_0$ are the VL stage's free parameters that can be varied independently and arbitrarily to optimize the VLLOT. Comparing to the traditional order-$(K-1)$ GenLOT, the number of free parameters is reduced by $\frac{M(M-2)}{4} - \frac{N(N-2)}{4}$. The reduction can be quite significant if the number of channels M is large and the number of long filters N is small. In the case that $N = 2$, the number of free parameters comes from $\mathbf{E}_{K-2}(z)$ only: $\hat{\mathbf{U}}_0$ and $\hat{\mathbf{V}}_0$ become singletons 1's. We shall see in a later section that the biorthogonal generalization results in two free parameters.

As aforementioned, with $\hat{\mathbf{G}}_0(z)$ peeled off, $\mathbf{E}_{K-2}(z)$ becomes the familiar polyphase matrix of an order-$(K-2)$ GenLOT, and it can be factorized into the familiar cascade structure in Eq.(2.26) where each cascading block $\mathbf{G}_i(z)$ has the form in Eq.(2.27). The complete factorization is given by

$$\mathbf{E}(z) \;=\; \hat{\mathbf{G}}_0(z)\,\mathbf{E}_{K-2}(z) \;=\; \hat{\mathbf{\Phi}}_0\,\hat{\mathbf{W}}\,\hat{\mathbf{\Lambda}}(z)\,\hat{\mathbf{W}}\,\hat{\mathbf{P}}_0 \prod_{i=K-2}^{1} \mathbf{G}_i(z)\,\mathbf{E}_0. \tag{6.16}$$

A detailed example of the complete lattice is illustrated in Figure 39.

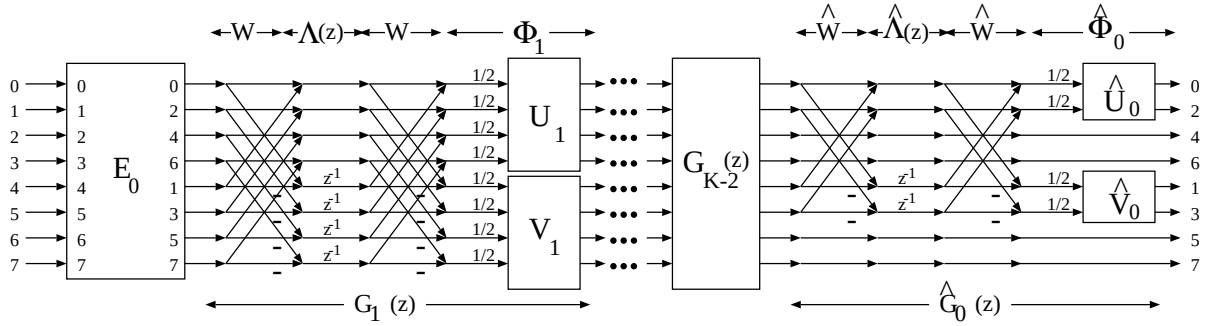

Figure 39: Detailed lattice structure for the VLLOT (drawn for $M = 8$ and $N = 4$).

Theorem 6.26 *The proposed factorization of* $\mathbf{E}(z)$ *in Eq.(6.16) is minimal, i.e., the lattice structure uses a minimal number of delays in the VLLOT implementation.*

Proof.

Recall that a structure is defined to be minimal when the required number of delays is equal to the degree of the transfer function [95]. For lossless systems, it can be proven [95] that $deg(\mathbf{E}(z)) = deg(|\mathbf{E}(z)|)$.

Exploiting the LP property of the FB polyphase matrix in Eq.(6.3), we have

$$\begin{aligned} deg(\mathbf{E}(z)) &= deg(|\mathbf{E}(z)|) \\ &= deg\left(\left| \begin{array}{cc} z^{-(K-1)}\mathbf{I}_N & \mathbf{0} \\ \mathbf{0} & z^{-(K-2)}\mathbf{I}_{M-N} \end{array} \right| \left| \begin{array}{cc} \mathbf{D}_L & \mathbf{0} \\ \mathbf{0} & \mathbf{D}_S \end{array} \right| \left| \begin{array}{c} \mathbf{E}_L(z^{-1}) \\ \mathbf{E}_S(z^{-1}) \end{array} \right| \left| \begin{array}{cc} \mathbf{0} & \mathbf{J} \\ \mathbf{J} & \mathbf{0} \end{array} \right| \right) \\ &= N(K-1) + (M-N)(K-2) - deg(\mathbf{E}(z)). \end{aligned}$$

Hence,

$$deg(\mathbf{E}(z)) = \frac{N(K-1) + (M-N)(K-2)}{2} = \frac{M(K-2)}{2} + \frac{N}{2}.$$

In the proposed factorization, we use $\frac{M(K-2)}{2}$ delays for $\mathbf{E}_{K-2}(z)$ and $\frac{N}{2}$ for $\hat{\mathbf{G}}_0(z)$, totaling the same number of delays as the degree of $\mathbf{E}(z)$. Therefore, the factorization is minimal. □

It is interesting to note that when N increases to M or decreases to 0, the VLLOT's required number of delay elements increases to $\frac{M(K-1)}{2}$ or decreases to $\frac{M(K-2)}{2}$ – consistent with the delays needed in the GenLOT's implementation [62]. Table 5 provides a comparison in implementation complexity of the popular DCT, LOT, and several low-order VLLOT.

Transform / Complexity	8x8 DCT	2x16 6x8 VLLOT	4x16 4x8 VLLOT	6x16 2x8 VLLOT	4x24 4x8 VLLOT	8x16 LOT
Number of Lattice Coefficients	12	12	14	18	16	24
Number of Delay Elements	0	1	2	3	4	4

Table 5: Complexity comparison between the DCT, the LOT, and various VLLOTs.

More general and complicated VLLOT can be constructed by a cascade of building blocks $\hat{\mathbf{G}}_i$ as follows

$$\mathbf{E}(z) \;=\; \hat{\mathbf{G}}_{\ell-1}(z) \cdots \hat{\mathbf{G}}_1(z)\, \hat{\mathbf{G}}_0(z)\, \mathbf{G}_{K-1}(z) \cdots \mathbf{G}_1(z)\, \mathbf{G}_0(z), \tag{6.17}$$

where $N_0 \geq N_1 \geq \cdots \geq N_{\ell-1}$ and each N_i is even. The longest filters have length $M(K+\ell)$ whereas the shortest filters have length MK. The general lattice structure is depicted in Figure 40.

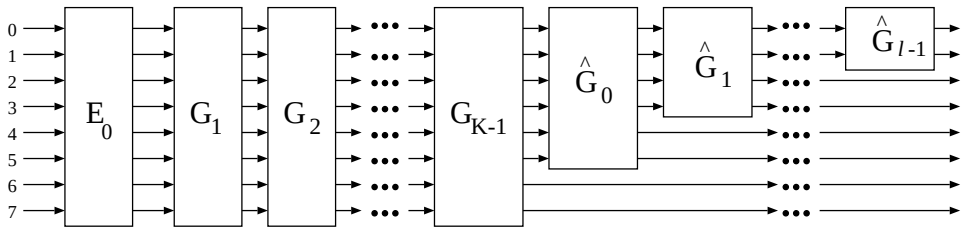

Figure 40: General lattice structure for the VLLOT.

Design Examples

Several VLLOT design examples are presented. Some of them are obtained from unconstrained nonlinear optimization where the lattice coefficients are the free parameters. In an alternative (and faster) design procedure, the filters are first obtained using the iterative method based on time-domain constraints [27]. Then, the lattice coefficients can be calculated from the resulting FB coefficients. In both optimization procedures, the cost function is the familiar combination of coding gain, DC leakage and attenuation around mirror frequencies as described in Section 4.7. The magnitude responses and the impulse responses of several new VLLOTs are depicted in Figure 41 – 43. Refer to Table 6 for a comparison of several objective properties of the design examples. Given the same order K, the VLLOT cannot match GenLOT in term of objective performance (coding gain and stopband attenuation for example) because it belongs to a subclass of GenLOT. However, VLLOT's variable-length basis functions make it an attractive transform candidate for perceptually-tuned image coders: reconstructed VLLOT images are more visually pleasant as testified in Chapter 7. Since the application we have in mind is image compression, all presented FB examples have high-frequency-band filters chosen to be short. The lattice structure does allow one to shorten other filters if he or

she desires to.

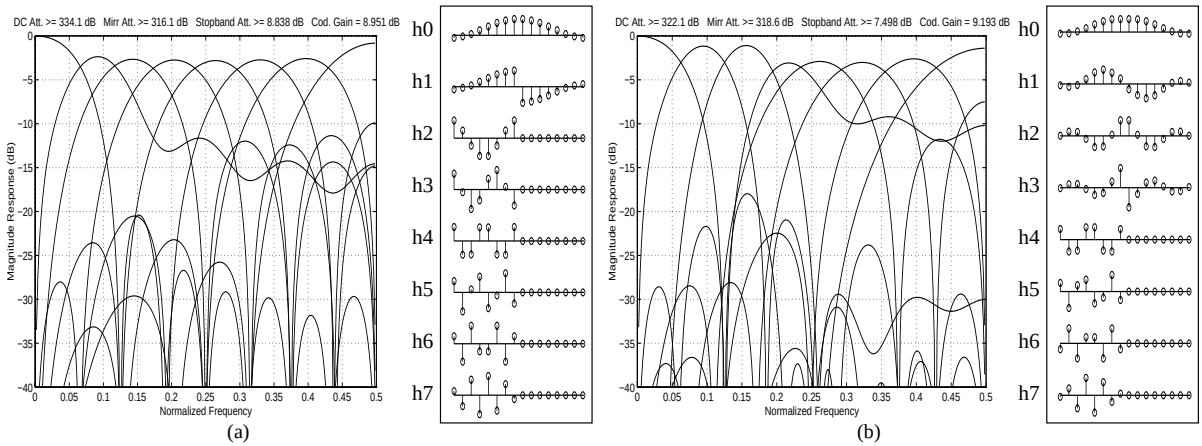

Figure 41: VLLOTs optimized for coding gain, DC attenuation, mirror frequency attenuation, and stopband attenuation. (a) Design example I: 2×16 6×8. (b) Design example II: 4×16 4×8.

6.2.3 Biorthogonal Lattice Structure

Obtaining the biorthogonal lattice structure for LPPRFB with VL filters from its orthogonal relative in the previous section is rather straightforward – the transpositional relationship between the polyphase matrices now becomes invertible. The orthogonal matrices $\hat{\mathbf{U}}_i$, $\hat{\mathbf{V}}_i$, $\mathbf{U}_i$, and $\mathbf{V}_i$ in the lattices in Figure 39 and 40 can be chosen to be invertible instead. These invertible matrices can then be completely parameterized by a set of rotation angles $\{\theta_i\}$ and diagonal multipliers $\{\alpha_i\}$ from their SVD representations as illustrated in Figure 20 of Section 4.5. The resulting biorthogonal lattice is called the variable-length generalized lapped biorthogonal transform (VLGLBT).

A more interesting discussion is on how we can exploit the newly-found flexibility of

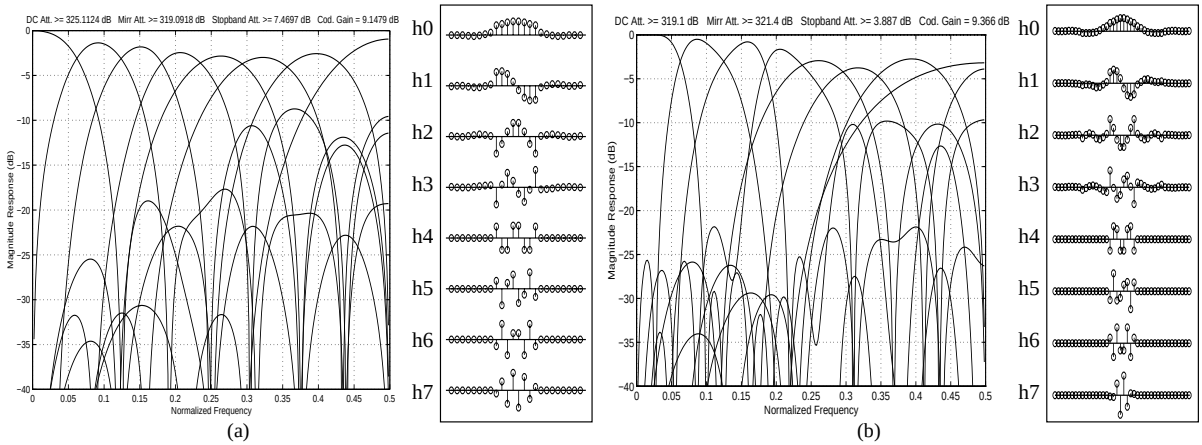

Figure 42: VLLOTs optimized for coding gain, DC attenuation, mirror frequency attenuation, and stopband attenuation. (a) Design example III: $4 \times 24 \;\; 4 \times 8$. (b) Design example IV: $4 \times 40 \;\; 4 \times 8$.

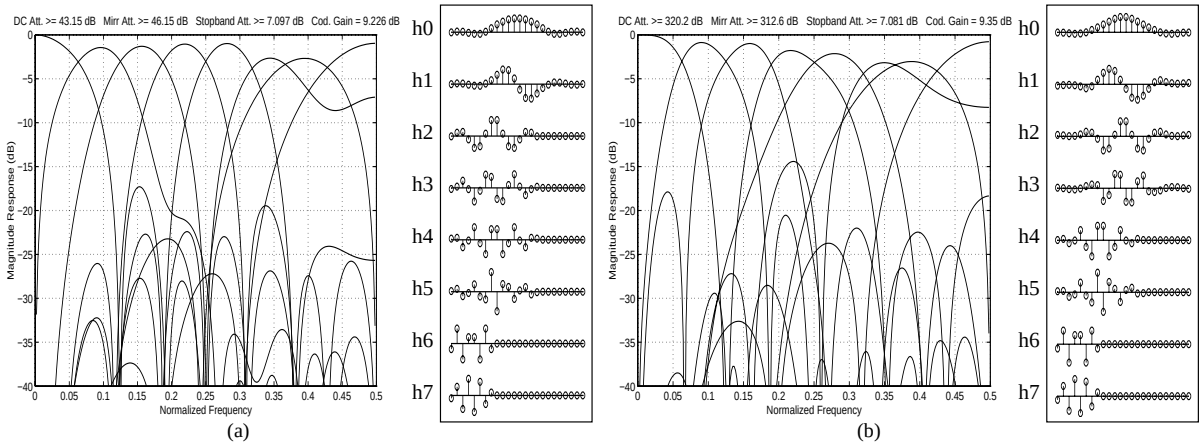

Figure 43: VLLOTs optimized for coding gain, DC attenuation, mirror frequency attenuation, and stopband attenuation. (a) Design example V: $2 \times 24 \;\; 4 \times 16 \;\; 2 \times 8$. (b) Design example VI: $4 \times 24 \;\; 2 \times 16 \;\; 2 \times 8$.

the VLGLBT to our advantage. Despite significant performance improvements, lapped transforms have not yet been able to dislodge the DCT in practical systems [98]. The most obvious reason is the increase in computational complexity. The rest of this section is devoted to the design of a high-performance, yet low-complexity, lapped transform to replace the DCT in the near future.

The VL structure $\hat{\mathbf{G}}_i(z) = \hat{\mathbf{\Phi}}_i\, \hat{\mathbf{W}}\, \hat{\mathbf{\Lambda}}(z)\, \hat{\mathbf{W}}$ where

$$\hat{\mathbf{\Phi}}_i = \begin{bmatrix} \hat{\mathbf{U}}_i & \mathbf{0} & \mathbf{0} \\ \mathbf{0} & \hat{\mathbf{V}}_i & \mathbf{0} \\ \mathbf{0} & \mathbf{0} & \mathbf{I_{M-N}} \end{bmatrix}$$

increases the length of N filters by M and leaves the rest intact. To minimize the transform's complexity, we choose $N = 2$ and the initial stage to be the DCT itself. In the orthogonal case, only trivial solution can be obtained (see Figure 41(a)) since the matrices $\hat{\mathbf{U}}_i$ and $\hat{\mathbf{V}}_i$ degenerate to singleton 1 or -1, and we do not have any free parameters for further transform optimization. In the more general biorthogonal case, nontrivial solutions exist. In fact, an example of such system has been presented earlier in Section 4.6. The invertible matrices $\hat{\mathbf{U}}_i$ and $\hat{\mathbf{V}}_i$ now becomes the lattice coefficients α_{i0} and α_{i1} as shown in the 2-channel PR lattice in Figure 22.

The transform's variable-length property allows us to design fast, low-complexity lapped transforms. The detailed lattice structure of the fast VLGLBT is depicted in Figure 44. Comparing to the DCT, the fast VLGLBT only requires 6 more multiplications, 8 more additions, and 2 more delays. An equivalent interpretation is to perform the DCT on the whole input signal, then 2 lowest-frequency coefficients from each of the

two neighboring blocks (one to the left and the other to the right) and 2 lowest-frequency coefficients from the current block are combined to produce the VLGLBT's transform coefficients. Despite its simplicity, the VLGLBT provides a significant improvement in image quality over the traditional DCT – little blocking and ringing artifacts at medium and high compression ratios. The coding results are presented in Chapter 7.

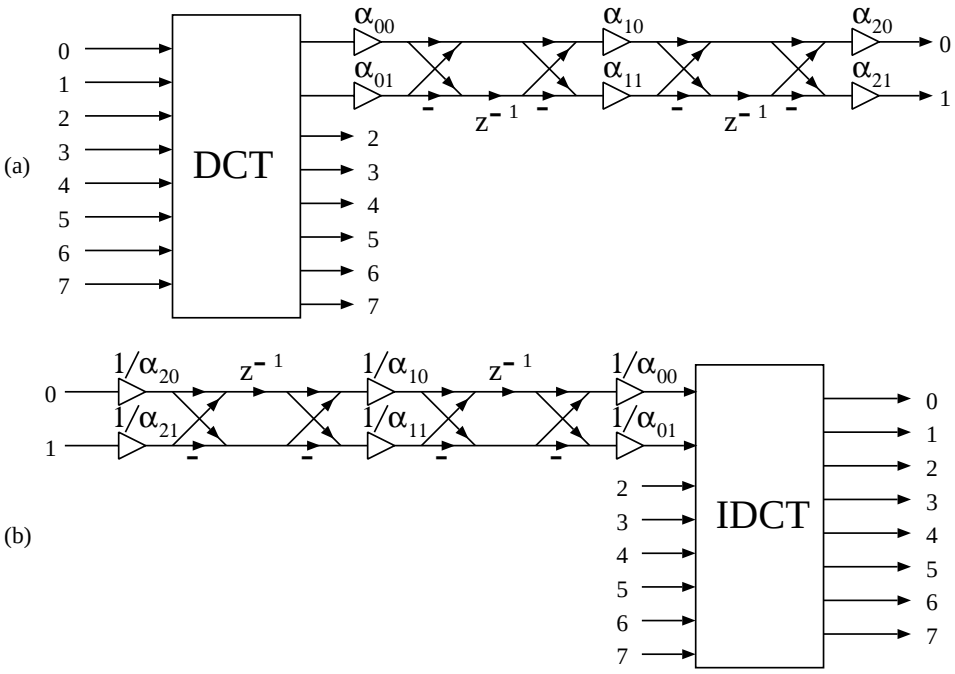

Figure 44: Detailed lattice structure of the fast VLGLBT. (a) Analysis bank. (b) Synthesis bank.

Design Examples

The fast VLGLBT optimized for image coding purpose is obtained using unconstrained nonlinear optimization where the lattice coefficients $\{\alpha_{00}, \alpha_{01}, \alpha_{10}, \alpha_{11}, \alpha_{20}, \alpha_{21}\}$ are the free parameters. Again, the cost function is a weighted combination of coding gain, DC

leakage, stopband attenuation, and mirror frequency attenuation. The frequency and impulse response of the fast VLGLBT's analysis and the synthesis bank are depicted in Figure 45(a) and Figure 45(b) respectively. Note that the last six filters of the VLGLBT come straight form the DCT's. Various properties of this VLGLBT can be found in Table 6.

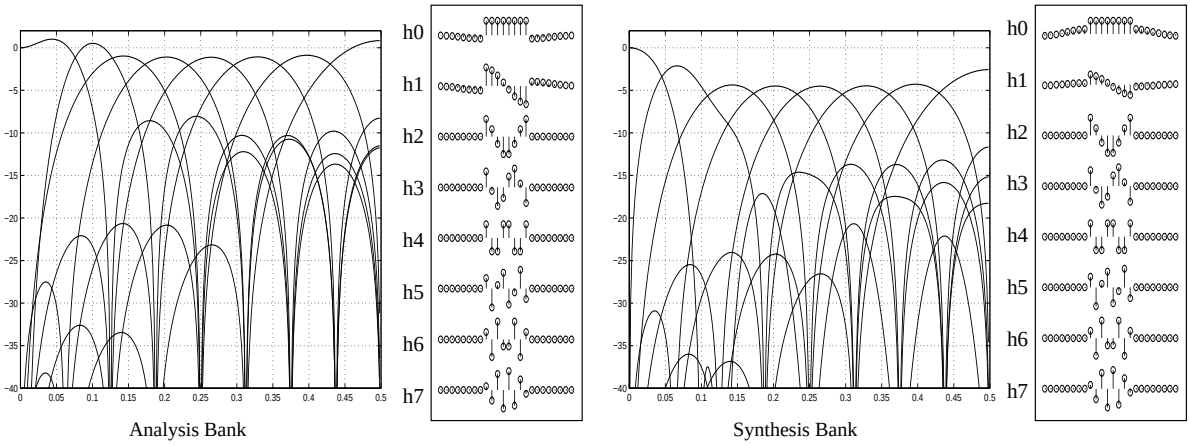

Figure 45: Fast VLGLBT. Design example VII: 2×24 6×8 optimized for coding gain, DC attenuation, mirror frequency attenuation, and stopband attenuation.

6.3 VLLOT via Orthogonal Complement Subspaces

In the lattice structure design method presented in the previous section, the filters' centers of symmetry are not aligned. The alignment of the bases is sometimes desired since it provides more accurate correlation between subband signals, and it can simplify the signal's symmetric extension [61], [63], [8] significantly. Only in cases that the length difference between the long and the short filters are even multiples of M, the alignment of the centers of symmetry can be obtained by shifting the short filters (at the cost of

adding more delay elements of course).

6.3.1 Problem Formulation and Existence Condition

In this section, a different design approach for VLLOTs whose filters all share the same center of symmetry is presented. These FB can be thought of as a subclass of GenLOT where the tail-end coefficients of some filters are forced to be zero. More specifically, given an M-channel GenLOT of length MK with M even, what are the relationships between the building blocks $\mathbf{U}_i$, $\mathbf{V}_i$ in Eq.(2.26) such that the resulting $M \times MK$ coefficients matrix $\mathbf{P}_K$ (storing the impulse responses row-rise) satisfies the following variable-length condition:

$$\mathbf{P}_K = \begin{bmatrix} \mathbf{X}_{N\times\frac{M}{2}} & \mathbf{X}_{N\times\frac{M}{2}} & \cdots & \mathbf{X}_{N\times\frac{M}{2}} & \mathbf{X}_{N\times\frac{M}{2}} \\ \mathbf{0}_{(M-N)\times\frac{M}{2}} & \mathbf{X}_{(M-N)\times\frac{M}{2}} & \cdots & \mathbf{X}_{(M-N)\times\frac{M}{2}} & \mathbf{0}_{(M-N)\times\frac{M}{2}} \end{bmatrix}, \tag{6.18}$$

where the rows of $\mathbf{P}_K$ might have been permuted so that the long filters are arranged on top. Simply speaking, we are studying M-channel LPPUFB where all of the filters share the same center of symmetry, N filters have length MK, and the remaining $(M-N)$ filters have length $M(K-1)$.

Theorem 6.27 *It is impossible to construct a VLLOT described in the problem formulation above with all symmetric (or all antisymmetric) filters being shortened by M taps.*

Proof.

It is a straightforward but tedious exercise to show that the left tail end of the GenLOT coefficient matrix turns out to be [62]

$$\mathbf{P}_K = \begin{bmatrix} \mathbf{U}_{K-1} \prod_{i=K-2}^{0} (\mathbf{U}_i - \mathbf{V}_i) & \mathbf{U}_{K-1} \prod_{i=K-2}^{1} (\mathbf{U}_i - \mathbf{V}_i) (\mathbf{U}_0 + \mathbf{V}_0) \mathbf{J} & \cdots \\ \mathbf{V}_{K-1} \prod_{i=K-2}^{0} (\mathbf{U}_i - \mathbf{V}_i) & \mathbf{V}_{K-1} \prod_{i=K-2}^{1} (\mathbf{U}_i - \mathbf{V}_i) (\mathbf{U}_0 + \mathbf{V}_0) \mathbf{J} & \cdots \end{bmatrix}. \quad (6.19)$$

Suppose that all antisymmetric filters are short, then $\mathbf{V}_{K-1} \prod_{i=K-2}^{0} (\mathbf{U}_i - \mathbf{V}_i) = \mathbf{0}_{\frac{M}{2}}$,

$$\begin{aligned} \Longleftrightarrow \quad & \mathbf{V}_{K-1}^T \mathbf{V}_{K-1} \prod_{i=K-2}^{0} (\mathbf{U}_i - \mathbf{V}_i) = \mathbf{V}_{K-1}^T \mathbf{0}_{\frac{M}{2}} \\ \Longleftrightarrow \quad & \prod_{i=K-2}^{0} (\mathbf{U}_i - \mathbf{V}_i) = \mathbf{0}_{\frac{M}{2}} \\ \Longleftrightarrow \quad & \mathbf{U}_{K-1} \prod_{i=K-2}^{0} (\mathbf{U}_i - \mathbf{V}_i) = \mathbf{0}_{\frac{M}{2}}. \end{aligned}$$

This means that all symmetric filters have to be short as well, and we are left with an order-$(K-2)$ GenLOT. On the other hand, if all symmetric filters are short, so are all antisymmetric filters. □

In the next subsection, we shall show that it is possible to construct various VLLOT if not all of the symmetric (or antisymmetric) filters are short. Equivalently, it is possible to obtain

$$\mathbf{U}_{K-1} \prod_{i=K-2}^{0} (\mathbf{U}_i - \mathbf{V}_i) = \begin{bmatrix} \mathbf{X}_{N \times \frac{M}{2}} \\ \mathbf{0}_{(\frac{M}{2}-N) \times \frac{M}{2}} \end{bmatrix} \text{ or } \mathbf{V}_{K-1} \prod_{i=K-2}^{0} (\mathbf{U}_i - \mathbf{V}_i) = \begin{bmatrix} \mathbf{X}_{N \times \frac{M}{2}} \\ \mathbf{0}_{(\frac{M}{2}-N) \times \frac{M}{2}} \end{bmatrix}, \quad (6.20)$$

or even both.

6.3.2 Design Procedure

Let us first consider the case with $(\frac{M}{2} - N)$ short symmetric filters of length $M(K-1)$. Define the product $\mathbf{Tu} \triangleq \mathbf{U}_{K-1} \prod_{i=K-2}^{1} (\mathbf{U}_i - \mathbf{V}_i)$. It is possible to split $\mathbf{Tu}$'s row space into $\nu \triangleq \mathcal{S}\{\mathbf{tu}_{1.}^T, \mathbf{tu}_{2.}^T, \ldots, \mathbf{tu}_{N.}^T\}$ and the corresponding orthogonal complement $\nu^{\perp}$ [95]. Now, if we choose $(\mathbf{U}_0 - \mathbf{V}_0)$ such that all of its columns lie in ν, then $\mathbf{U}_{K-1} \prod_{i=K-2}^{0} (\mathbf{U}_i - \mathbf{V}_i) = \mathbf{Tu}(\mathbf{U}_0 - \mathbf{V}_0)$ will take the desired form $\begin{bmatrix} \mathbf{X}_{N \times \frac{M}{2}} \\ \mathbf{0}_{(\frac{M}{2}-N) \times \frac{M}{2}} \end{bmatrix}$. Following is an ordered outline of the designing steps:

- Choose arbitrary $\frac{M}{2} \times \frac{M}{2}$ orthogonal matrices $\mathbf{U}_{K-1}$, $\mathbf{B}$, and $\mathbf{U}_i, \mathbf{V}_i, i = 1, 2, \ldots, K-2$.
- Obtain the product $\mathbf{Tu} = \mathbf{U}_{K-1} \prod_{i=K-2}^{1} (\mathbf{U}_i - \mathbf{V}_i)$.
- Find an orthonormal basis for the first N rows of $\mathbf{Tu}$. Find an orthonormal basis for the corresponding orthogonal complement. From these orthonormal row vectors, form the unitary matrix $\mathbf{T}$.
- Obtain the first stage's building blocks by choosing

$$\mathbf{U}_0 = \mathbf{T} \begin{bmatrix} \mathbf{Q}_1 & \mathbf{0}_{N \times (\frac{M}{2}-N)} \\ \mathbf{0}_{(\frac{M}{2}-N) \times N} & \mathbf{Q}_3 \end{bmatrix} \mathbf{B} \quad \text{and} \quad \mathbf{V}_0 = \mathbf{T} \begin{bmatrix} \mathbf{Q}_2 & \mathbf{0}_{N \times (\frac{M}{2}-N)} \\ \mathbf{0}_{(\frac{M}{2}-N) \times N} & \mathbf{Q}_3 \end{bmatrix} \mathbf{B},$$

  where $\mathbf{Q}_1, \mathbf{Q}_2$ are any $N \times N$ orthogonal matrices, and $\mathbf{Q}_3$ is any $(\frac{M}{2} - N) \times (\frac{M}{2} - N)$ orthogonal matrix.

With these particular choices of $\mathbf{U}_0$ and $\mathbf{V}_0$, the columns of the difference matrix $(\mathbf{U}_0 - \mathbf{V}_0)$ can be easily verified to belong to the predefined subspace ν:

$$\mathbf{U}_0 - \mathbf{V}_0 \;=\; \mathbf{T}\begin{bmatrix} \mathbf{Q}_1 & \mathbf{0} \\ \mathbf{0} & \mathbf{Q}_3 \end{bmatrix}\mathbf{B} - \mathbf{T}\begin{bmatrix} \mathbf{Q}_2 & \mathbf{0} \\ \mathbf{0} & \mathbf{Q}_3 \end{bmatrix}\mathbf{B} \;=\; \mathbf{T}\left(\begin{bmatrix} \mathbf{Q}_1 - \mathbf{Q}_2 & \mathbf{0} \\ \mathbf{0} & \mathbf{0} \end{bmatrix}\right)\mathbf{B}.$$

The rotation angles of the arbitrary orthogonal matrices are the free parameters that can be tuned to optimize the VLLOT for any further desired criterion. Note that we only have to put constraints on the first and last stage of GenLOT's lattice structure to obtain VLLOT of the same order. These two stages control the orthogonality between rows and columns of the building blocks to reduce the length of $(\frac{M}{2}-N)$ filters by M. The constraints added to obtain VL reduce the total number of free parameters to optimized by

$$\begin{pmatrix} M/2 \\ 2 \end{pmatrix} - \left[2\begin{pmatrix} N \\ 2 \end{pmatrix} + \begin{pmatrix} M/2 - N \\ 2 \end{pmatrix}\right].$$

The reduction is independent of the order K and can be significant for large M.

The same method can be applied to shorten any N antisymmetric filters as long as N is less than $\frac{M}{2}$. If only N antisymmetric filters and N symmetric filters are desired to be long, we have to ensure that the matrix $\mathbf{Tv} \stackrel{\triangle}{=} \mathbf{V}_{K-1}\prod_{i=K-2}^{1}(\mathbf{U}_i - \mathbf{V}_i)$ is appropriately chosen such that its row space can be split into the same two orthogonal subspaces ν and $\nu^{\perp}$. We propose the following solution

- Choose $\mathbf{V}_{K-1} = \begin{bmatrix} \mathbf{Q}_4 & \mathbf{0}_{N\times(\frac{M}{2}-N)} \\ \mathbf{0}_{(\frac{M}{2}-N)\times N} & \mathbf{Q}_5 \end{bmatrix}\mathbf{U}_{K-1}$, where $\mathbf{Q}_4$, $\mathbf{Q}_5$ are, respectively, arbitrary $N \times N$ and $(\frac{M}{2} - N) \times (\frac{M}{2} - N)$ orthogonal matrices.

With this particular choice of $\mathbf{V}_{K-1}$, both of the VL properties in Eq.(6.20) can be satisfied simultaneously:

$$\begin{aligned}
\mathbf{V}_{K-1}\prod_{i=K-2}^{0}(\mathbf{U}_i-\mathbf{V}_i) &= \begin{bmatrix} \mathbf{Q}_4 & \mathbf{0}_{N\times(\frac{M}{2}-N)} \\ \mathbf{0}_{(\frac{M}{2}-N)\times N} & \mathbf{Q}_5 \end{bmatrix} \mathbf{U}_{K-1}\prod_{i=K-2}^{0}(\mathbf{U}_i-\mathbf{V}_i) \\
&= \begin{bmatrix} \mathbf{Q}_4 & \mathbf{0}_{N\times(\frac{M}{2}-N)} \\ \mathbf{0}_{(\frac{M}{2}-N)\times N} & \mathbf{Q}_5 \end{bmatrix} \begin{bmatrix} \mathbf{X}_{N\times\frac{M}{2}} \\ \mathbf{0}_{(\frac{M}{2}-N)\times\frac{M}{2}} \end{bmatrix} \\
&= \begin{bmatrix} \mathbf{Q}_4\,\mathbf{X}_{N\times\frac{M}{2}} \\ \mathbf{0}_{(\frac{M}{2}-N)\times\frac{M}{2}} \end{bmatrix}.
\end{aligned}$$

In this case, $\mathbf{V}_{K-1}$ contains $\frac{N(N-1)}{2} + \frac{(M-2N)(M-2N-2)}{8}$ degrees of freedom instead of $\frac{M(M-2)}{4}$. Again, the reduction in the amount of free rotation angles is significant for large M.

This design method using orthogonal complement subspaces keys on the relationship between the GenLOT's building blocks $\mathbf{U}_i$ and $\mathbf{V}_i$ to obtain the coefficient matrix $\mathbf{P}$ directly. Hence, it can be classified as a time-domain design method. The resulted system is guaranteed to have LP as well as PR. Furthermore, the filters can have different lengths, yet all centers of symmetry are aligned. The FB can still be represented by a lattice structure. However, the VL property is not robust under the quantization of lattice coefficients.

6.3.3 Design Examples

Several VLLOT design examples using the orthogonal complement subspace method are presented in Figure 46 and Figure 47. Notice that the filters have the same center of symmetry in all design examples. Refer to Section 4.7 for a description of the design procedure and various design aspects. Transform properties of Design example VIII and Design example IX can be found in Table 6.

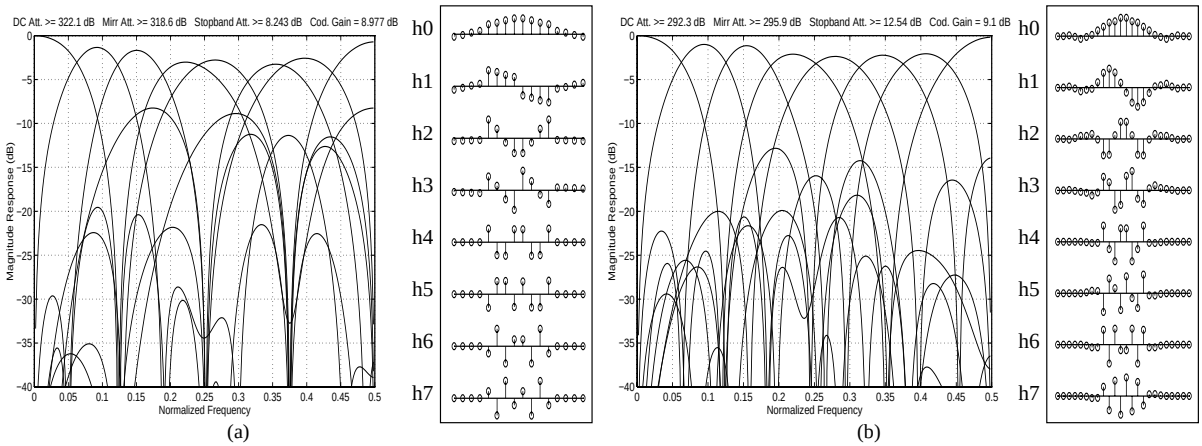

Figure 46: VLLOTs designed by the orthogonal complement subspace method. (a) Design example VIII: 4×16 4×8 optimized for coding gain and DC attenuation. (b) Design example IX: 4×24 4×16 optimized for coding gain, stopband attenuation, DC and mirror frequency attenuation.

Transform Property	Transform							
	8x8 DCT	8x16 LOT	2x16 6x8 VLLOT (I)	4x24 4x8 VLLOT (III)	4x24 2x16 2x8 VLLOT (VI)	4x16 4x8 VLLOT (VIII)	4x24 4x16 VLLOT (IX)	2x24 6x8 VLGLBT
Coding Gain (dB)	8.83	9.22	8.95	9.15	9.35	8.98	9.10	9.23
DC Attenuation (-dB)	310.62	312.56	334.10	325.11	320.20	322.12	292.30	314.38
Stopband Attenuation (-dB)	9.96	19.38	8.84	7.47	7.08	8.24	12.54	8.05
Mirror Freq. Attenuation (-dB)	322.10	317.24	316.10	319.09	312.60	318.60	295.93	309.76

Table 6: Comparison of VLLOT and VLGLBT properties.

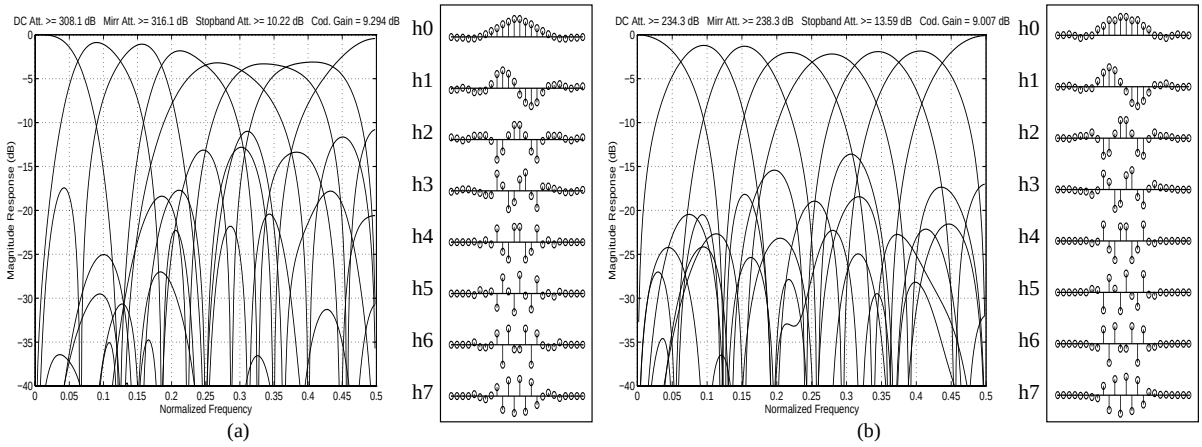

Figure 47: VLLOTs designed by the orthogonal complement subspace method. (a) Design example X: $4 \times 24 \quad 4 \times 16$ optimized primarily for coding gain. (b) Design example XI: $4 \times 24 \quad 4 \times 16$ optimized primarily for stopband attenuation.

6.4 Summary

In this chapter, the theory, design, and lattice structure of LPPRFBs with filters of different lengths have been presented and analyzed. The proposed lattice structure is robust under coefficient quantization: it retains all attractive properties of the new FBs (LP, PR, and variable-length), and it is minimal resulting in a fast and efficient implementation. The lattice is proven to span the complete class of permissible solutions: the number of long filters must be even; half of the long filters are symmetric and the other half are anti-symmetric, and so are the short filters. An alternate design method that keys on the relationship between the lattice coefficients to obtain variable-length filters is also discussed.

The new family of FBs can be interpreted as a class of general lapped orthogonal/biorthogonal transforms with basis functions of variable lengths, called VLLOT and

VLGLBT. The initial stage of these transforms can be chosen to be the DCT so that existing fast software and hardware implementation can be retained. The VL subclass of LPPRFBs finds application in transform-based image compression since it relies on its long basis functions to reconstruct smooth signal components while uses its short basis functions to represent edges and textures. Experimental results presented in the next chapter show the great promise of the proposed transform: blocking artifact is avoided while ringing artifact is suppressed. It is certainly a step towards a better understanding of how to design filter banks that are most suited to the human visual system.

Chapter 7

Application in Image Coding

7.1 Introduction

As previously mentioned in Chapter 2, one of the most popular and successful FB application is in image coding. Block transform coding and subband coding have been two dominant techniques in existing image compression standards and implementations. Both methods actually exhibit many similarities: relying on a certain FB to convert the input image to a more decorrelated representation, then utilizing the same basic building blocks such as bit allocators, quantizers, and entropy coders to achieve compression.

This chapter serves one single purpose: to demonstrate the tremendous potential of the novel multi-band LPPRFBs presented earlier in Chapter 4–6. Given a fixed quantization and entropy coding framework, new FBs in this dissertation consistently offer significant improvements over current popular transforms such as the wavelet transform, the DCT, and the LOT. Extensive coding comparisons are carried out with two next-generation image coding schemes: progressive transmission coding and and its perceptually-tuned version. This chapter also attempts to shed some light onto a deeper understanding of wavelets, lapped transforms, their relation, and their performance in

image compression from a multirate filter bank perspective.

7.2 Progressive Image Transmission

7.2.1 A New Philosophy

Block transform coders enjoyed early successes in image compression due to their low complexity in implementation and their reasonable performance. The most popular block transform coder is the current image compression standard JPEG [58] which utilizes the 8×8 DCT at its transformation stage. At high bit rates (1 bpp and up), JPEG offers almost visually lossless reconstruction image quality. However, when more compression is needed (i.e., at lower bit rates), annoying blocking artifacts show up because of two reasons: (i) the DCT bases are short, non-overlapped, and have discontinuities at the ends; (ii) JPEG processes each image block independently. So, inter-block correlation has been completely abandoned.

The development of the lapped orthogonal transform [47] and various generalized versions presented throughout this dissertation help solve the blocking problem to a certain extent by borrowing pixels from the adjacent blocks to produce the transform coefficients of the current block. The lapped transform outperforms the DCT on two counts: (i) from the analysis viewpoint, it takes into account inter-block correlation, hence, provides better energy compaction that leads to more efficient entropy coding of the coefficients; (ii) from the synthesis viewpoint, its basis functions decay asymptotically

to zero at the ends, reducing blocking discontinuities drastically. However, earlier lapped-transform-based image coders [47], [62], [94] have not utilized global information to their full advantage: the quantization and the entropy coding of transform coefficients are still independent from block to block.

Recently, subband coding has emerged as the leading standardization candidate in future image compression systems thanks to the development of the discrete wavelet transform. Wavelet representation with implicit overlapping and variable-length basis functions produces smoother and more perceptually pleasant reconstructed images. Moreover, wavelet's multiresolution characteristics have created an intuitive foundation on which simple, yet sophisticated, methods of encoding the transform coefficients are developed. Exploiting the relationship between the parent and the offspring coefficients in a wavelet tree, progressive wavelet coders [73], [71], [110] can effectively order the coefficients by bit planes and transmit more significant bits first. This coding scheme results in an embedded bit stream along with many other advantages such as exact bit rate control and near-idempotency (perfect idempotency is obtained when the transform maps integers to integers). In these subband coders, global information is taken into account fully.

From a frequency domain point of view, the wavelet transform simply provides an octave-band representation of signals. The dyadic wavelet transform is analogous to a non-uniform-band lapped transform. It can sufficiently decorrelate smooth images; however, it has problems with images with well-localized high frequency components,

leading to low energy compaction. In this chapter, we shall demonstrate that the embedded framework is not only limited to the wavelet transform; it can be utilized with uniform-band lapped transforms as well. In fact, some of the lapped transforms presented in previous chapters can provide much finer frequency spectrum partitioning and superior energy compaction over the wavelet transform, leading to significant improvements in embedded image coding.

7.2.2 The Wavelet Transform and Progressive Image Transmission

Progressive image transmission is perfect for the recent explosion of the internet. The wavelet-based progressive image coding approach first introduced by Shapiro [73] relies on the fundamental idea that more important information (defined here as what decreases a certain distortion measure the most) should be transmitted first. Assume that the distortion measure is the mean-squared error (MSE), the transform is paraunitary, and transform coefficients $c_{i,j}$ are transmitted one by one, it can be proven that the mean squared error decreases by $\frac{|c_{i,j}|}{N}$, where N is the total number of pixels [15]. Therefore, larger coefficients should be transmitted first. If one bit is transmitted at a time, this approach can be generalized to ranking the coefficients by bit planes and the most significant bits are transmitted first [64]. The progressive transmission scheme results in an embedded bit stream (i.e., it can be truncated at any point by the decoder to yield the best corresponding reconstructed image). The algorithm can be thought of as an elegant

combination of a scalar quantizer with power-of-two stepsizes and an entropy coder to encode wavelet coefficients.

Embedded algorithm relies on the hierarchal coefficients' tree structure that we called a *wavelet tree*, defined as a set of wavelet coefficients from different scales that belong in the same spatial locality as demonstrated in Figure 48(a), where the tree in the vertical direction is circled. All of the coefficients in the lowest frequency band make up the *DC band* or the *reference signal* (located at the upper left corner). Besides these DC coefficients, in a wavelet tree of a particular direction, each lower-frequency *parent node* has four corresponding higher-frequency *offspring nodes*. All coefficients below a parent node in the same spatial locality is defined as its *descendents*. Also, define a coefficient $c_{i,j}$ to be *significant* with respect to a given threshold T if $|c_{i,j}| \geq T$, and *insignificant* otherwise. Meaningful image statistics have shown that if a coefficient is insignificant, it is very likely that its offspring and descendents are insignificant as well. Exploiting this fact, the most sophisticated embedded wavelet coder SPIHT can output a single binary marker to represent very efficiently a large, smooth image area (an insignificant tree). For more details on the algorithm, the reader is referred to [71].

Although the wavelet tree provides an elegant hierarchical data structure which facilitates quantization and entropy coding of the coefficients, the efficiency of the coder still heavily depends on the transform's ability in generating insignificant trees. For non-smooth images that contain a lot of texture, the wavelet transform is not as efficient in signal decorrelation comparing to transforms with finer frequency selectivity and superior energy compaction. Multi-band lapped transforms hold the edge in this area.

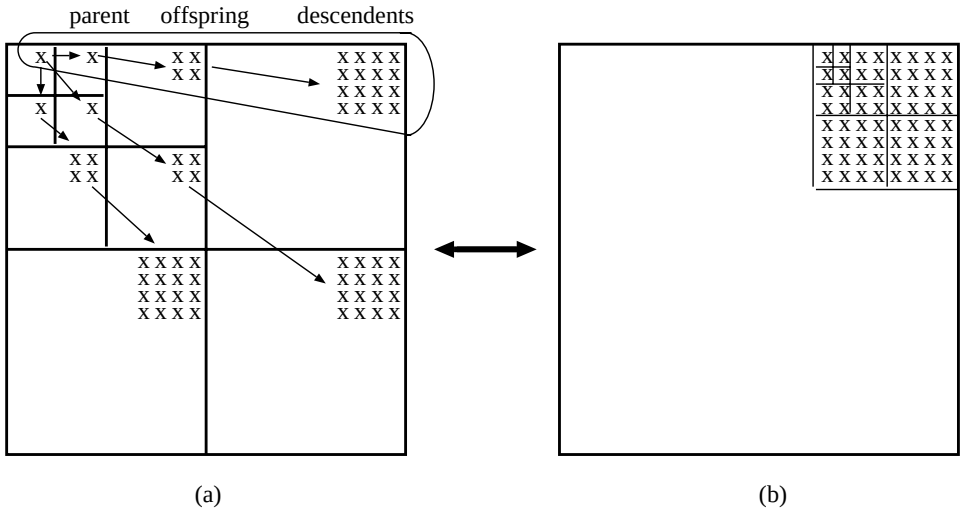

Figure 48: Wavelet and block transform analogy.

7.2.3 Wavelet and block transform analogy

Instead of obtaining an octave-band signal decomposition, one can have a finer uniform-band partitioning as depicted in Figure 49 (drawn for $M = 8$). The finer frequency partitioning compacts more signal energy into a fewer number of coefficients and generates more insignificant ones, leading to an enhancement in the performance of the zerotree algorithm. However, uniform filter bank also has uniform downsampling (all subbands now have the same size). A parent node does not have four offspring nodes as in the case of the wavelet representation. How would one come up with a new tree structure that still takes full advantage of the inter-scale correlation between block-transform coefficients?

The above question can be answered by investigating an analogy between the wavelet and block transform as illustrated in Figure 48. The parent, the offspring, and the descendents in a wavelet tree cover the same spatial locality, and so are the coefficients of

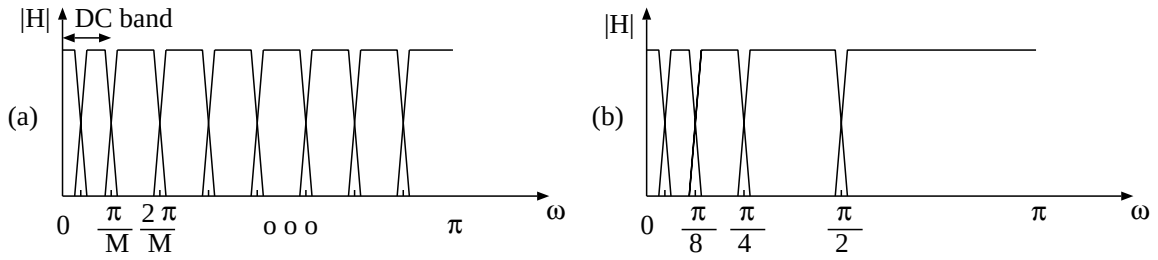

Figure 49: Frequency spectrum partitioning. (a) M-channel uniform-band transform. (b) Dyadic wavelet transform.

a transform block. In fact, a wavelet tree in an L-level decomposition is analogous to a 2^L-channel transform's coefficient block. The difference lies at the bases that generate these coefficients. It can be shown that a 1D L-level wavelet decomposition, if implemented as a lapped transform, has the following coefficient matrix:

$$\mathbf{P}_L = \begin{bmatrix} h_0[n] * h_0[\frac{n}{2}] * \cdots * h_0[\frac{n}{2^{L-2}}] * h_0[\frac{n}{2^{L-1}}] \\ h_0[n] * h_0[\frac{n}{2}] * \cdots * h_0[\frac{n}{2^{L-2}}] * h_1[\frac{n}{2^{L-1}}] \\ h_0[n] * h_0[\frac{n}{2}] * \cdots * h_1[\frac{n}{2^{L-2}}] \\ h_0[n] * h_0[\frac{n}{2}] * \cdots * h_1[\frac{n}{2^{L-2}}] \\ \vdots \\ h_1[n] \\ h_1[n] \\ h_1[n] \\ h_1[n] \end{bmatrix}. \tag{7.1}$$

From the coefficient matrix $\mathbf{P}_L$, we can observe several interesting and important characteristics of the wavelet transform through the block transform's prism:

- The wavelet transform can be viewed as a lapped transform with filters of variable

lengths. For an L-level decomposition, there are 2^L filters.

- Each basis function has linear phase; however, they do not share the same center of symmetry.
- The block size is defined by the length of the longest filter. If $h_0[n]$ is longer and has length N_0, the top filter covering the DC component turns out to be the longest, and it has a length of $(2^L - 1)(N_0 - 1) + 1$. For the biorthogonal wavelet pair with $h_0[n]$ of length 9 and $h_1[n]$ of length 7 and three levels of decomposition, the eight resulting basis functions have respective lengths of $57, 49, 21, 21, 7, 7, 7$, and 7.
- For a 6-level decomposition using the same $9-7$ pair, the length of the longest basis function grows to 505! The huge amount of overlapped pixels explains the smoothness of the reconstructed images where blocking artifacts have been completely eliminated.

Each block of lapped transform coefficients represents a spatial locality similarly to a tree of wavelet coefficients. Let $\mathcal{O}(i,j)$ be the set of coordinates of all offspring of the node (i,j) in an M-channel block transform ($0 \leq i,j \leq M-1$), then $\mathcal{O}(i,j)$ can be represented as follows:

$$\mathcal{O}(i,j) \;=\; \{(2i,2j),(2i,2j+1),(2i+1,2j),(2i+1,2j+1)\}. \tag{7.2}$$

All $(0,0)$ coefficients from all transform blocks form the DC band, which is similar to the wavelet transform's reference signal, and each of these nodes has only three offsprings: $(0,1)$, $(1,0)$, and $(1,1)$. This is a straightforward generalization of the structure first proposed in [107]. The only requirement here is that the number of channel M has to

be a power of two. Figure 50 demonstrates through a simple rearrangement of the block transform coefficients that the redefined tree structure above does possess a wavelet-like multiscale representation. The quadtree grouping of the coefficients is far from optimal in the rate-distortion sense; however, other parent-offspring relationships for uniform-band transform such as the one mentioned in [73] do not facilitate the further usage of various entropy coders to increase the coding efficiency.

Figure 50: Demonstration of the analogy between M-channel uniform-band transform and wavelet representation.

Figure 50 shows that there still exists correlation between DC coefficients. To decorrelate the DC band even more, several levels of wavelet decomposition can be used depending on the input image size. Besides the obvious increase in the coding efficiency of DC coefficients thanks to a deeper coefficient trees, wavelets provide variably longer bases for the signal's DC component, leading to smoother reconstructed images, i.e., blocking artifacts are further reduced. Regularity objective can be added in the transform design process to produce M-band wavelets, and a wavelet-like iteration can be carried out using uniform-band transforms as well. The complete coder's diagram is depicted in Figure 51.

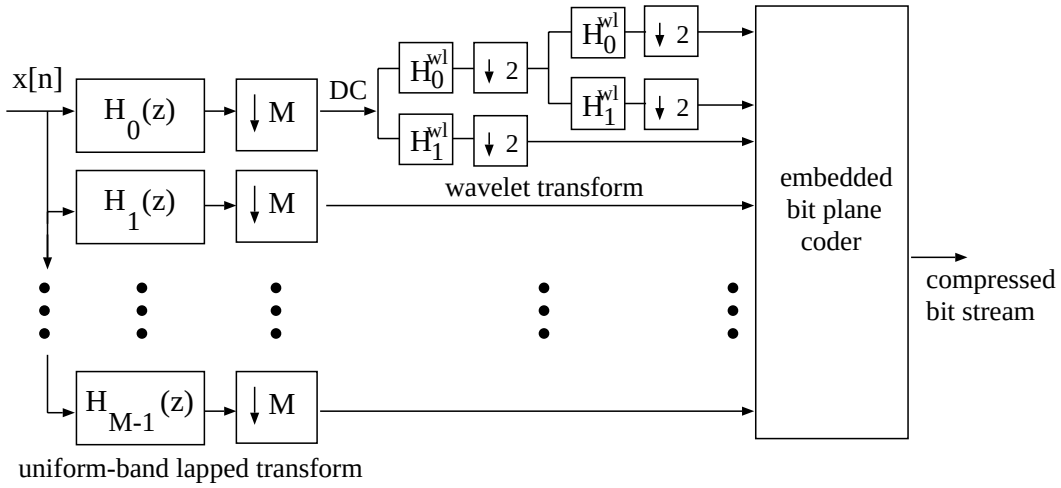

Figure 51: The LT-based progressive coder's diagram.

7.2.4 Coding Results

The objective coding results (PSNR in dB) for standard 512×512 Lena, Barbara, and Goldhill test images are tabulated in Table 7. The transforms in comparison are

- 9/7-tap biorthogonal wavelet [3].
- 8×8 DCT [67] shown in Figure 9.
- 8×16 LOT [45] shown in Figure 11.
- 8×40 GenLOT [89] shown in Figure 13.
- 4×24 4×8 VLLOT in Figure 42(a) of Chapter 6.
- 2×24 6×8 VLGLBT in Figure 45 of Chapter 6.
- 8×16 GLBT in Figure 24 of Chapter 4.
- 16×32 GLBT in Figure 25 of Chapter 4.

Except the 9/7-tap biorthogonal wavelet, all of the transforms listed are multi-band uniform LPPRFB, and their transform coefficients are encoded as described in Section

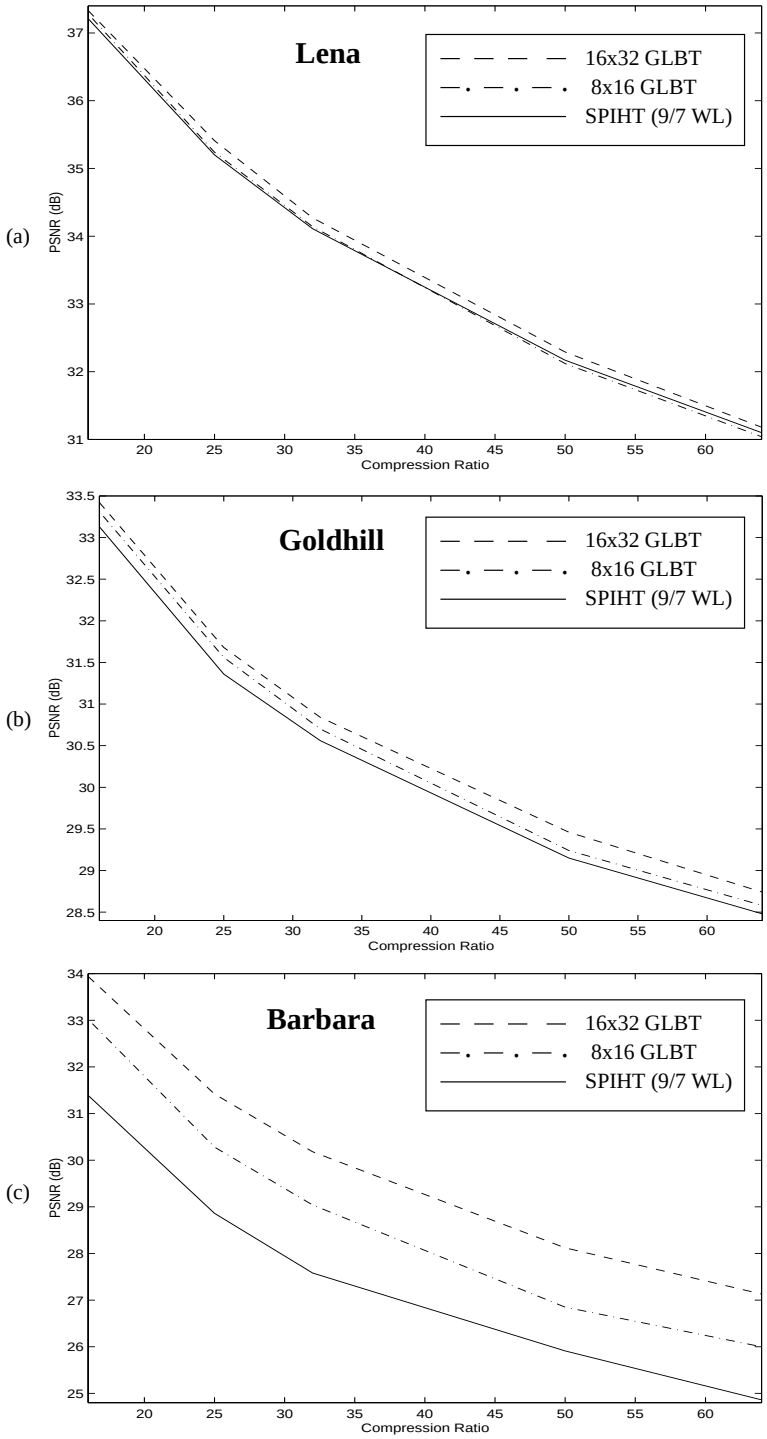

Figure 52: Rate-distortion curves of image coding examples. (a) Lena. (b) Goldhill. (c) Barbara.

(a)

Lena	Progressive Transmission Image Coders							
Comp. Ratio	SPIHT (9/7 WL)	8 x 8 DCT	8 x 16 LOT	8 x 40 GenLOT	4x24 4x8 VLLOT	2x24 6x8 VLGLBT	8 x 16 GLBT	16 x 32 GLBT
1:8	40.41	39.91	40.05	40.43	40.18	39.89	40.35	40.43
1:16	37.21	36.38	36.72	37.32	36.85	36.51	37.28	37.33
1:32	34.11	32.90	33.56	34.23	33.61	33.25	34.14	34.27
1:64	31.10	29.67	30.48	31.16	30.48	30.15	31.04	31.18
1:100	29.35	27.80	28.62	29.31	28.62	28.31	29.14	29.38
1:128	28.38	26.91	27.61	28.35	27.64	27.48	28.19	28.39

(b)

Goldhill	Progressive Transmission Image Coders							
Comp. Ratio	SPIHT (9/7 WL)	8 x 8 DCT	8 x 16 LOT	8 x 40 GenLOT	4x24 4x8 VLLOT	2x24 6x8 VLGLBT	8 x 16 GLBT	16 x 32 GLBT
1:8	36.55	36.25	36.63	36.80	36.49	36.22	36.69	36.78
1:16	33.13	32.76	33.18	33.36	33.06	32.76	33.31	33.42
1:32	30.56	30.07	30.56	30.79	30.51	30.25	30.70	30.84
1:64	28.48	27.93	28.36	28.60	28.35	28.17	28.58	28.74
1:100	27.38	26.65	27.09	27.40	27.10	27.06	27.33	27.62
1:128	26.73	26.01	26.48	26.79	26.46	26.36	26.71	26.96

(c)

Barbara	Progressive Transmission Image Coders							
Comp. Ratio	SPIHT (9/7 WL)	8 x 8 DCT	8 x 16 LOT	8 x 40 GenLOT	4x24 4x8 VLLOT	2x24 6x8 VLGLBT	8 x 16 GLBT	16 x 32 GLBT
1:8	36.41	36.31	37.43	38.08	36.83	36.22	37.84	38.43
1:16	31.40	31.11	32.70	33.47	31.86	31.12	33.02	33.94
1:32	27.58	27.28	28.80	29.53	27.99	27.42	29.04	30.18
1:64	24.86	24.58	25.70	26.37	25.10	24.86	26.00	27.13
1:100	23.76	23.42	24.34	24.95	23.96	23.74	24.55	25.39
1:128	23.35	22.68	23.37	24.01	23.24	23.23	23.49	24.56

Table 7: Objective coding results (PSNR in dB). (a) Lena. (b) Goldhill. (c) Barbara.

7.2.3. All computed PSNR quotes in dB are obtained from a real compressed bit stream with all overheads included. The rate-distortion curves in Figure 52 and the tabulated coding results in Table 7 clearly demonstrate the superiority of the GLBT over current transforms of choice. For a smooth image like Lena where the wavelet transform can sufficiently decorrelate, SPIHT offers a comparable performance. However, for a highly-textured image like Barbara, the 8×40 GenLOT, the 8×16 GLBT, and the 16×32 GLBT coder can provide a PSNR gain of more than 2 dB over a wide range of bit rates. Unlike other block transform coders whose performance dramatically drops at very high compression ratios, the new LT-based progressive coders are consistent throughout as illustrated in Figure 52. Lastly, better decorrelation of the DC band provides around $0.3 - 0.5$ dB improvement over an earlier DCT embedded coder [107].

Figure 53 - 56 confirm the superiority of the new lapped transforms in reconstructed image quality as well. Figure 53 shows reconstructed Barbara images at 1:32 using various block transforms. Comparing to JPEG, blocking artifacts are already remarkably reduced in the DCT-based coder in Figure 53(a). Blocking is completely eliminated when the DCT is replaced by appropriately-designed lapped transforms as shown in Figure 53(c)-(d) and Figure 54. A closer look in Figure 55(a)-(c) (where only 256×256 image portions are shown so that artifacts can be more easily seen) reveals that besides blocking elimination, the 8×16 GLBT can preserve texture beautifully (the table cloth and the clothes pattern in the Barbara image) while keeping the edges relatively clean. Comparing to SPIHT, the reconstructed images have an overall sharper and more natural look with more defining edges and more evenly reconstructed texture regions. Although the PSNR

difference is not as striking in the Goldhill image, the improvement in perceptual quality is rather significant as shown in Figure 55(d)-(f). Even at 1:100, the reconstructed Goldhill image in Figure 54(d) is still visually pleasant: no blocking and not much ringing.

Figure 56 demonstrates the impressive performance of the fast VLGLBT in Section 6.2.3. As expected, the VLGLBT offers a $0.3 - 0.5$ dB improvement over the DCT at medium and low bit rates. It is inferior to much more complex transforms like the 9/7-tap wavelet and the 8×16 GLBT. However, we stress that the VLGLBT is designed mainly to improve the reconstructed image quality. Zoom-in portions of the reconstructed images in Figure 56 confirms the VLGLBT's high potential in this most crucial criterion: blocking is avoided while ringing is suppressed. In fact, the low-complexity VLGLBT is even better than the "optimal" LOT [45] in blocking elimination. More objective and subjective evaluation of block-transform-based progressive coding can be found at the web site

`http://saigon.ece.wisc.edu/~waveweb/Coder/index.html`.

As previously mentioned, the improvement over wavelets keys on the lapped transform's ability to capture and separate localized signal components in the frequency domain. In the spatial domain, this corresponds to images with directional repetitive texture patterns. To illustrate this point, the lapped-transform-based coder is compared against the FBI Wavelet Scalar Quantization (WSQ) standard [112]. When the original 768×768 gray-scale fingerprint image shown in Figure 57(a) is compressed at $1 : 13.6$ (43366 bytes) by the WSQ coder, Bradley *et al* reported a PSNR of 36.05 dB. Using the 16×32 GLBT in Figure 25, a PSNR of 38.09 dB can be achieved at the same compression

(a) (b)

(c) (d)

Figure 53: Barbara coded at 1:32 using various transforms. (a) 8×8 DCT. (b) 8×16 LOT. (c) 8×16 GLBT. (d) 16×32 GLBT.

(a) (b)

(c) (d)

Figure 54: Goldhill coded by the 16×32 GLBT. (a) 1:16, 33.42 dB. (b) 1:32, 30.84 dB. (c) 1:64, 28.74 dB. (d) 1:100, 27.62 dB.

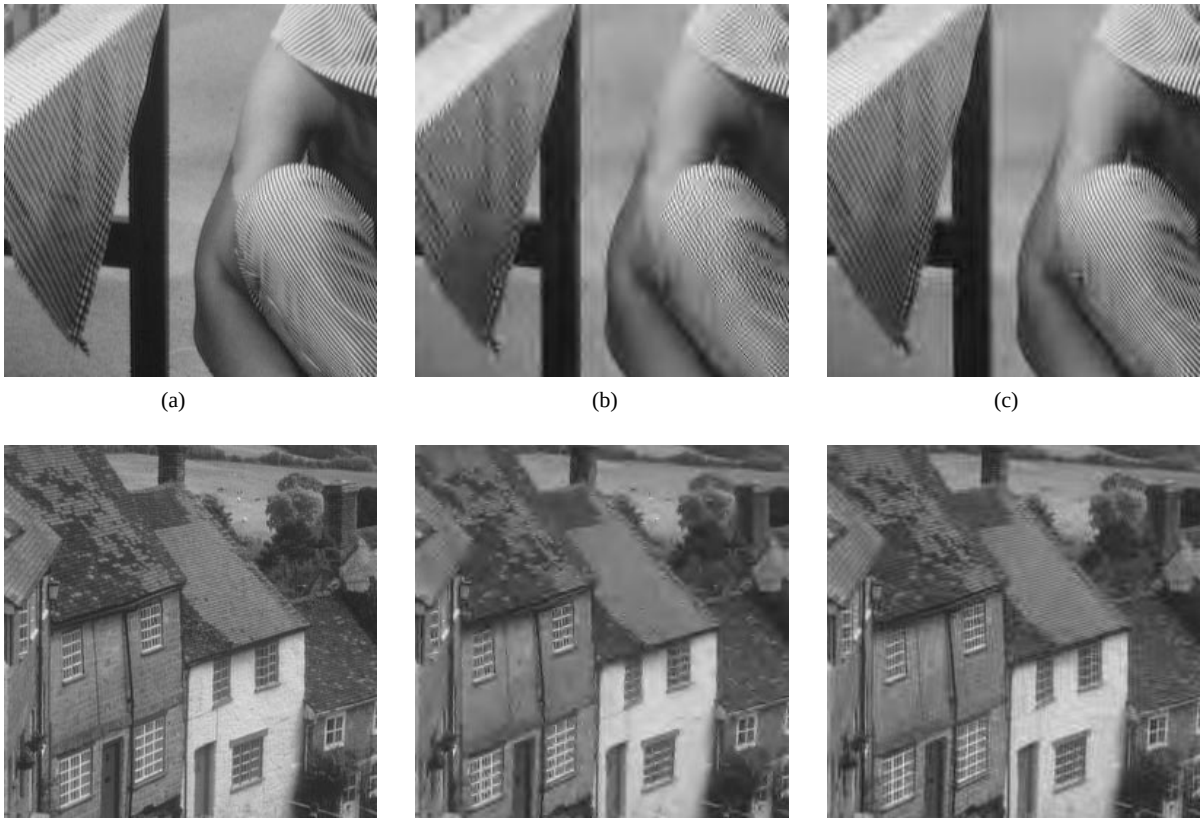

Figure 55: Perceptual comparison between the wavelet and the LT embedded coder. Enlarged portions. (a) Original Barbara image. (b) SPIHT at 1:32. (c) 8×16 GLBT embedded coder at 1:32. (d) Original Goldhill. (e) SPIHT at 1:32. (f) 8×16 GLBT embedded coder at 1:32.

Figure 56: Perceptual comparison between various transforms at 1:32 compression ratio. Enlarged portions. (a) Original Lena image. (b) 8×8 DCT. (c) 2×24 6×8 VLGLBT. (d) 8×16 LOT. (e) 8×16 GLBT. (f) 9/7-tap wavelet.

ratio. At the same level of PSNR, the GLBT coder can compress the image down to 1 : 20 where the reconstructed image is shown in Figure 57(b). To put this in perspective, the wavelet-packet-based SFQ coder in [109] reported a PSNR of only 37.30 dB at 1:13.6 compression ratio. At 1 : 18.036 (32702 bytes), the WSQ's reconstructed image shown in Figure 57(c) has a PSNR of 34.42 dB while the GLBT coder produces 36.57 dB. At the same distortion level, the GLBT coder can compress the image down to a compression ratio of 1:27 (21845 bytes) as shown in Figure 57(d). Notice the high visual quality of the reconstructed images in Figure 57(b) and (d): no disturbing blocking and ringing artifacts.

7.3 Progressive Perceptual Image Coding

7.3.1 Motivation

The embedded image coder presented in the previous section yields excellent performance in the mean-square sense. However, one important aspect that it has not taken into account is the perceptual quality of the reconstructed images. It has been widely known that PSNR is not the ultimate judge in image quality [31]. Although some improvements in this aspect can be addressed at the transform stage as discussed throughout the dissertation, taking another step forward requires much more sophisticated perceptually-tuned coders – the main motivation and objective of this section. Instead of aiming for the highest PSNR between the original and the coded image, we propose a progressive

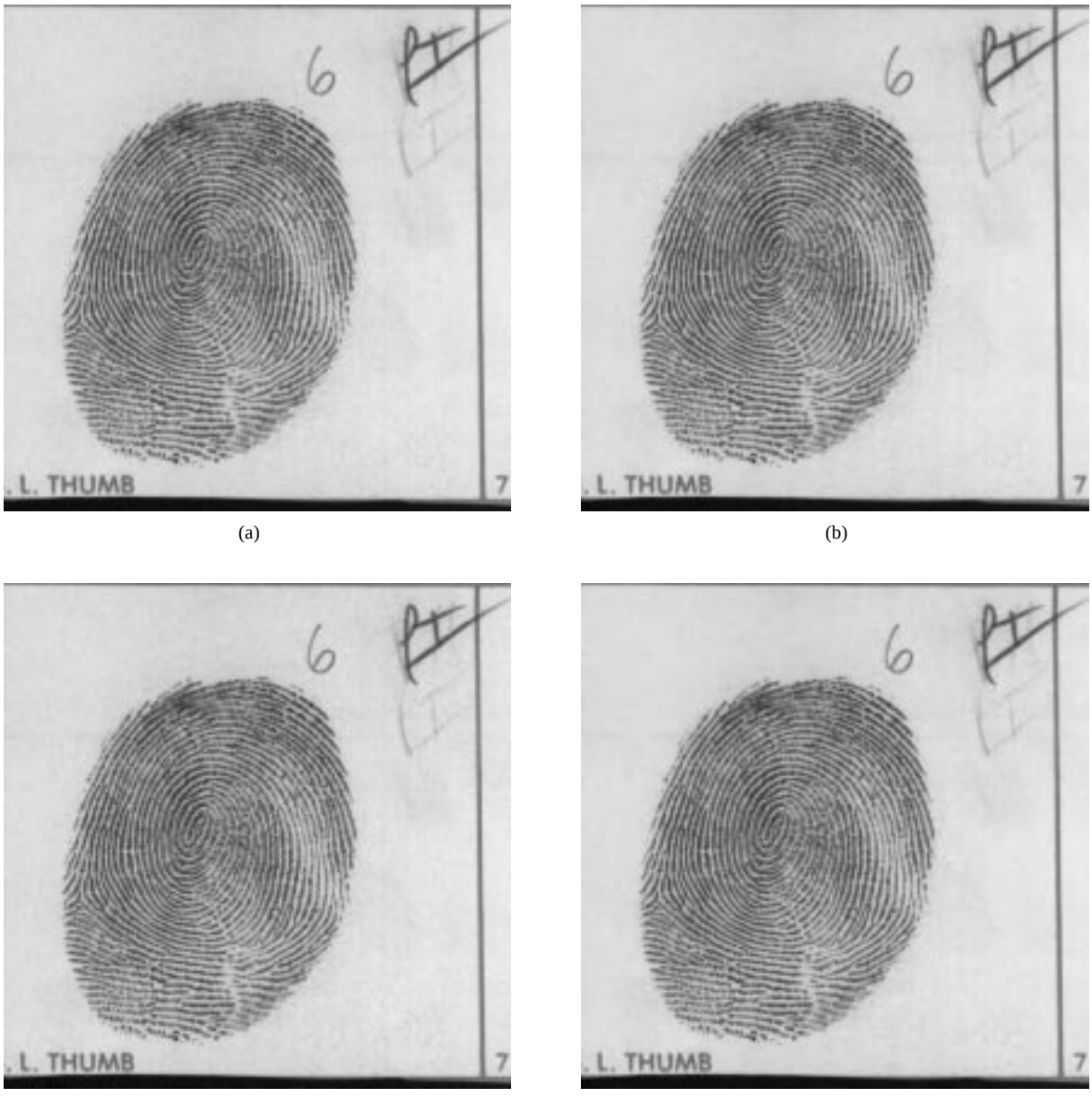

Figure 57: Fingerprint compression example. (a) Original Fingerprint image (589824 bytes). (b) Coded by the 16×32 GLBT coder at 1:20 (29490 bytes), 36.05 dB. (c) Coded by the WSQ coder at 1:18.036 (32702 bytes), 34.42 dB. (d) Coded by the 16×32 GLBT coder at 1:27 (21845 bytes), 34.42 dB.

coder that incorporates many prominent properties of the Human Visual System (HVS) to yield visually pleasant reconstructed images.

7.3.2 Approach

The novel embedded coder features a locally adaptive perceptual masking thresholder that computes, based on the contents of the original image, the maximum amount of noise energy that can be injected at each transform coefficient such that the reconstructed image is still perceptually distortion-free. The adaptive thresholder is used as a pre-processor to a block-based embedded image coder. Perceptually normalized block-transform coefficients less than their corresponding masking thresholds can be set to zero before the normal embedded quantization and bit plane coding step. The result is a visually-tuned embedded coder which is capable of transparent coding when all bit planes are encoded. Visually insignificant coefficients are never included in the compressed bit-stream. If lower bit rates are desired, the decoder and possibly the encoder simply deal with the higher bit planes of the visually significant coefficients. Excellent reconstructed image quality without annoying blocking and ringing artifacts can still be obtained at low bit rates.

The perceptually-tuned embedded coder can be divided into the following stages: the transform stage, the perceptual pre-quantization stage, the texture masking thresholding stage, and the embedded coding stage. The new components added on top of the embedded transform coder in Section 7.2 are the perceptual pre-quantizer and the texture

masking thresholder.

7.3.3 The Perceptual Pre-Quantizer

The pre-quantizer accounts for the HVS's frequency and luminance sensitivity. It is implemented from the DCT detection model presented in [59] and the LOT model in [60]. The JND step sizes are measured and modeled from the visible sensitivity of the transform's basis functions, taking into account different pixel sizes, different viewing distances, and also different display luminance. In other words, the JND profile provides a quantization table **Q** (that is dependent on the viewing conditions and the transform) for coefficient normalization. The higher the JND, the less visually sensitive the coefficient is. This is similar to the quantization stage in JPEG. In fact, the familiar quantization tables in JPEG [58] can be used here without any significant loss in perceptual quality.

7.3.4 Texture Masking Thresholder

In the perceptual normalization process, local image statistics have not been exploited. The image-dependent texture masking thresholder here employs a similar idea to the masking model presented in [87] where the authors use a mapping of the DCT frequency responses onto the Cortex transform space to estimate the texture energy, i.e., the amount of spatial details in each HVS's critical band of each image block. A threshold elevation factor for each DCT coefficient of that particular block can then be computed from the amount of texture energy. More simply stated, the threshold elevation model provides

a more "aggressive" quantization table with larger quantization stepsizes for coefficients in an image locality containing significant texture energy. Since the HVS cannot detect quantization noise in highly textured image regions as well as in smooth background regions [31], [10], [69], appropriate elevation of the quantization stepsizes will improve the coding efficiency of these textured regions without any loss in perceptual quality.

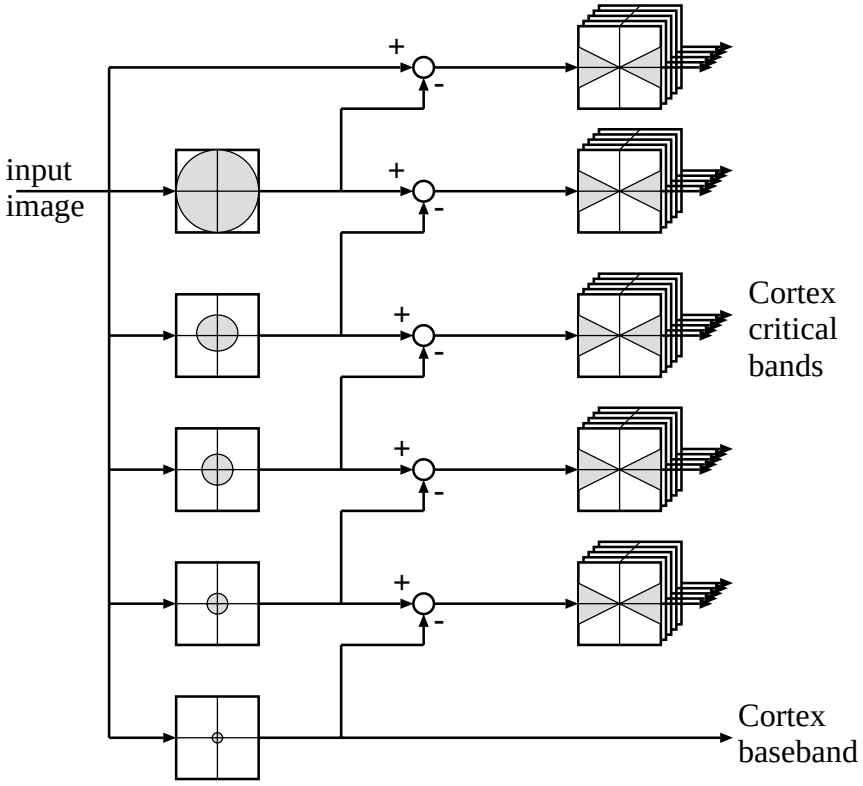

Figure 58: Implementation of the Cortex filter bank.

The Cortex transform shown in Figure 58 is a 2D non-maximally decimated filter bank which has been proven to be a rather accurate model of the HVS's critical bands [31]. It is a combination of octave-band ring filters and directional fan filters. Instead of mapping the block transform onto the Cortex transform [87] as depicted in Figure 59, we propose a fast and simple, yet still effective, approximation of this process by replacing

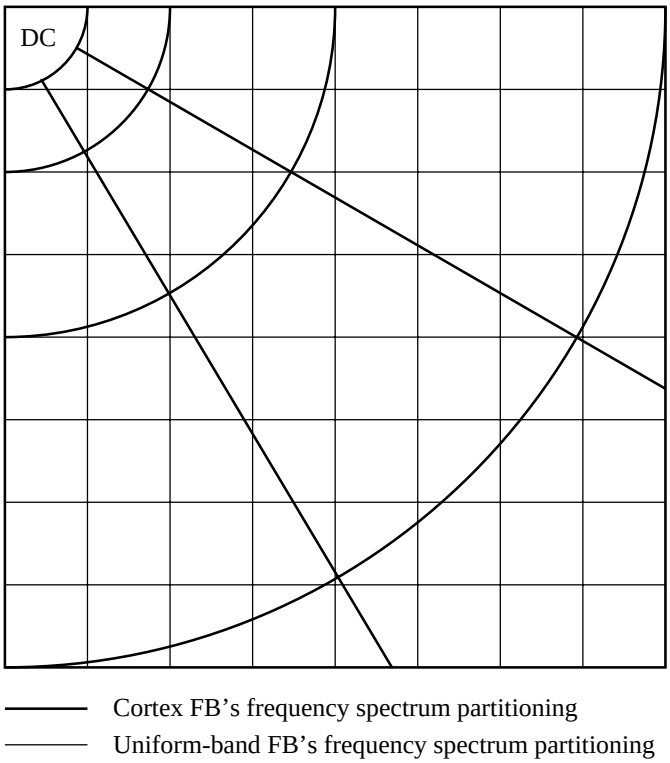

Figure 59: Transform mapping to estimate texture energy in each Cortex band.

the ring filters by square separable ones and employing three stair-case fan filters: one vertical, one horizontal, and one diagonal. The Cortex band approximation is illustrated in Figure 60 where the darker lines mark the boundaries between critical bands and coefficients belonging to one vertical critical band are labeled X. Note that the frequency partitioning of the approximated HVS critical bands is very similar to the dyadic wavelet representation known to be well-matched to psychovisual HVS models.

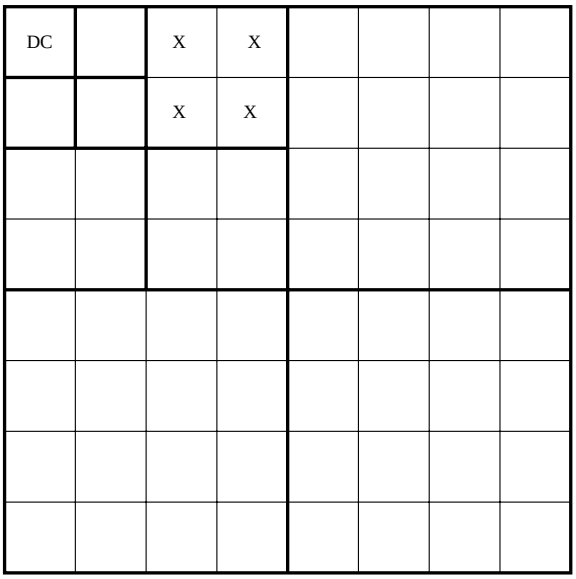

Figure 60: Approximation of the HVS critical bands.

For each Cortex band $\mathbf{C}_i$ in an image block, the variance σ_i of all coefficient members is calculated with the zero-mean assumption. The variance is then used to calculate the threshold elevation factor as shown in Figure 61 where the parameters *min, max, low, high* are tuned by subjective testing. The product of the elevation factor and the corresponding quantization table $\mathbf{Q}$ entry from the pre-quantizer is the coefficient's masking threshold. If a coefficient's absolute value is smaller than its masking threshold, it is labeled "visually

insignificant" and set to zero.

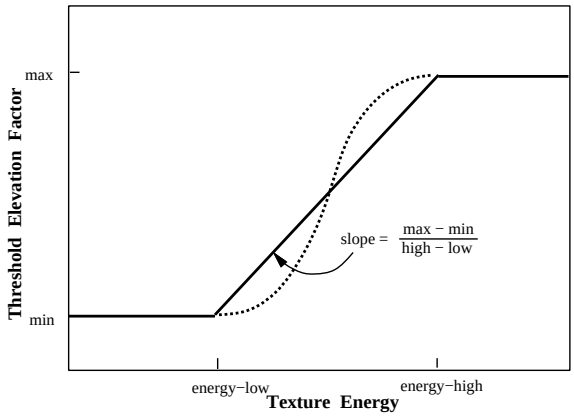

Figure 61: A Typical Threshold Elevation Model.

7.3.5 Complete Coder

The complete perceptual coder diagram is shown in Figure 62. Without the perceptual normalizer and the texture masking thresholder, the coder is reduced to the PSNR-tuned lapped-transform-based progressive image coder presented in the previous section. Without the thresholder and if the encoding process is terminated at the end of a certain bit plane, the coder simply provides a method of encoding the transform coefficients quantized with a quantization table scaled by a power of two. If the two perceptual modules are designed appropriately and all bit planes are encoded as in [72], the reconstructed image is visually lossless. As other embedded coding schemes [73], [71], [110], the new coder has exact bit rate control. Moreover, it also has robust perceptual control – only coefficients pre-determined to be visually significant are involved in the coding process. If the user wishes to compress an image with a bit budget lower than the transparent

level, only higher bit planes of the visually significant coefficients are encoded. The scaling of the quantization matrix is performed implicitly and automatically to fit the given budget.

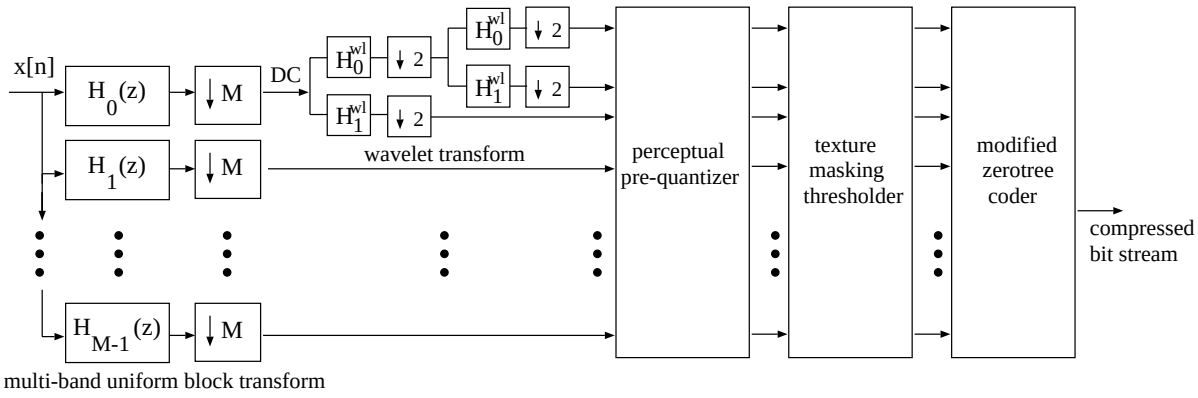

Figure 62: The complete perceptual coder diagram.

7.3.6 Coding Results

Coding results clearly confirm the superiority of the perceptually-tuned coder in term of the visual quality of reconstructed images. On the standard 512×512 test image Barbara at a compression ratio of 30:1, the standard baseline JPEG's reconstructed image has a PSNR of 24.84 dB. The image quality is unacceptable as expected: annoying blocking artifact shows up everywhere as illustrated in Figure 63(a). Our DCT-based coder yields a much more perceptually pleasant coded image despite having a lower PSNR of 24.73 dB. Figure 63(b) shows the reconstructed image where blocking is reduced significantly, especially in smooth image regions. Blocking is more severe in texture regions; however, it is partially masked. It takes JPEG nearly twice the bit budget to yield a compressed image of comparable quality.

If the DCT is replaced by the high-performance 8×16 GLBT in Chapter 4, blocking artifact is completely eliminated whereas ringing is still kept at a minimum level. Notice the astounding PSNR difference between the PSNR-tuned and the perception-tuned version: almost 4 dB! The objectively tuned coder in Section 7.2 offers an excellent PSNR of 29.77 dB. (The wavelet-based embedded coder SPIHT [71] in this case only yields 28.52 dB.) However, as noted in Figure 63(d), aiming for PSNR has the coder spending many unnecessary bits in the texture regions, leaving some ringing at strong edges. The perceptually-tuned coder spends its bit budget more judiciously: bits that are normally used on heavy textured regions (the table cloth, the clothes, the chairs behind) are now allocated to visually sensitive features, like the face, the elbows, and the table edges as shown in Figure 63(c) – (d). For more in-depth subjective evaluation of perceptual block-transform-based progressive image coding, the reader is again referred to the url address `http://saigon.ece.wisc.edu/~waveweb/Coder/index.html`.

7.4 Summary

This chapter presents two high-performance image coding frameworks, both based on M-channel uniform-band LPPRFBs and zerotree entropy coding. Image coding examples show that the novel M-channel LPPRFBs, when appropriately designed and utilized, offer the highest objective performances up to date, easily outdistance state-of-the-art wavelets by a significant margin. On the other hand, the perceptually-tuned embedded image coder yields remarkably high visual-quality performance despite its simplicity.

(a) (b)

(c) (d)

Figure 63: Coding results of Barbara image at 30:1 compression ratio. (a) Standard baseline JPEG, 24.84 dB (b) Perceptually coded by DCT, 24.73 dB. (c) Perceptually coded by 8×16 GLBT, 25.88 dB (d) Coded by 8×16 GLBT, PSNR-tuned, 29.77 dB.

Both coding framework offers many advantages:

- They are both fast and relatively simple.
- They do not need any kind of training, optimization, segmentation, and classification.
- Both of them employ block transforms at the transformation stage, facilitating and increasing the efficiency of local texture masking.
- The transforms have fast, robust, efficient, and modular structures, ideal for VLSI implementations.
- The block-based nature of the transforms also increases the parallelism of computation.
- The coder has progressive image transmission and nearly all of its attractive characteristics, such as embedded quantization and exact bit rate control. Only idempotency is sacrificed in the perceptually-tuned coder.

Chapter 8

Conclusion

8.1 Summary

This dissertation focuses on the theory, structure, design, implementation, and application in image compression of discrete-time FIR linear phase perfect reconstruction filter banks with arbitrary M channels and arbitrary-length filters. This class of FBs is purposely chosen to have high practical values: linear phase, FIR, real (sometimes even rational and integer) filter coefficients, and exact reconstruction.

The approach consistently taken throughout the dissertation is to parameterize the FBs by various lattice structures based on the factorization of the analysis and synthesis polyphase transfer matrices. From a slightly different point of view, the factorization allows the construction of a highly complex system from a cascade of identical low-order building blocks, each is carefully designed to propagate structurally the most desired properties, namely linear phase and perfect reconstruction. In other words, in the lattice representation, both of these crucial properties are retained regardless of the quantization of lattice coefficients to any desired level. The lattice structure offers a powerful characterization in both FB design and implementation. From a design perspective, the lattice

coefficients can be varied independently and arbitrarily without affecting the LP and PR properties. Secondary FB properties such as high coding gain and low stopband attenuation can be further achieved using unconstrained optimization techniques. From an implementation perspective, the cascading construction provides a fast, efficient, robust, and modular structure which lends itself nicely to hardware realization in VLSI.

In the particular application of image coding, M-channel LPPRFBs in this dissertation can be interpreted as lapped transforms which elegantly solve the annoying blocking artifact problem in widely-used block-transform-based image coders. Borrowing image pixels from the neighboring blocks to produce the transform coefficients of the current block, the lapped transform takes into account inter-block correlation, provides higher energy compaction, and is capable of eliminating completely discontinuities between block boundaries on the reconstruction stage. Image compression demonstrations show that our novel transforms offer significant improvements in coding performance, both objectively and subjectively, over the popular DCT, LOT, and even state-of-the-art wavelets in the current literature. Coding performance aside, the block-based nature of the transforms also provide several other advantages:

- capable of processing large signals under limited memory constraint
- increasing computational parallelism
- facilitating region-of-interest coding/decoding.

The specific results of the dissertation are summarized below.

8.1.1 Necessary Existence Conditions for LPPRFBs

The LP property of the filters imposes certain symmetry constraints on the components of the FB's polyphase matrices. Manipulating the symmetrical forms of these transfer functions, we are able to obtain in Chapter 3 a restrictive set of permissible conditions on the filter lengths and symmetry polarity (symmetric/antisymmetric) for LPPRFBs in general. The symmetry of the polyphase matrices and the necessary conditions for existence play key roles in the derivation of complete and minimal lattice structures in later chapters.

8.1.2 The Generalized Lapped Biorthogonal Transform

Chapter 4 introduces the first complete and minimal lattice structure for a large class of M-channel FIR LPPRFBs: all analysis and synthesis filters have the same length $L = KM$. The novel SVD-based lattice can be viewed as an efficient and robust representation of the generalized lapped biorthogonal transforms (GLBT) with arbitrarily large overlapped samples KM. The lattice actually covers all solutions (both orthogonal and biorthogonal) in the class of practical FBs under consideration. The relaxation of the orthogonal constraint allows the FB to have significantly different analysis and synthesis basis functions which can then be tailored to fit a particular class of signals or applications. For a fixed quantization and entropy coding scheme, this class of FBs yields the highest coding performance comparing to other sate-of-the-art transforms reported in previous works.

8.1.3 Lapped Transforms of Arbitrary Block Size

Conceptually, the result in Chapter 5 is a simple, straightforward step towards unifying the field of LPPRFB design: the length constraint $L = KM$ in the GLBT's lattice is now relaxed to $L = KM + \beta$. The derivation of the general solution is not trivial in any standard. In the lapped transform language, the amount of overlap is not constrained to be a multiple of the number of channels anymore. The window size of the transform can be chosen arbitrarily.

8.1.4 Most General Solution: LPPRFB with Filters of Variable Length

Chapter 6 presents our most general LPPRFB solution: the filters can be chosen to have variable lengths $L_i = K_i M + \beta$. Besides having all of the attractive properties of previously-introduced transforms, this new class of FBs can take advantage of its VL property: the long overlapping basis functions are used to represent slowly-changing signal components and to avoid blocking artifacts, while the short basis functions are reserved for high-frequency signal components to limit ringing artifacts. These transforms named VLLOT and VLGLBT also provide a trade-off between performance and complexity. Extremely fast transforms (taking only several more additions and multiplications comparing to the DCT) with impressive subjective performance can be obtained.

8.1.5 Completeness and Minimality

Most of the lattice structures in this dissertation are proven to completely span the set of all possible solutions and to employ the least number of delay elements in the FB's implementation. This shows that the results are both general and practical.

8.1.6 Design Aspects

Numerous design examples obtained from standard nonlinear optimization programs are presented throughout Chapter 4 – 6. Many design criteria, secondary FB's properties, and their connection to image coding performance are considered and investigated: coding gain, attenuation at DC, attenuation around mirror frequencies, stopband attenuation of both analysis and synthesis filters, etc.

8.1.7 Application in image coding

Chapter 7 demonstrates that multi-band LPPRFBs are capable of providing significant improvements over current popular transforms such as the wavelet transform, the DCT, and the LOT. Extensive coding comparison are carried out with two next-generation image coding schemes: multiple-pass embedded coding and perceptually-tuned progressive coding. The embedded coder based on our new FBs outperforms some of the best image coders published recently in the literature. The improvement in PSNR over SPIHT, one of the highest performance wavelet-based embedded coder, can reach up to an astounding 2.6 dB. The perceptually-tuned coder which gears towards the human perception instead

of PSNR yields exceptional reconstructed image quality.

8.2 Future Research Directions

Despite tremendous successes mentioned above, much more work remains to be done in the field of filter banks, multirate systems, and their applications. In fact, the dissertation raises more new questions and reveals more open problems for future research than it actually resolves. A list of future research directions as well as open problems, some specific, others general, is compiled below. Some of the items in the list are already works in progress [29], [30], [23], [57].

8.2.1 Integer-Coefficient Transforms

M-channel LPPRFB with dyadic rational coefficients can lead to faster, more efficient, multiplierless, and low-powered systems [29], [30]. This highly practical class of transforms can also give rise to a unifying framework for both lossy and lossless image coding.

8.2.2 M-band Wavelets

Imposing regularity constraints (vanishing moments) on the lowpass filter of LPPRFBs leads to orthogonal/biorthogonal M-band wavelets. Moreover, direct mathematical imposition of regularity on the lattice coefficients results in M-band wavelets with fast, efficient, and robust implementation. The simple example in Section 4.6 demonstrates the feasibility of the idea.

8.2.3 Asymmetrical Systems

The analysis and synthesis polyphase matrices of all FBs presented in this dissertation have the same order. We have not biased one bank over the other: both have the same level of complexity. In many practical systems – for instance archiving or systems with low memory and limited resources like mobile phones, inexpensive printers – it is desirable to have extremely fast and low-complexity synthesis bank. This calls for asymmetrical FB design where the synthesis bank may have much lower order than the analysis. Another possible approach is to relax the PR constraint and to try to approximate the analysis bank by the fewest number of operations in the synthesis bank.

8.2.4 Filter Banks in Higher Dimension

Various other generalization to higher dimension can be taken: nonseparable multi-dimensional LPPRFB to handle multi-dimensional signals [57]; multi-FBs and multi-wavelets to better adapt to signals that are vector-valued in nature, i.e., color images, video, etc. The same factorization approach can be applied in straightforward manners.

8.2.5 Application in Image Compression

On image compression, high-order context modeling [106], [9], better quantization scheme [108], better rate-distortion optimizations and estimation [42], and subband classification methods [33] can be applied to the GLBT's transform coefficients to push the rate-distortion performance even further. Similarly, a more general data structure that better

fits the uniform-band nature of the transforms should also improve the coding efficiency [23] as well.

8.2.6 Other Potential Applications

The new transforms can benefit numerous other applications. The most obvious is the application in video coding. Since the LT prove to be a much better alternative than the DCT in still image coding, it is also capable of replacing the DCT in MPEG video coder [39], [111] as well. Its close relationship with the DCT and its low complexity facilitate the modification in both hardware and software. Other potential applications include speech and audio coding; processing, analysis, and compression of medical signals (ECG, MRI, mammograms...); transmultiplexers in communication; robust signal transmission over wireless and lossy channels [24].

In short, the results in this thesis deepen our understanding of multirate systems and filter banks, have a rich mathematical foundation, offer a unique blend of theory and practice, and provide many new, powerful tools for signal processing, understanding, and communication.

Bibliography

[1] S. O. Aase and T. A. Ramstad, "On the optimality of nonunitary filter banks in subband coders," *IEEE Trans. on Image Processing,* vol. 4, pp. 1585-1591, Dec. 1995.

[2] A. Akansu and M. J. T. Smith, eds., *Subband and Wavelet Transforms*, Kluwer Academic, Hingham, MA, 1995.

[3] M. Antonini, M. Barlaud, P. Mathieu, and I. Daubechies, "Image Coding Using the Wavelet Transform," *IEEE Trans. on Image Processing,*, vol. 1, pp. 205-220, Jan. 1992.

[4] S. Basu and H. M. Choi, "On multichannel linear-phase perfect-reconstruction filter banks," *Proc. IEEE Int. Conf. on Acoustics, Speech, and Signal Processing*, pp. 145-148, Detroit, 1994.

[5] C. Brislawn, "A simple lattice architecture for even-order linear-phase perfect reconstruction filter banks," *Proc. IEEE-SP Int. Symp. on Time-Frequency and Time-Scale Analysis,* pp. 124-127, Philadelphia, 1994.

[6] R. C. Calderbank, I. Daubechies, W. Sweldens, and B. L. Yeo, "Wavelet transforms that map integers to integers," preprint, to appear in *Applied and Computational Harmonic Analysis,* 1998.

[7] S. C. Chan, "The generalized lapped transform (GLT) for subband coding applications," *Proc. IEEE Int. Conf. on Acoustics, Speech, and Signal Processing,* pp. 1508-1511, Detroit, May 1995.

[8] L. Chen, T. Q. Nguyen and K. pp. Chan, "Symmetric extension methods for parallel M-channel perfect-reconstruction linear-phase FIR analysis/synthesis systems," *IEEE Trans on Signal Processing,* vol. 43, pp. 2505-2511, Nov. 1995.

[9] C. Chrysafis and A. Ortega, "Efficient context-based entropy coding for lossy wavelet image compression," *Proc. Data Compression Conference*, pp. 241-250, Snowbird, Mar. 1997.

[10] T. N. Cornsweet, *Visual Perception*, Academic Press, New York, 1970.

[11] R. E. Crochiere and L. R. Rabiner, *Multirate Digital Signal Processing*, Prentice-Hall, Englewood Cliffs, NJ, 1983.

[12] I. Daubechies, *Ten Lectures on Wavelets,* CBMS Conference Series, SIAM, Philadelphia, 1992.

[13] I. Daubechies, "Orthonormal bases of compactly supported wavelets," *Comm. Pure Appl. Math.,* vol. 41, pp. 909-996, 1988.

[14] I. Daubechies and W. Sweldens, "Factoring wavelet transforms into lifting steps," preprint, to appear in *J. Fourier Anal. Appl.*, vol. 4, 1998.

[15] R. A. DeVore, B. Jawerth, and B. J. Lucier, "Image compression through wavelet trasnform coding," *IEEE Trans on Information Theory*, vol. 38, pp. 719-746, March, 1992.

[16] Gantmacher, F. R., *The Theory of Matrices*, Chelsea Publishing Company, 1977.

[17] H. Gharavi and A. Tabatabai, "Sub-band coding of monochrome and color images," *IEEE Trans. on Circuits and Systems,* vol. 35, pp. 207-214, 1988.

[18] A. Gersho and R. M. Gray, *Vector Quantization and Signal Compression*, Kluwer Academic Publishers, Hingham, MA, 1992.

[19] W. Givens, "Computation of plane unitary rotations transforming a general matrix to triangular form," *SIAM Journal of Appl. Math.*, vol. 6, pp. 26-50, 1958.

[20] R. C. Gonzalez and R. E. Woods, *Digital Image Processing*, Addison-Wesley, Reading, MA, 1993.

[21] R. A. Gopinath and C. S. Burrus, "Wavelet transforms and filter banks", in *Wavelets: A Tutorial in Theory and Applications*, C. K. Chui, ed., Academic Press, San Diego, 1992.

[22] P. N. Heller, T. Q. Nguyen, H. Singh, and W. K. Carey, "Linear-phase M-band wavelets with application to image coding," *Proc. IEEE Int. Conf. on Acoustics, Speech, and Signal Processing*, Detroit, May 1995.

[23] M. Helsingius, T. D. Tran, and T. Q. Nguyen, "A GenLOT-based progressive image coder for low resolution images," *Proc. IEEE Int. Conf. on Image Processing*, Chicago, Oct. 1998.

[24] S. S. Hemami, "Reconstruction Optimized Lapped Orthogonal Transforms for Robust Image Transmission," *IEEE Trans. on Circuits and Systems for Video Technology*, Special Issue on Wireless Visual Communications, April 1996.

[25] R. A. Horn and C. R. Johnson, *Matrix Analysis*, Cambridge University Press, 1985.

[26] B. R. Horng and A. N. Willson, Jr., "Lagrange multiplier approaches to the design of two-channel perfect reconstruction linear phase FIR filter banks," *IEEE Trans. on Signal Processing*, vol. 40, pp. 364-374, Feb. 1992.

[27] M. Ikehara and T.Q. Nguyen, " Time-domain design of perfect reconstruction filter banks with linear phase", *Proc. IEEE Int. Conf. on Acoustics, Speech, and Signal Processing*, Munich, April 1997.

[28] M. Ikehara, T. D. Tran, and T. Q. Nguyen, "Linear phase paraunitary filter banks with unequal-length filters," *Proc. IEEE Int. Conf. on Image Processing*, Santa Barbara, Oct. 1997.

[29] M. Ikehara, T. D. Tran, and T. Q. Nguyen, "Generalized lapped biorthogonal transform with integer coefficients," *Proc. of IEEE Int. Conf. on Image Processing*, Chicago, Oct. 1998.

[30] M. Ikehara, T. D. Tran, and T. Q. Nguyen, "Generalized lapped biorthogonal transform with integer coefficients," in preparation, to be submitted to *IEEE Trans. on Signal Processing*, 1998.

[31] N. S. Jayant, J. D. Johnston, and R. J. Safranek, "Signal compression based on models of human perception," *Proc. of the IEEE*, vol. 81, pp. 1358-1422, Oct. 1993.

[32] N. S. Jayant and P. Noll *Digital Coding of Waveforms*, Prentice-Hall, Englewood Cliffs, NJ, 1989.

[33] R.L. Joshi, H. Jafarkhani, J.H. Kasner, T.R. Fischer, N. Farvardin, M.W. Marcellin, and R. H. Bamberger, "Comparison of different methods of classification in subband coding of images," *IEEE Trans. Image Processing,* 1997.

[34] J. Katto and Y. Yasuda, "Performance evaluation of subband coding and optimization of its filter coefficients," *SPIE Proc. Visual Communication and Image Processing*, pp. 95-106, Boston, Nov. 1991.

[35] H. Kiya, M. Yae, and M. Iwahashi, "A linear-phase two-channel filter bank allowing perfect reconstruction", *Proc. IEEE Int. Symp. Circuits and Systems*, pp. 951-954, San Diego, May 1992.

[36] H. Kiya, K. Nishikawa, and M. Iwahashi, "A development of symmetric extension method for subband image coding," *IEEE Trans. on Image Processing*, vol. 3, pp. 78-81, Jan. 1994.

[37] C. Kok and T. Q. Nguyen, "Nonnegative scaling function and applications in image coding," *Proc. 29th Asilomar Conference on SSC,* Monterey, Oct. 1995.

[38] C. W. Kok, T. Nagai, M. Ikehara, and T. Q. Nguyen, "Structures and factorization of linear phase paraunitary filter banks," *Proc. IEEE Int. Symp. on Circuits and Systems*, Hong Kong, June 1997.

[39] D. J. Le Gall, "The MPEG video compression algorithm," *Image Communication*, vol. 4, pp. 129-140, 1992.

[40] J. S. Lim, *Two-Dimensional Signal and Image Processing*, Prentice Hall, Englewood Cliffs, NJ, 1990.

[41] Y. P. Lin and P. P. Vaidyanathan, "Linear phase cosine modulated maximally decimated filter banks with perfect reconstruction," *IEEE Trans. on Signal Processing*, vol. 42, pp. 2525-2539, Nov. 1995.

[42] S. M. LoPresto, K. Ramchandran, and M. T. Orchard, "Image coding based on mixture modeling of wavelet coefficients and a fast estimation-quantization framework," *Proc. Data Compression Conference*, pp. 221-230, Snowbird, Mar. 1997.

[43] S. Mallat, "A theory for multiresolution signal decomposition: the wavelet representation," *IEEE Trans. on Pattern Anal. and Machine Intel.*, vol. 11, pp. 674-693, July 1989.

[44] S. Mallat, "Multiresolution approximations and wavelet orthonormal bases of $L^2(R)$," *Trans. of Amer. Math. Soc.*, vol 315, pp. 69-87, Sept. 1989.

[45] H. S. Malvar and D. H. Staelin, "The LOT: transform coding without blocking effects," *IEEE Trans. on Signal Processing*, vol. 37, pp. 553-559, Apr. 1989.

[46] H. S. Malvar and D. H. Staelin, "Lapped transforms for efficient transform/subband coding," *IEEE Trans. on Acoustics, Speech, and Signal Processing*, vol. 38, pp. 969-978, June 1990.

[47] H. S. Malvar, *Signal Processing with Lapped Transforms*, Artech House, Norwood, MA, 1992.

[48] H. S. Malvar, "Biorthogonal and nonuniform lapped transforms for transform coding with reduced blocking and ringing artifacts," *IEEE Trans. on Signal Processing*, Special Issue on Multirate Systems, Filter Banks, Wavelets, and Applications, vol. 46, pp. 1043-1053, Apr. 1998.

[49] H. S. Malvar, "Lapped biorthogonal transforms for transform coding with reduced blocking and ringing artifacts," *Proc. IEEE Int. Conf. on Acoustics, Speech, and Signal Processing*, Munich, April 1997.

[50] F. Mintzer, "Filters for distortion-free two-band multirate filter banks", *IEEE Trans. on Acoustics, Speech, and Signal Processing*, vol. 33, pp. 626-630, June 1985.

[51] K. Nayebi, T. P. Barnwell, III, and M. J. T. Smith, "Time-domain filter bank analysis: A new design theory," *IEEE Trans. on Signal Processing*, vol. 40, pp. 1412-1429, June 1992.

[52] J. A. Nelder and R. Mead, "A simplex method for function minimization," *Computer Journal*, vol. 7, pp. 308-313.

[53] T. Q. Nguyen and P. P. Vaidyanathan, "Two channel PR FIR QMF structures which yield linear-phase analysis and synthesis filters", *IEEE Trans. on Acoustics, Speech, and Signal Processing*, vol. 37, pp. 676-690, May 1989.

[54] T. Q. Nguyen and P. P. Vaidyanathan, "Structures for M-channel perfect-reconstruction FIR QMF banks which yield linear-phase filters," *IEEE Trans. on Acoustics, Speech, and Signal Processing*, vol. 38, pp.433-446, March 1990.

[55] T. Q. Nguyen, "Digital filter banks design – quadratic-constrained formulation," *IEEE Trans. on Signal Processing*, vol. 43, pp. 2103-2108, Sept. 1995.

[56] A. V. Oppenheim and R. W. Schafer, *Discrete-time Signal Processing*, Prentice-Hall, Englewoods Cliffs, NJ, 1989.

[57] S. Oraintara, T. D. Tran, and T. Q. Nguyen, "On the study of diamond-shape filter banks and an application in image compression," *Proc. IEEE DSP Workshop*, Bryce Canyon National Park, Utah, Aug. 1998.

[58] W. B. Pennebaker and J. L. Mitchell, *JPEG: Still Image Compression Standard,* Van Nostrand Reinhold, New York, NY, 1993.

[59] H. A. Peterson, A. J. Ahumada Jr, and A. B. Watson, "An Improved Detection Model for DCT Coefficient Quantization," *Human Vision, Visual Processing, and Digital Display IV*, pp. 1-10, 1993.

[60] R. L. de Queiroz and K. R. Rao, "HVS weighted progressive transmission of images using the LOT," *Journal of Electronic Imaging*, vol. 1, pp. 328-338, July 1992.

[61] R. L. de Queiroz and K. R. Rao, "On reconstruction methods for processing finite-length signals with paraunitary filter banks," *IEEE Trans. on Signal Processing*, vol. 43, pp. 2407-2410, Oct. 1995.

[62] R. L. de Queiroz, T. Q. Nguyen, and K. R. Rao, "The GenLOT: generalized linear-phase lapped orthogonal transform," *IEEE Trans. on Signal Processing,* vol. 40, pp. 497-507, March 1996.

[63] R. L. de Queiroz, *On Lapped Transforms*, PhD Thesis, The University of Texas, Arlington, TX, Dec. 1994.

[64] M. Rabbani and P. W. Jones, *Digital Image Compression Techniques,* SPIE Opt. Eng. Press, Bellingham, Washington, 1991.

[65] K. Ramchandran, Z. Xiong, K. Asai and M. Vetterli, "Adaptive transforms for image coding using spatially-varying wavelet packets", *IEEE Trans. on Image Processing*, vol. 5, pp. 1197-1204, July, 1996.

[66] T. A. Ramstad, S. O. Aase, J. H. Husoy, *Subband Compression of Images: Principles and Examples*, Elsevier, 1995.

[67] K. R. Rao and P. Yip, *Discrete Cosine Transform: Algorithms, Advantages, Applications*, New York, NY, Academic Press, 1990.

[68] P. Rieder, J. Götze, J. A. Norsek, and C. S. Burrus, "Parameterization of orthogonal wavelet transforms and their implementation," *IEEE Trans. on Circuits and Systems - II: Analog and Digital Signal Processing*, vol. 45, pp. 217-226, Feb. 1998.

[69] R. J. Safranek and J. D. Johnston, "A perceptually-tuned sub-band image coder with image dependent quantization and post-quantization data compression," *Proc. IEEE Int. Conf. on Acoustics, Speech, and Signal Processing,* pp. 1945-1948, 1989.

[70] P. Saghizadeh and A. N. Willson, Jr., "A generic approach to the design of M-channel uniform-band perfect-reconstruction linear phase FIR filter banks," *Proc. IEEE Int. Conf. on Acoustics, Speech, and Signal Processing*, pp. 1300-1303, Detroit, May 1995.

[71] A. Said and W. A. Pearlman, "A new fast and efficient image codec based on set partitioning in hierarchical trees," *IEEE Trans. on Circuits and Systems for Video Technology,* vol. 6, pp. 243-250, June 1996.

[72] A. Said and W. A. Pearlman, "An image multiresolution representation for lossless and lossy compression," *IEEE Trans. on Image Processing,* vol. 5, pp. 1303-1310, Sept. 1996.

[73] J. M. Shapiro, "Embedded image coding using zerotrees of wavelet coefficients," *IEEE Trans. on SP,* vol. 41, pp. 3445-3462, Dec. 1993.

[74] M. J. T. Smith and T. P. Barnwell, III, "Exact reconstruction techniques for tree-structured subband coders," *IEEE Trans. Acoustics, Speech, and Signal Processing*, pp. 434-441, June 1986.

[75] A. K. Soman, P. P. Vaidyanathan, and T. Q. Nguyen, "Linear-phase paraunitary filter banks: theory, factorizations and applications," *IEEE Trans. on Signal Processing*, vol. 41, pp. 3480-3496, Dec. 1993.

[76] P. Steffen, P. N. Heller, R. A. Gopinath, C. S. Burrus, "Theory of regular M-band wavelets," *IEEE Trans. on Signal Processing,* vol. 41, pp. 3497-3511, Dec. 1993.

[77] G. Strang and T. Q. Nguyen, *Wavelets and Filter Banks*, Wellesley-Cambridge Press, Wellesley, MA, Second Edition, 1998.

[78] W. Sweldens, "The lifting scheme: A construction of second generation wavelets," *SIAM J. Math. Anal.*, vol. 29, pp. 511-546, 1997.

[79] T. D. Tran, *A Locally Adaptive Perceptual Masking Threshold Model for Image Coding*, Master Thesis, Massachusetts Institute of Technology, Cambridge, MA, May 1994.

[80] T. D. Tran and T. Q. Nguyen, "On M-channel linear-phase FIR filter banks and application in image compression," *IEEE Trans. on Signal Processing,* vol. 45, pp. 2175-2187, Sept. 1997.

[81] T. D. Tran and T. Q. Nguyen, "A progressive transmission image coder using linear phase filter banks as block transforms," submitted to *IEEE Trans. on Image Processing,* May 1997.

[82] T. D. Tran, M. Ikehara, and T. Q. Nguyen, "Linear phase paraunitary filter bank with filters of different lengths and its application in image compression," submitted to *IEEE Trans. on Signal Processing* in Dec. 1997.

[83] T. D. Tran, R. L. de Queiroz, and T. Q. Nguyen, "Linear phase perfect reconstruction filter bank: lattice structure, design, and application in image coding," submitted to *IEEE Trans. on Signal Processing* in Apr. 1998.

[84] T. D. Tran, T. Q. Nguyen, Y. H. Hu, R. J. Safranek, and R. L. de Queiroz, "Progressive perceptual image coding," in preparation, to be submittied to *IEEE Trans. on Image Processing.*

[85] T. D. Tran, R. de Queiroz, and T. Q. Nguyen, "Generalized lapped biorthogonal transform with variable-length basis functions," in preparation, to be submitted to *IEEE Trans. on Signal Processing.*

[86] T. D. Tran and T. Q. Nguyen, "On arbitrary-length M-channel linear-phase FIR filter banks," *Proc. 29th Asilomar Conference on SSC,* Monterey, Oct. 1995.

[87] T. D. Tran and R. J. Safranek, "A locally adaptive perceptual masking threshold model for image coding," *Proc. IEEE Int. Conf. on Acoustics, Speech, and Signal Processing,* Atlanta, May 1996.

[88] T. D. Tran and T. Q. Nguyen, "Generalized lapped orthogonal transform with unequal-length basis functions," *Proc. IEEE Int. Symp. on Circuits and Systems*, Hong Kong, June 1997.

[89] T. D. Tran and T. Q. Nguyen, "A progressive transmission image coder using linear phase paraunitary filter banks," *Proc. 31st Asilomar Conference on SSC,* Pacific Grove, Nov. 1997.

[90] T. D. Tran, T. Q. Nguyen, and Y. H. Hu, "A perceptually-tuned block-transform-based progressive transmission image coder," *Proc. 31st Asilomar Conference on SSC,* Pacific Grove, Nov. 1997.

[91] T. D. Tran and T. Q. Nguyen, "A lapped transform embedded image coder," *Proc. IEEE Int. Symp. on Circuits and Systems*, Monterey, May 1998.

[92] T. D. Tran, R. de Queiroz, and T. Q. Nguyen, "The generalized lapped biorthogonal transform," *Proc. IEEE Int. Conf. on Acoustics, Speech, and Signal Processing*, Seattle, May 1997.

[93] T. D. Tran, R. de Queiroz, and T. Q. Nguyen, "Variable-length generalized lapped biorthogonal transform," *Proc. IEEE Int. Conf. on Image Processing*, Chicago, Oct. 1998.

[94] S. Trautmann and T. Q. Nguyen, "Comparison of linear phase perfect reconstruction in wavelet transform based image compression," *Conference on Information Sciences and Systems*, Baltimore, March 1995.

[95] P. P. Vaidyanathan, *Multirate Systems and Filter Banks*, Prentice Hall, Englewood Cliffs, NJ, 1993.

[96] P. P. Vaidyanathan and P. Q. Hoang, "Lattice structures for optimal design and robust implementation of two-channel perfect-reconstruction QMF banks," *IEEE Trans. on Acoustics, Speech, and Signal Processing,* vol. 36, pp. 81-94, Jan. 1988.

[97] P. P. Vaidyanathan, "Theory and design of M-channel maximally decimated quadrature mirror filters with arbitrary M, having perfect reconstruction property," *IEEE Trans. on Acoustics, Speech, and Signal Processing*, vol. 35, pp. 476-492, Apr. 1987.

[98] M. Vetterli and J. Kovačević, *Wavelets and Subband Coding*, Prentice Hall, Englewood Cliffs, NJ, 1995.

[99] M. Vetterli, "A theory of multirate filter banks," *IEEE Trans. on Acoustics, Speech, and Signal Processing*, vol. 35, pp. 356-372, March 1987.

[100] M. Vetterli and C. Herley, "Wavelets and filter banks: theory and design," *IEEE Trans. on Signal Processing*, vol. 40, pp 2207-2232, Sept. 1992.

[101] M. Vetterli and D. Le Gall, "Perfect-reconstruction filter banks : some properties and factorizations", *IEEE Trans. on Acoustics, Speech, and Signal Processing*, vol. 37, pp. 1057-1071, July 1989.

[102] J. E. Volder, "The CORDIC trigonometric computing technique," *IRE Trans. on Electron. Comput.*, vol. EC-8, pp. 330-334, 1959.

[103] J. W. Woods and S. D. O'Neil, "Subband coding of images," *IEEE Trans. on Acoustics, Speech, and Signal Processing*, vol. 34, pp. 1278-1288, Oct. 1986.

[104] J. W. Woods (Ed.), *Subband Coding of Images*, Kluwer Academic, Hingham, MA, 1991.

[105] X. Wu and N. Memon, "Context-based, Adaptive, Lossless Image Codec", *IEEE Trans. on Communications*, vol. 45, no. 4, pp. 437-444, April 1997.

[106] X. Wu, "High-order context modeling and embedded conditional entropy coding of wavelet coefficients for image compression," preprint, submitted to *IEEE Trans. on Image Processing*, 1998.

[107] Z. Xiong, O. Guleryuz and M. T. Orchard, "A DCT-based embedded image coder", *IEEE Signal Processing Letters*, vol. 3, pp. 289-290, Nov. 1996.

[108] Z. Xiong, K. Ramchandran and M. T. Orchard, "Space-frequency quantization for wavelet image coding", *IEEE Trans. Image Processing*, vol. 6, pp. 677-693, May 1997.

[109] Z. Xiong, K. Ramchandran and M. T. Orchard, "Wavelet packets image coding using space-frequency quantization," preprint, to appear in *IEEE Trans. Image Processing*, 1998.

[110] "Compression with Reversible Embedded Wavelets," RICOH Company Ltd. submission to ISO/IEC JTC1/SC29/WG1 for the JTC1.29.12 work item, 1995. Can be obtained on the World Wide Web, address: `http://www.crc.ricoh.com/CREW`.

[111] Recommendation H.262, ISO/IEC 13818. "Generic coding of moving picture & associates audio," Draft international standard of MPEG-2. Also see `http://www.mpeg.org/`.

[112] "Wavelet Scalar Quantization Gray Scale Fingerprint Image Compression Specification," Criminal Justice Information Services, FBI, Washington, DC, 1993.